Modelling of groundwater flow conditions at the contaminated site of a former dry-cleaning facility

Master's thesis in Infrastructure and Environmental Engineering

JOHANNA NILSSON

DEPARTMENT OF DEPARTMENT OF ARCHITECTURE AND CIVIL ENGINEERING
DIVISION OF GEOLOGY AND GEOTECHNICS

CHALMERS UNIVERSITY OF TECHNOLOGY
Gothenburg, Sweden 2023
www.chalmers.se

MASTER'S THESIS ACEX30

Modelling of groundwater flow conditions at the contaminated site of a former dry-cleaning facility

Master's Thesis in the Master's Programme Infrastructure and Environmental Engineering

JOHANNA NILSSON

Department of Architecture and Civil Engineering

Division of Geology and Geotechnics

Engineering Geology

CHALMERS UNIVERSITY OF TECHNOLOGY

Göteborg, Sweden 2023

Modelling of groundwater flow conditions at the contaminated site of a former dry-cleaning facility
Master's Thesis in the Master's Programme Infrastructure and Environmental Engineering

JOHANNA NILSSON

Examensarbete ACEX30

Institutionen för arkitektur och samhällsbyggnadsteknik

Chalmers tekniska högskola, 2023

Department of Architecture and Civil Engineering
Division of Geology and Geotechnics
Engineering Geology
Chalmers University of Technology

SE-412 96 Göteborg
Sweden
Telephone: + 46 (0)31-772 1000

Modelling of groundwater flow conditions at the contaminated site of a former dry-cleaning facility

Master's thesis in the Master's Programme Infrastructure and Environmental Engineering

JOHANNA NILSSON

Department of Architecture and Civil Engineering
Division of Geology and Geotechnics
Engineering Geology
Chalmers University of Technology

ABSTRACT

The thesis aims to investigate the hydrogeological conditions at the site of a former dry-cleaning facility where contamination of chlorinated ethenes (PCE and TCE) has been documented. This is done through the development of a steady-state numerical groundwater flow model in the widely used software Visual MODFLOW Flex. As an initial step of the modelling process, a conceptual site model was developed and presented. The site model includes two adjacent tunnels situated in the shallow bedrock, for which the impact on the local groundwater system is unknown. Using the calibrated model, a sensitivity analysis was performed, identifying crucial hydraulic parameters and boundary conditions which could be subject to further investigation to minimize model uncertainties regarding the calculated groundwater inflow to the nearby tunnels and the travel time of particles situated at the former dry cleaner's location within the hydrogeologic system.

The model suggests that the two tunnels have a significant impact on the hydrogeological system to the west of the former dry-cleaner. The site of the former building is located at a groundwater divide, and the developed numerical model was not able to reproduce groundwater heads both west and south-east of the former dry-cleaner. The groundwater levels south-east of the former dry-cleaning facility are found to be governed by unknown hydraulic conditions, which were not identified and included in the conceptual model. The performed sensitivity analysis indicates that the boundary conditions of recharge and drain leakance of the tunnels need to be investigated further to reduce uncertainties of the model. The developed model suggests that the tunnels, primarily the sewage tunnel, act as a contaminant pathway of chlorinated ethenes present in groundwater flowing from the contaminated site.

Key words: Hydrogeology, groundwater, numerical modelling, MODFLOW, VMF, DNAPLs, chlorinated ethenes

Modellering av grundvattenflödesförhållanden vid den förorenad platsen för en nedlagd kemtvätt

Examensarbete inom mastersprogrammet Infrastruktur och miljöteknik

JOHANNA NILSSON

Institutionen för arkitektur och samhällsbyggnadsteknik
Avdelningen för geologi och geoteknik
Teknisk geologi
Chalmers tekniska högskola

SAMMANFATTNING

Syftet med arbetet är att undersöka de hydrogeologiska förhållandena på platsen för en tidigare kemtvättanläggning där förorening av de klorerade lösningsmedlen tetrakloreten (PCE) och trikloreten (TCE) har dokumenterats. Detta har gjorts genom att utveckla av en stationär (steady-state) numerisk grundvattenmodell i programvaran Visual MODFLOW Flex samt utförandet av en känslighetsanalys av den kalibrerade modellen. Som ett första steg i modelleringsprocessen utarbetades och presenterades en konceptuell modell av platsen, vilket inkluderar två närbelägna bergtunnlar vars påverkan på det lokala grundvattensystemet till stor del är okänd. Känslighetsanalysen används för att identifiera avgörande hydrauliska parametrar och randvillkor som skulle kunna vara föremål för ytterligare undersökning för att minimera osäkerheter i modellen avseende grundvatteninflödet till två närliggande bergtunnlar och den beräknade flödestiden för partiklar vid platsen för kemtvätten.

Den utvecklade modellen tyder på att de två bergstunnlarna har en betydande påverkan på det hydrogeologiska systemet väster om den nedlagda kemtvätten. Den tidigare byggnaden är belägen vid en grundvattendelare, och den numeriska modellen kunde inte återskapa grundvattennivåer både väster och sydost om den tidigare kemtvätten. Det anses troligt att grundvattennivåerna sydost om den tidigare kemtvättanläggningen styrs av parametrar som inte har identifierats eller inkluderades i den konceptuella modellen. Den genomförda känslighetsanalysen indikerar att randvillkoren för grundvattenbildning och faktorn för genomsläpplighet (leakance) av bergtunnlarna bör undersökas närmare för att minska osäkerheterna i modellen. Den utvecklade modellen indikerar att tunnlarna, främst avloppstunneln, fungerar som en spridningsväg för de klorerade lösningsmedel som förekommer i det grundvatten som flödar från den förorenade platsen.

Nyckelord: Hydrogeologi, grundvatten, numerisk modellering, MODFLOW, VMF, klorerade lösningsmedel.

Contents

Aknowledgements

This thesis was performed as the final part of my studies at Chalmers University of Technology. This project would not have been possible without the support of a number of people. Firstly, I would like to thank Anna Vickman, my supervisor at WSP, for the opportunity to do my master thesis at WSP and for the invaluable guidance, support, and numerous insightful discussions on the subject of groundwater modelling. I would also like to express my thanks to my supervisor and examiner Lars Rosén for providing valuable input and feedback to the project.
Furthermore, I would like to extend my gratitude to Saba Joodaki at WSP in Stockholm for all the support regrading modelling in VMF and for answering all my numerous questions. I would also like to thank Julia Inkapööl and Inger Johansson at WSP in Stockholm for providing all the available material and data of the project, and for providing feedback regarding the thesis.
Finally, I would like to extend my thanks to everyone at the WSP Hydrogeology in Göteborg for the support in the project and for the inclusion into the group.

Johanna Nilsson, Göteborg, August 2023

List of acronyms

CSM	Conceptual site model
DCE	Dichloroethene/Dichloroethylene
DNAPLs	Dense non-aqueous phase liquids
FD/ FDM	Finite difference (method)
FEM	Finite element method
GIS	Geographic information system
GUI	Graphic user interface
GWM	Groundwater model
MAE	Mean absolute error
MIP	Membrane interface probe
PCE	Perchloroethylene/Tetrachloroethene/Tetrachloroethylene
SGU	Geological Survey of Sweden
TCE	Trichloroethene/Trichloroethylene
TCE	Trichloroethylene/Trichloroethene
USGS	United States Geological Survey
VMF	Visual MODFLOW Flex

Glossary

MODFLOW	Finite-difference (FD) computer code that is used for simulating groundwater flow in three dimensions, developed by the USGS.
RH2000	The Swedish national height reference system (Lantmäteriet, n.d.-a).
SWEREF 99 TM	The Swedish national map projection (Lantmäteriet, n.d.-).

1 Introduction

The majority of of the Earth's freshwater (70%) is bound in glaciers and other ice formations (Fitts, 2012). Surface waters, such as lakes and rivers, accounts for only a small fraction of all freshwater, instead the majority of the freshwater that is not bound in ice occurs as groundwater beneath the Earth's surface. Many regions around the world depend heavily on groundwater as their primary source of drinking water and for irrigation. In addition, groundwater sustains the base flow of rivers and has an important role in supporting crucial ecosystem services (Dennedy-Frank, 2019), a role that is often largely unappreciated.

With the continually rapid urbanisation and climate change, the impact of anthropogenic activities on hydrogeological systems becomes an increasing issue. Human activities such as groundwater exploitation, physical alterations of the Earth's surface, and the emissions of pollutants, together with the complex dynamics of the hydrologic cycle contribute to an increased vulnerability of aquifers in an anthropogenic environment (Burri et al., 2019). The degradation of groundwater quality is a widely recognized concern.

1.1 Background

Chlorinated solvents are considered some of the most challenging groundwater contaminants in industrialized countries (Pankow & Cherry, 1996). The two chlorinated ethenes tetrachloroethene (PCE) and trichloroethene (TCE) are common contaminants of soil and groundwater at sites with a history of activities connected to dry cleaning facilities. PCE and TCE are categorized as dense non-aqueous phase liquids (DNAPLs), as they have certain chemical and physical characteristics, often giving rise to complicated spreading in the surface. As both substances are considered carcinogenic according to the International Agency of Research on Cancer (IARC, 2008; IARC, 2014), these contaminated sites are of great concern. The behaviour of chlorinated ethenes in the subsurface is highly dependent on site-conditions, geologic properties, and subsurface anisotropies.

Numerical hydrogeological flow modelling is an essential tool in the field of hydrogeology. Numerical flow models are mainly used to predict the behaviour of a hydrogeologic system in reaction to anthropogenic activities such as exploitation of groundwater or changes in the natural conditions, such as climate change (Rapantova et al., 2017). The coupling of solute transport models with flow models provides a possibility to model the distribution of a solute through the processes of advection, dispersion, and various chemical reaction.

However, in addition to this, numerical flow models can have a wide range of applications, some of which have less straightforward aims. Groundwater flow models are based on a synthesis of information of geology, hydrogeology, geography, and hydrology. As is pointed out by Rapantova et al. (2017) numerical models contribute to an increased understanding of the modelled area, as they provide a three-dimensional visualisation of the flow field and the conditions of the subsurface. Thus, groundwater models can be used in order to gain a better understanding of the hydrogeological system, and as a tool to test and analyse assumptions of the system and its dynamics (Kresic, 2007). Knowledge of the geology and hydrogeology are key requirement for management and remediation of a contaminated area. Thereby, numerical flow modelling is highly applicable to cases of groundwater contamination.

Given the numerous sources of uncertainty inherent in numerical groundwater modelling, it is essential to examine the ways in which various uncertainties impact the results of the model. This is done through the performance of a sensitivity analysis, where the influence of parameters and boundary condition on the model is assessed. The sensitivity analysis results in quantitative relationships between the model results and the hydraulic properties or boundary conditions of the aquifer (ASTM, 2016).

In this thesis a conceptual and numerical groundwater flow model is developed of the area surrounding a former dry-cleaning facility in eastern Sweden. The activity of the dry cleaner has caused contamination of soil and groundwater by chlorinated ethenes. The site has been under investigation for a long time, with a wide range of data gathered. Investigations indicate drainage of contaminated groundwater through a sewage and a stormwater tunnel located in proximity to the former dry cleaner, which are largely unexplored. Thus, there is a need to achieve further understanding the dynamics of the hydrogeological system at the site and to investigate the impact of the two tunnels.

1.2 Aim and research questions

The aim of the thesis and to gain a deeper understanding of the hydrogeological conditions and flow patterns at the site of a former dry-cleaning facility where contamination of chlorinated ethenes is established, through the development of a steady-state numerical groundwater flow model. Using the developed model, the drainage of groundwater through two tunnels situated within the studied area, as well as the calculated particle travel time from the source area of the site, is investigated. A sensitivity analysis is performed on the calibrated model in order to investigate the impact of variations in parameters and boundary conditions to the model results, thus determining which parameters are most important to focus investigations on in order to reduce the model uncertainties.

With the presented aim, the following research questions have been defined:

- What insight can the developed model give about the spreading of chlorinated ethenes in groundwater originating from the source area of the former dry-cleaning facility?
- What impact does the tunnels located west of the site have on the hydrogeological system?
- How does the groundwater inflow to the tunnels and the computed particle travel time from the site of the former dry-cleaning facility vary with different assumptions of hydraulic properties and boundary conditions?
- Which model parameters and boundary conditions should be investigated further in order to limit uncertainties in the model predictions of tunnel inflow and computed particle travel time?

1.3 Limitations

The following limitations apply to the thesis:

- The thesis is based on previously gathered data from the site. No additional investigations are conducted as part of the thesis.
- The thesis is focused on the contamination of chlorinated ethenes although various additional contaminants have been detected at the studied site.
- While contaminants have been detected in several phases at the studied area, only solute transport in groundwater is considered in the study.

- The thesis does not engage in risk assessment, or the management and remediation of contamination of soil, bedrock, and groundwater.
- The thesis is focused on numerical groundwater flow modelling and does not engage in transport modelling of contaminates. Particle tracking is used to investigate the principal flow paths, which can be used to give a theoretical estimation of the advective transport of non-reactive contaminants along the principal flow paths.
- The sensitivity analysis focuses on a selected array of parameters which during the during the model calibration process were deemed of interest of further investigation.

1.4 Method and thesis structure

The methodology of the thesis is composed of a number of steps, which are illustrated in Figure 1. First, a literature review was conducted to provide a theoretical background to the thesis. The literature review is presented in **Chapter 2**, and presents the necessary theoretical background of groundwater flow, groundwater flow modelling as well as chlorinated ethenes and solute transport. Textbooks available through Chalmers University of Technology's library has been used as the basis of the literature review. Anderson et al. (2015), Woessner & Poeter (2020) and Kresic (2007) served as the basis for the theoretical background on groundwater flow and groundwater flow modelling. Pankow & Cherry (1996) and Fetter (1993) were the main sources used in developing a theoretical foundation on chlorinated ethenes. To complement the textbook literature, the bibliographic databases Web of Science and Scopus were used. A wide range of search stings were used, and the search strategy was based on snowballing. Grey literature, as defined by (Schöpfel, 2010) have been used as a secondary complement when needed.

Thereafter, a conceptual site model (CSM) was developed, containing a wide range of information relevant to the hydrogeologic conditions of the site. The former dry-cleaning facility and the CSM is presented in **Chapter 3.** Information on the geology, hydrogeology, hydrology, and contamination of chlorinated solvents at the studied area has been gathered and complied into a CSM. As a part of the CSM, calculations of the water balance and the groundwater recharge were performed as well as evaluation of the hydraulic properties of the rock. Throughout the project, the CSM was continually updated and amended with new information.

The process of developing the numerical model is detailed in **Chapter 4.** The process contains a number of steps and was, as is illustrated in Figure 1, largely iterative. After calibration of the model is deemed sufficient, a sensitivity analysis was performed to examine how variations of specific parameters and boundary conditions will impact the developed numerical model. As a part of the investigation of the impact of the rock tunnels on the developed model, the area of influence of the rock tunnels was derived. The findings of the model and the results of the sensitivity analysis are presented in **Chapter 5.** This is followed by a discussion of the obtained results and the used methodology in **Chapter 6.** Finally, the conclusions of the thesis are presented in **Chapter 7.**

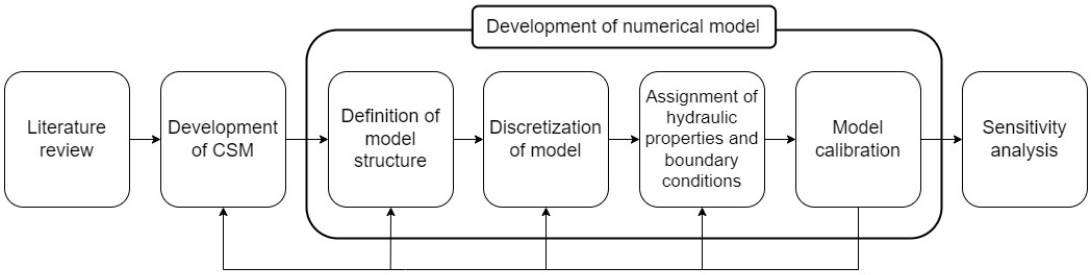

Figure 1. Illustration of the methodology of the thesis.

2 Theory

The following chapter provides a theoretical background to the thesis, covering the basics of groundwater flow, the foundation of numerical groundwater modelling and the transport of chlorinated ethenes in the subsurface

2.1 Terminology

A wide range of terminology is used in hydrogeology, and there is a need to define some terms used in this thesis. The term *groundwater* refers to water that occurs in the saturated zone of the subsurface. The *water table* constitutes the top of the *saturated zone*, in which the pore spaces of a porous media are fully saturated, see Figure 2. The *unsaturated zone* (or vadose zone) is the area located between the land surface and the water table, where the pore spaces can contain both water and air (Woessner & Poeter, 2020).

There are a number of different ways of categorizing the occurrence of groundwater in the subsurface. Geologic formations can be classified into distinct *hydrostratigraphic units*, defined as a continuous geological material (a geologic formation or part of a geologic formation) that has similar hydraulic properties (Anderson et al., 2015). Hydrostratigraphic units can be categorized as aquifers and confining units. An *aquifer* is a saturated geologic formation that stores and transmits a significant amount of potable water (Kresic, 2007). The definition is somewhat subjective, as the terms significant amount and potable can be subject to interpretation. A number of terms, such as aquitard and aquiclude can be used to describe hydrogeologic units that does not constitute an aquifer. Here however, the more modern term confining unit (or confining bed) is used. A *confining unit* is a geologic unit with low permeability that may store but does not transmit significant amounts of water (Anderson et al., 2015).

An *unconfined aquifer* is an aquifer that has the water table as its upper boundary, where the hydraulic head of the aquifer at the water table is equal to the atmospheric pressure (Kresic, 2007). An aquifer that is bound above by a confining bed is referred to as a *confined aquifer*. The potentiometric surface is the imaginary surface that the groundwater would rise to if not restricted in a confined aquifer, as is illustrated in Figure 2. The pressure of the groundwater in confined aquifers is usually higher than atmospheric pressure.

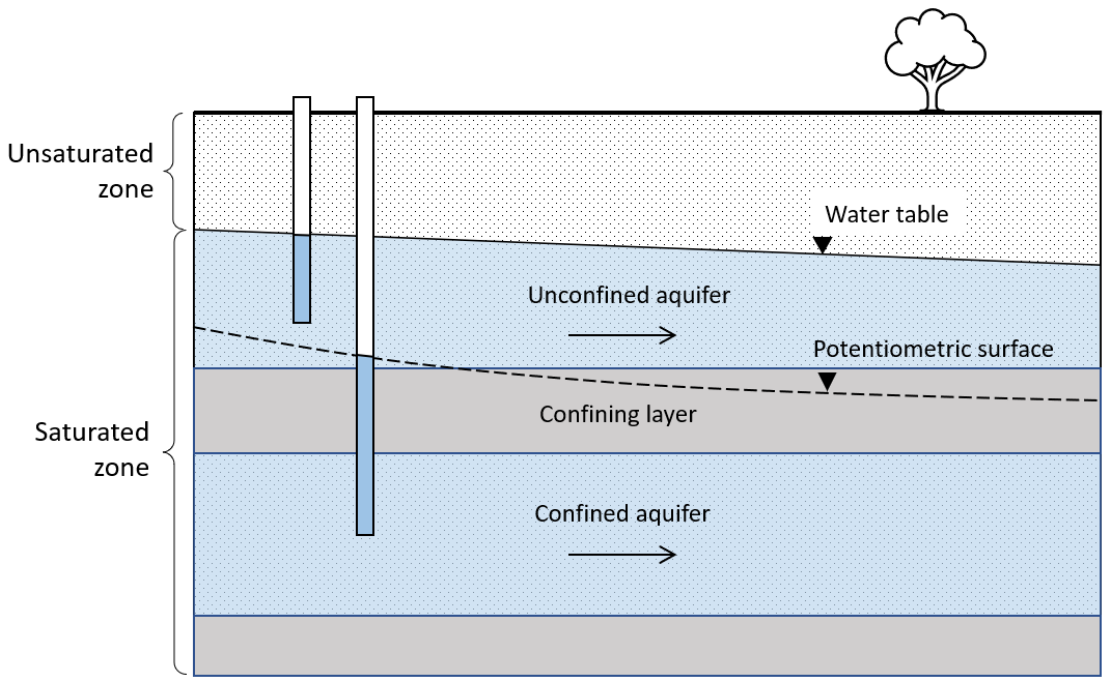

Figure 2. Cross-section of an unconfined and confined aquifer, separated by a confining unit. Based on Cohen & Cherry (2020).

2.2 Groundwater flow

Darcy's law is the fundamental equation that describes the flow through a porous media. Darcy's law defines the relationship between groundwater flow, hydraulic conductivity and hydraulic head gradient (Woessner & Poeter, 2020) which is presented in equation (1),

$$Q = -KA\frac{dh}{dl} \tag{1}$$

where Q is the flow (m^3/s), K is the hydraulic conductivity (m/s), A is the cross-sectional area (m^2) and $\frac{dh}{dl}$ is the gradient of the hydraulic head (-). Hydraulic conductivity describes the ease of which a fluid passes through a porous material and has the unit m/s, however, it is not a velocity. The hydraulic conductivity is dependent on both the material properties of the aquifer (the intrinsic permeability K_i) and the properties of water (density, viscosity, and temperature). Freeze & Cherry (1979) presents the relationship between the hydraulic conductivity and the intrinsic permeability in equation (2),

$$K = K_i\frac{g\rho}{\mu} \tag{2}$$

where K is the hydraulic conductivity (m/s), K_i the intrinsic permeability (m^2), g the acceleration of gravity (m/s^2), ρ the density of the fluid (kg/m^2) and μ the viscosity of the fluid (kg/m·s). The intrinsic permeability (often referred to as just permeability) is a constant that describes the influence of the material properties that have an effect on the flow (Woessner & Poeter, 2020).

2.2.1 Spatial and directional variation of hydraulic conductivity

The value of hydraulic conductivity ranges over many orders of magnitude in geologic materials, corresponding to an extreme variety in groundwater flow velocities (Fitts, 2012). Subsurface geologic materials have an irregular and complex distribution of

hydraulic conductivity. Thus, two important concepts that has to be discussed in regard to hydraulic conductivity are anisotropy and heterogeneity, illustrated in Figure 3.

Variations of the hydraulic conductivity with direction, means that the material is considered anisotropic. A geologic formation is considered isotropic if the hydraulic conductivity at a point in the formation is the same regardless of direction (K_x=K_y=K_z). No geologic material is perfectly isotropic, however it may be deemed a reasonable assumption due to the simplifications it produces in calculations (Fitts, 2012). In most sediments (and sedimentary rock) the hydraulic conductivity in the horizontal direction can be considered the same (K_x=K_y), however the vertical hydraulic conductivity (K_z) is usually slightly lower (Woessner & Poeter, 2020). This is due to depositional processes, where micro-layering is produced, giving rise to anisotropy in the vertical direction. The horizontal flow is thereby often dominant Hölting & Coldwey (2019).

Looking at the larger scale, the concepts of homogeneity and heterogeneity can be used to describe a formation or material. In general, the hydraulic conductivity will vary with space within a geologic structure, which is referred to as heterogeneity. Freeze & Cherry (1979) state that if the hydraulic conductivity is dependent on the location within the geologic formation, the formation is heterogeneous; if it is independent on the location, the formation is considered homogeneous.

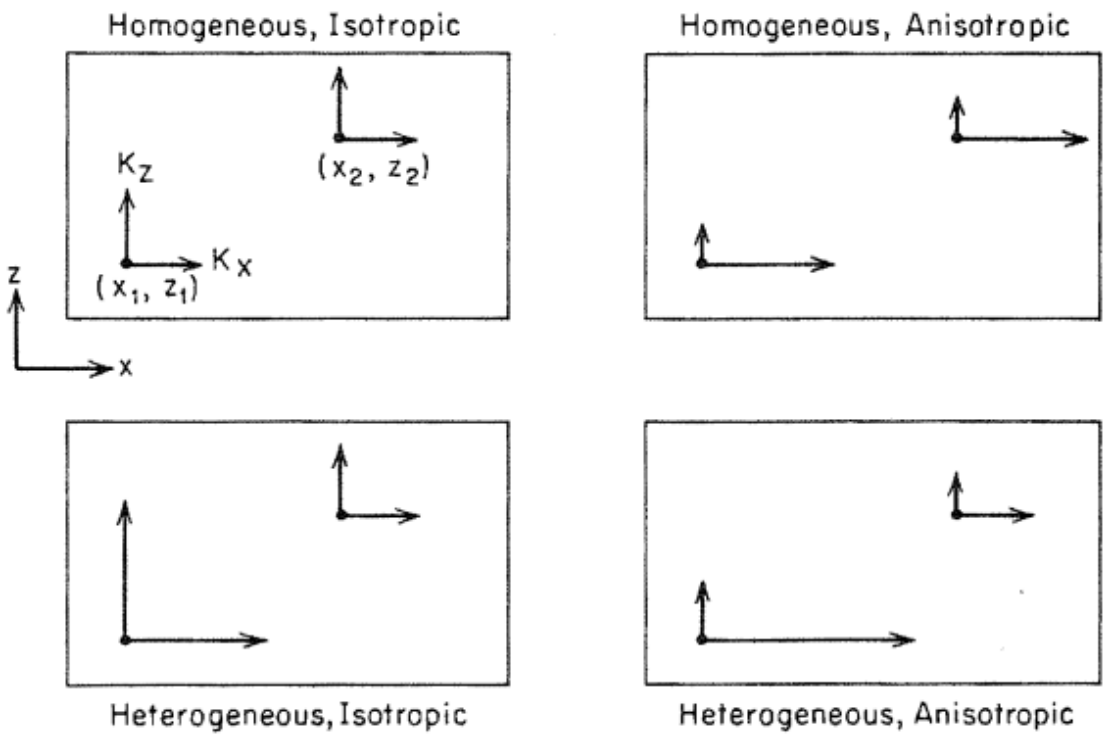

Figure 3. Illustration of the concepts of anisotropy and heterogeneity (Freeze & Cherry, 1979). The two points are located within a coordinate system in a geologic formation, with the length of the arrows indicating the size of the hydraulic conductivity along the principal axes.

2.2.2 Effective porosity

Porosity refers to the ratio of the volume of the pore spaces to the total volume of a porous media. As pointed out by Anderson et al. (2015) the concept of effective porosity is relatively simple, however it is hard to define quantitatively. Some of the

pores of a medium are not part of the flow path of the groundwater and are therefore not contributing to the transmission or storage of groundwater. These are pores that are not interconnected, such as pores that form "dead ends" or have such small connection so that water cannot flow through them (Woessner & Poeter, 2020). Effective porosity (n_e) can be defined according to equation (3),

$$n_e = \frac{V_I}{V_T} \tag{3}$$

as the ratio of the interconnected pore volume (V_I) to the total pore volume (V_T). As Fetter (1993) defines it, effective porosity is the porosity through which groundwater flow occurs. The complexity of the evaluation effective porosity is discussed in detailed by Stephens et al. (1998). Ideally, the effective porosity would be estimated from field tests, however this is not commonly done. Instead of using derivation from field tests or lab testing, the effective porosity is often estimated based on experience or literature, especially for modelling where the effective porosity can be estimated from model calibration.

2.2.3 Water balance

The water balance of a hydrogeologic system is based on the principle of mass conservation. The law of water balance states that the inflow to any groundwater system is equal to the outflow plus any change in storage during a specific time period, which is accompanied by change in head, according to equation (4):

$$Inflow = Outflow \pm \Delta Storage \tag{4}$$

The *inflow* component in equation (4) typically include recharge from precipitation and inflows from other sources such as artificial recharge or from hydrogeologic units outside the system boundaries (Anderson et al., 2015). The *outflow* component includes processes such as evapotranspiration and other types of losses of groundwater from the system, such as pumping from wells. Figure 4 illustrates the water balance of a hydrogeologic system without any interaction with surface water bodies or artificial infiltration or pumping.

The renewal of groundwater is highly dependent on groundwater recharge, which can be defined as processes that lead to an increase of stored water in the form of groundwater (Barthel et al., 2021). Groundwater recharge is highly complex, influenced by numerous factors and interactions, each with their own dynamic. Groundwater recharge processes also vary depending on location and with the seasons, as they are highly dependent on site-specific factors such as topography, land use, vegetation, geology, and climate. Thereby groundwater recharge cannot be directly measured, and instead has to be evaluated indirectly through connected processes and properties (Barthel et al., 2021). The presence of urban infrastructure also has an effect on the groundwater recharge processes, further complicating quantification.

A range of methods of estimation of groundwater recharge exist. Barthel et al. (2021) present the most common methods for estimation of groundwater recharge that are used in Sweden. As the infiltration capacity of the soils in Sweden are normally considered to be good, and percolation and infiltration of recharge are considered the dominant groundwater recharge processes, a common approach is to assume the groundwater recharge to be equal to the net precipitation (precipitation minus the evapotranspiration). As the infiltration capacity of the soil is considered greater than the precipitation intensity, all precipitation in the groundwater basin will infiltrate to the groundwater (Rodhe et al., 2006).

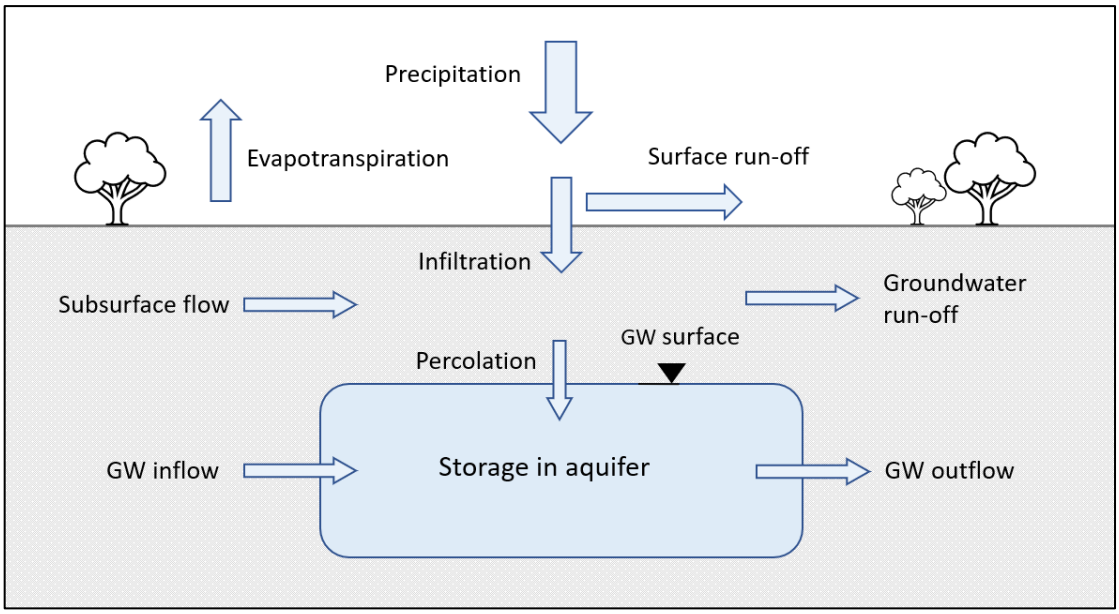

Figure 4. A conceptual hydrogeological water balance.

2.3 Groundwater flow modelling

Two basic principles form the basis of all models of groundwater flow; the first one is conservation of mass, according to which water cannot be destroyed or created, and the second one is Darcy's law (Anderson et al., 2015). The mathematical model of groundwater flow consists of a governing equation, boundary conditions, and initial conditions. The governing equation describes the processes within the problem domain, and the boundary conditions define flow into and out of the domain (Anderson et al., 2015). The initial conditions specify values of the dependent variable (head) at the start of the simulation. The three-dimensional transient groundwater flow in heterogeneous and anisotropic conditions is described by the governing (differential) equation (5),

$$\frac{\partial}{\partial x}\left(K_{xx}\frac{\partial h}{\partial x}\right)+\frac{\partial}{\partial y}\left(K_{yy}\frac{\partial h}{\partial y}\right)+\frac{\partial}{\partial z}\left(K_{zz}\frac{\partial h}{\partial z}\right)+Q_s'=S_s\frac{\partial h}{\partial t} \tag{5}$$

where K_{xx}, K_{yy}, and K_{zz} denotes the hydraulic conductivity along the coordinate axes, h the hydraulic head (variable of interest), Q_s' the volumetric flux per unit volume representing sources and sinks of water, S_s the specific storage and t the time.

There are generally three types of boundary conditions that are applied in groundwater modelling: specified head boundary (Neumann condition), specified flow boundary (Dirichlet condition) and head-dependent boundary (Cauchy condition) (Anderson et al., 2015). The head-dependent boundary relates a boundary head to a boundary flow and is sometimes referred to as a mixed condition. A *constant head boundary* is a version of the specified head boundary where the head is set to the same value along the whole boundary. A *no-flow boundary* is a special case of specified flow where the flow through the boundary is set to zero.

The mathematical model of groundwater flow can be solved both analytically and numerically. Analytical solutions are numerically exact and continuous both in space and time but require simplifications to be able to produce a closed-form solution and are thereby limited to simple systems (Anderson et al., 2015). Numerical models use an approximation of the governing equation in order to calculate the groundwater head at discrete points. Thereby numerical models can solve the three-dimensional transient

governing equation under complex (heterogenous and anisotropic) initial conditions and boundary conditions, as often is the case for practical groundwater problems.

2.3.1 Finite-difference method

Two types of numerical methods are widely used in groundwater modelling: the finite-difference method (FDM) and the finite-element method (FEM). Of these, the FDM is most common due to it being more mathematically simpler. The principles of the FDM (as used in the groundwater flow model MODFLOW) are described in great detail by Harbaugh (2005). The model is discretized using a rectangular grid, forming blocks referred to as *cells*. The location of each cell is described by an indexing system, where the index *i* denotes rows, *j* denotes columns and *k* denotes layers, see Figure 5. A node is placed within each cell, which is the location at which the hydraulic head is calculated for. In addition to space, time is also needed to be discretized. Time is broken down into *time steps*, and for each time step the head is calculated. An equation is set up for each cell (with a variable head), forming a system of equations that form an approximation of the mathematical model of groundwater flow (equation 5). The equations are solved simultaneously for the distribution of the hydraulic heads at time t=1 (Harbaugh, 2005). At each time step, this set of equations is reformulated, so that a new system of equations is created. The unknows of this new system is the distribution of heads at time t=2. This set of equations is solved, the equations are reformulated, and the process repeats itself again.

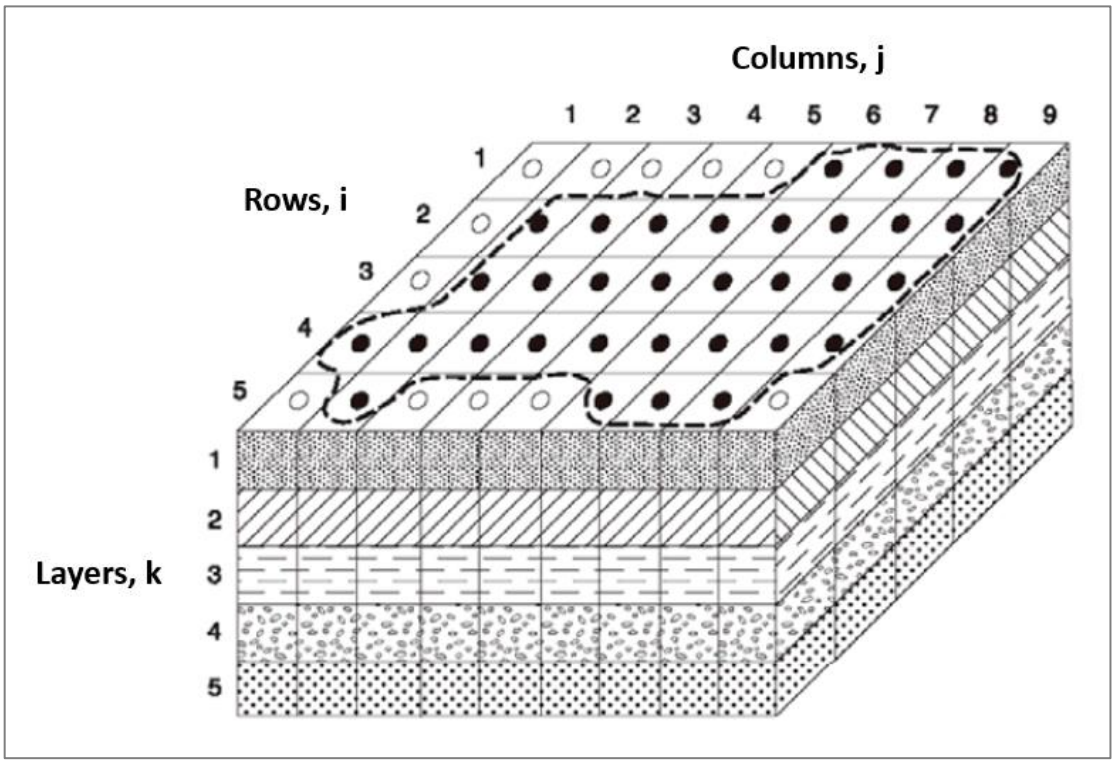

Figure 5. Discretization of an aquifer using the finite-difference method. The dotted line represents the boundary of the aquifer. Active cells are denoted by a black dot, and inactive cells by a white dot. Modified from Harbaugh (2005).

The set of equations created for each time step is solved iteratively, meaning the calculation is repeated and refined until a (approximate) solution is deemed to have been found (Harbaugh, 2005). Each iteration of the calculations produces an interim head value. As the derived solution of each iteration of calculations gets closer to a solution that would satisfy the set of equations, the change between these interim head values becomes smaller and smaller. The iterative process is stopped when the solution is deemed to have converged. The judgement of when the solution has converged is highly subjective. Therefore, a closure criterion is defined, that specifies the change between the computed heads at which the iterations are to be stopped. A number of the maximum number of iterations is typically also specified.

2.3.2 Conceptual site model

The development of a hydrogeological conceptual site model (CSM) is essential in modelling, as it provides a framework for the development of the numerical model. A CSM can be defined in a variety of ways. According to Kresic & Mikszewski (2012) a hydrogeological CSM is a description of factors that govern and/or contribute to the movement of groundwater. Anderson et al. (2015) defines a hydrogeological CSM as "a qualitative representation of a groundwater system that conforms to hydrogeological principles and is based on geological, geophysical, hydrological, hydrogeochemical, and other ancillary information". The CSM aims to summarize all the available information of the hydrogeological system.

The CSM represents a simplification of a complex reality as it is inevitably based on assumptions and a qualitative interpretation of the conditions at the site. As is stated by Enemark et al. (2019), the conceptual model is considered a major source of uncertainty in numerical groundwater modelling.

2.3.3 Calibration

The groundwater model only simulates a portion of a complex natural system. The model is always a simplification, and the true conditions are unknown. The performance of the model, and therefore the conceptual understanding of the nature of the hydrogeological system and its surroundings, is therefore assessed through comparison of output to field observations (Anderson et al., 2015).

Calibration is used to solve the inverse problem that a groundwater model comprises, with the aim of identifying a set of unknowns (input parameters) that produce an output of hydraulic heads and fluxes that accurately corresponds to the field observations (Anderson et al., 2015). This means that the hydrogeological framework, hydraulic properties, and boundary conditions of the model are continuously evaluated and refined (within a deemed reasonable interval) as a part of a series of successive runs of the model. This process is therefore highly subjective, dependent on the perception and of the modeller. There is also the problem of non-uniqueness, as several different sets of model inputs can produce nearly identical model outputs (Middlemis et al., 2001).

During calibration, the degree of correspondence between output of the model and observations is evaluated through graphical comparison and the use of statistical tools. Model error can be expressed in a range of ways, of which many are based on hydraulic head residuals. The residual hydraulic head (r_i) at a certain point (i) is defined according to equation (6),

$$r_i = X_{calc} - X_{obs} \tag{6}$$

as the difference between the computed (X_{calc}) and the observed hydraulic head (X_{obs}) (Waterloo Hydrogeologic, 2022). The maximum and minimum residual refers to the largest and smallest difference in hydraulic head. The *residual mean* (or mean error) is the average residual value. As both positive and negative values are included in the mean, the residuals may cancel out each other, producing a mean close to zero (Anderson & Woessner, 2015). The *mean absolute error* (MAE) is the average of the absolute value of the residuals, thus giving a better indicator of the model fit than the residual mean (Waterloo Hydrogeologic, 2022).

The ASTM (2016) categorizes model parameters into four Sensitivity Types:

> I – Variation of an input parameter cause insignificant changes in the calibration performance of the model and the model output.
>
> II – Variations in the parameter causes significant changes in the calibration performance, but insignificant changes in the model output.
>
> III – Variations in the parameter cause significant changes in both the calibration performance and the model output.
>
> IV – Variations in the parameter causes insignificant changes in the calibration performance, but significant changes in the model output.

A parameter of Sensitivity Type I or 2 is of little interest as the variation in value has little effect on the model (ASTM, 2016). The same is true for a parameter with Sensitivity Type 3, as the change in the parameter causes the model to become uncalibrated. Thereof, parameters of Sensitivity Type 4 are of the highest concern, as variation in a parameter that has a clear impact on the results of the model, while still being considered calibrated.

2.4 Chlorinated ethenes

Tetrachloroethene (PCE) and trichloroethene (TCE) have been used extensively in dry cleaning and for degreasing because of their excellent solvent properties. They are often referred to under the collective name chlorinated solvents, which constitutes a large group of organic solvents that contain chlorine atoms in their molecular structure (Cwiertny & Scherer, 2010). PCE and TCE have been manufactured and used in a variety of industries since 1920s, and their presence in groundwater have been known since the 1950s (Pankow & Cherry, 1996). Environmental concerns were first raised in the 1970s as the issue of chlorinated haloforms in chlorinated drinking water was raised. However, these chemicals were not recognized as significant groundwater pollutants until the late 1980s.

The physical and chemical properties of chlorinated ethenes make them particularly likely of causing extensive contamination of groundwater resources (Pankow & Cherry, 1996). Chlorinated ethenes have a limited solubility in water and a high density relative to water and are therefore categorized as dense non-aqueous phase liquids (DNAPLs). According to the IARC (2014) TCE is considered carcinogenic (group 1) and PCE is considered probably carcinogenic to humans (group 2A).

2.4.1 Degradation process

PCE and TCE can undergo both abiotic and biotic (microbial) degradation in the subsurface through a variety of processes. The degradation processes are highly dependent on geochemical and microbiological conditions at the location, as well as co-contaminants present (Tobiszewski & Namieśnik, 2012). Reductive dechlorination

is the principal biodegradation process for highly chlorinated ethenes and can take place under anoxic conditions. Each chloride atom is removed and replaced by a hydrogen atom in a stepwise procedure, during which PCE will form the intermediates TCE, DCE isomers and vinyl chloride (Leeson et al., 2013) according to the degradation pathway illustrated in Figure 6. Several bacterial species have been found to have the ability to reductively dechlorinate chlorinated ethenes, however the process is often incomplete (Tobiszewski & Namieśnik, 2012). This may lead to the accumulation of degradation products in an aquifer. Vinyl chloride, one of the intermediates of the process, is considered a known carcinogen (category 1A) according to the IARC (2008). The theoretical end product of the degradation process is ethene, which is a non-toxic substance.

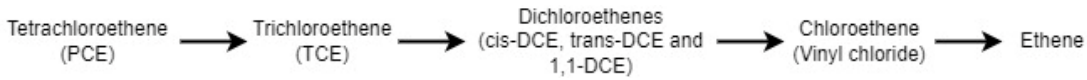

Figure 6. Degradation pathway of PCE. Based on Sun et al. (2004).

2.4.2 Spatial spreading of DNAPLs

DNAPLs have a potential to spread substantially in the subsurface due to their relatively low solubility, high density, and low viscosity. If a sufficiently large quantity of DNAPL is spilled, it will be able to travel through the unsaturated zone and penetrate the water table, as illustrated in Figure 7. The movement of DNAPLs in the saturated zone is governed by heterogeneities and the structure of the media (Pankow & Cherry, 1996), as it will spread through preferential pathways. Even subtle heterogeneities can have a direct effect on the spreading pathway, making the movement of DNAPLs in the saturated zone highly unpredictable.

In the subsurface, the DNAPLs will distribute into different physical states referred to as phases; air, soil, water, and free phase (Puigserver et al., 2022). DNAPL may occur as a vapour plume (air phase) in the unsaturated zone. In the saturated zone, the DNAPL will travel laterally in the subsurface until it encounters layer with significantly lower permeability where it will gather or travel laterally along the layer. At these locations, DNAPLs might be present in free phase, meaning a continuous body of significant volume that occupies all the pore spaces of the material (Kresic, 2007). DNAPL may also spread into the matrix of the low-permeable media through diffusion. Other than free-phase, residual DNAPL might be found in the subsurface, referring to drops and ganglia in pore spaces that has been disconnected from the continuous DNAPL body by water (Kresic, 2007; Pankow & Cherry, 1996). The DNAPL will slowly dissolve to the groundwater, forming a plume that travels with the groundwater flow (Pankow & Cherry, 1996), as shown in Figure 7. The free-phase, or residual DNAPL can act as a potential source of dissolved contaminants in the groundwater over a long time period.

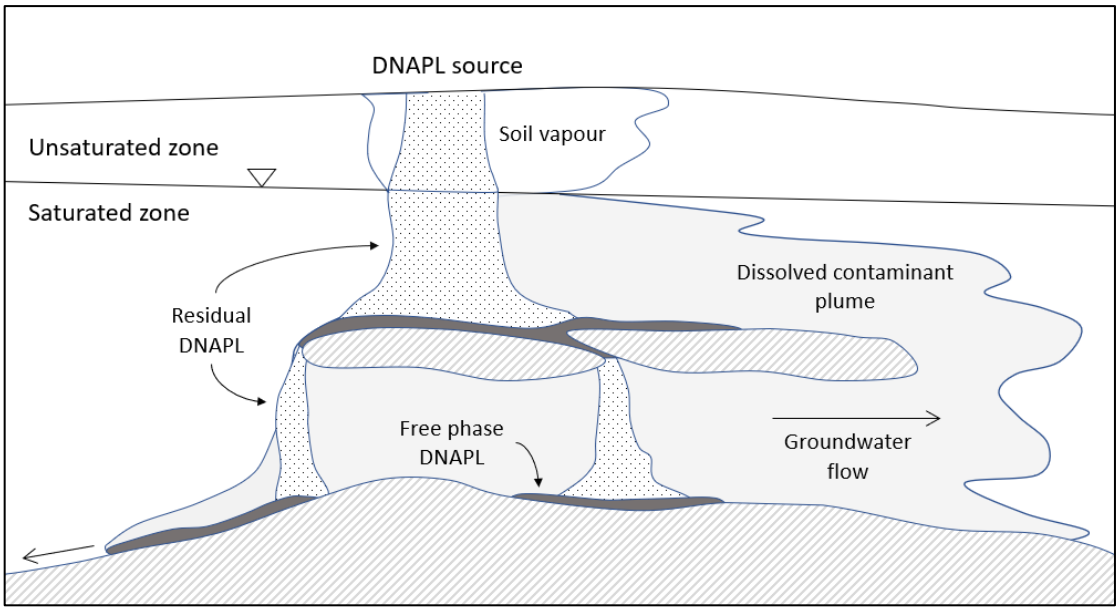

Figure 7. The transport and spreading of DNAPLs in the subsurface. Based on figure by Kresic (2007).

2.4.3 Solute transport

The two driving processes in the transport of a dissolved substance in groundwater are advection and dispersion. Advective flow is the movement of a dissolved substances through the movement of the fluid it is dissolved in, and it refers to the movement of the bulk of the dissolved substance (Fitts, 2012). In the subsurface, the average linear groundwater velocity, v_L describes the rate of the flow that crosses the pore spaces of a unit cross-section (Fetter, 1993), and is defined as equation (7),

$$v_L = \frac{q}{n_{ef}} = \frac{1}{n_{ef}} K \frac{dh}{dl} \tag{7}$$

where n_{ef} is the effective porosity of the porous material (see Section 2.2.2), and q is the specific discharge (m/s) which is equal to the $K$is hydraulic conductivity (m/s) times the $\frac{dh}{dl}$ is the hydraulic gradient (-). The specific discharge is another way of presenting Darcy's equation, describing the discharge per unit area of a cross-section. The average liner groundwater velocity thereby describes the average velocity that a solute would have in in groundwater if not reaction with solids (sorption) or subject to chemical reactions (Fitts, 2012).

Contaminant movement is also affected by the process of dispersion, where a solute move from an area with high concentration toward an area with a lower concentration (Fetter, 1993), causing the solute to spread and decrease in concentration. Dispersion is caused by the processes of molecular diffusion and mechanical dispersion, however in flowing groundwater these processes cannot be separated. Mechanical dispersion refers to the process in which solutes are through microscopic variations in velocity mechanically mixed during advective transport.

3 Conceptual site model

This chapter presents the investigated site and the developed conceptual site model (CSM). The CSM is divided into several sections, each covering the geology, hydrogeology, topography and hydrology, and contamination of soil and groundwater at the site.

3.1 The former dry-cleaning facility

The thesis is focused on the case study of the former dry-cleaning facility located in Stockholm County. The facility was active between the years 1946 and 1969 and has caused extensive contamination of chlorinated solvents in mainly soil and groundwater (WSP, 2019a). The former property and building of the dry-cleaning facility are shown in Figure 8. The area has gone through substantial redevelopment since the activities of the dry cleaner ended in 1969. Aerial photos from 1971 show that the building of the dry-cleaning service had been demolished and that the today present dual carriageway was under construction (WSP, 2019a). Construction of a light-rail line crossing the former property and building of the dry-cleaning facility was started in 2009. Apartment buildings are located east of the former property of the dry-cleaning facility. In addition, the area is today covered by a wide range of sub-surface infrastructure, such as electricity cables, district heating and stormwater- and sewage pipes and tunnels. The site has been under investigation by WSP since 2017. Extensive sampling and analysis of a wide range of media has been performed. Other than soil and groundwater, sampling of soil gas, tree cores, indoor air in adjacent residential buildings, as well as air and water from storm water- and sewage pipes (superficial pipes and tunnels) has been performed (WSP, 2023a; WSP 2023b).

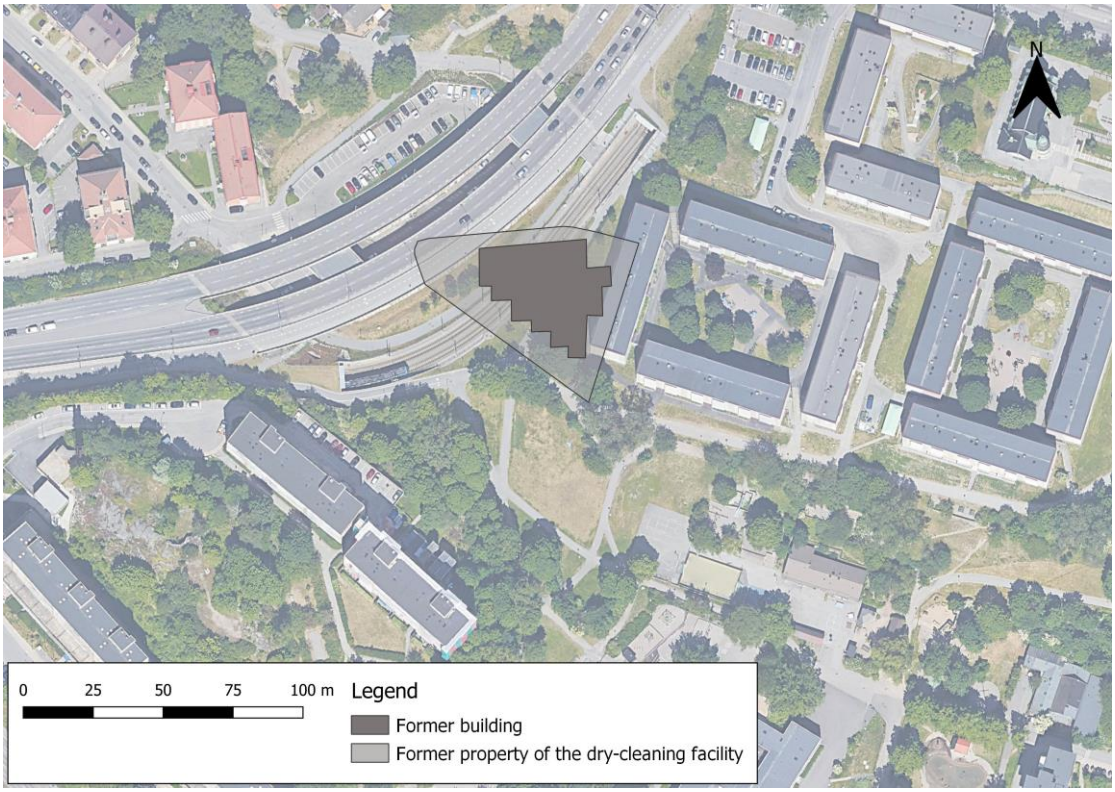

Figure 8. The former location of the building and property of the dry-cleaning facility.

3.2 Geology

Figure 9 shows a soil map of the area. The studied area is located below the highest shoreline from the latest glaciation and is dominated by deep bedrock valleys, filled with clay. A glaciofluvial esker, containing a separate aquifer, is located along the bay. The aquifer is part of a 60 km long esker that stretches northwest through several municipalities and provinces of Sweden (Eriksson, 2009). A detailed map of the esker is found in Appendix A. The glaciofluvial esker was formed during the retreat of the latest glacier around 11 700 years ago (Andréasson, 2015) in the north-north-western direction and forms a range of hills through the area composed of sand with a core of gravel. As the glacier continued to recede, the region found itself situated below sea level of what would form the Baltic Sea. The ridges of the esker were exposed to forces of sea currents and waves, reworking and redepositing the glaciofluvial material and filling the bedrock valleys surrounding the esker with postglacial sand. At the later stages and after the glacial period, the area of Uppland was located below sea level during several different stages of the Baltic Sea, thus making the deposition of glacial and postglacial clay possible, filling the valleys (Andréasson, 2015). With the postglacial land uplift, the area was slowly lifted above sea level. As can be seen in Figure 9, the area is to a large extent covered by a layer of backfilled material with unknown origin. This material has not been formed through natural processes at the site, and has a varied composition, containing sand, gravel and occasionally clay.

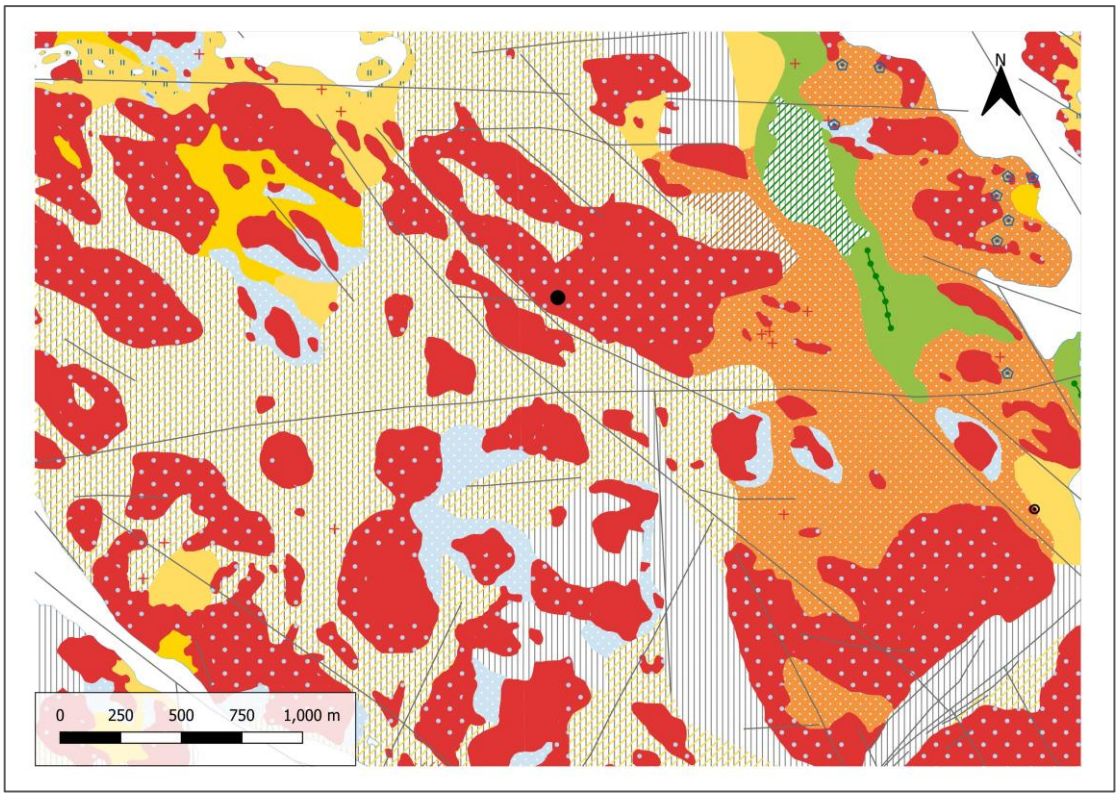

Figure 9. *Map over soil types in the study area (1:25 000 – 1:1:100 000) created in GIS from WMS data (SGU, n.d.-a, SGU, n.d.-b). Bedrock is indicated by red, with blue dots indicating a surface layer of glacial till. Grey stripes indicate a base layer of filling material. Yellow indicates glacial clay (darker yellow) and postglacial clay (lighter yellow), with yellow stripes indicating an underlying layer of postglacial clay. Orange indicates postglacial sand. Green indicates glaciofluvial sediment. Blue with white dots indicates sandy glacial till. Weak zones of the bedrock are indicated by grey lines.*

Figure 9 indicates bedrock with a thin or discontinuous surface layer of glacial till at the location of the former dry-cleaner. Investigations of the soil stratigraphy around the former dry-cleaning facility, however, give a different result than the SGU soil map; the bedrock depression (with filling material and clay) that stretches southeast-northwest along a weak zone, extend to the location of the dry cleaner. Based on probing and soil sampling at the site (WSP, 2023a) three stratigraphic layers can be recognized in the immediate area of the former dry-cleaning facility:

- filling material, between 1-4 m thick (modelled as 2.5 m);
- clay (with some occurrences of silt), varying thickness between 3-6 m;
- fine sand (with coarser sand on top of bedrock), varying thickness across the area.

The bedrock in the area consists of crystalline rock, with rock types from the Svecofennian orogeny (Persson, 1998). The structurally most important directions in the larger area are according to Persson (1998) east-west, west-northwest and northwest, which is in line with the SGU mapping of weak zones that stretch across the study area, see Figure 9. Notably, directly south (and west) of the former dry-cleaning facility, a weak zone stretches northwest towards the lake, coinciding with the buried bedrock valley.

3.3 Hydrogeology

An unconfined, discontinuous hydrogeological unit is found in the filling material in the area (WSP, 2023b). A deeper aquifer is found in the sand layer below the clay, which acts as a confining unit. The approximate extent of the confined aquifer and the estimated flow direction based on previous hydrogeological investigations is presented in Appendix B. Thus, three hydrogeologic units can be found at the site; an upper unconfined aquifer, a confined aquifer as well as groundwater in the bedrock (WSP, 2023b). The conceptual hydrostratigraphy of the investigated area is presented in Figure 10.

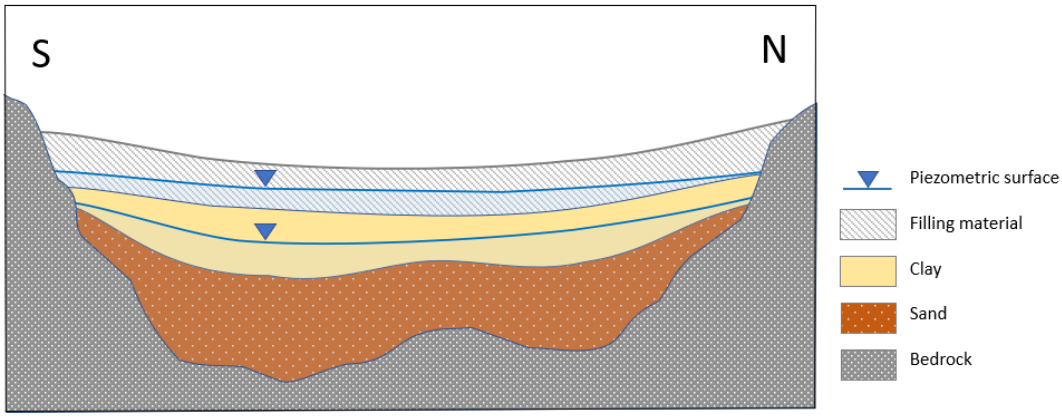

Figure 10. Conceptual illustration of a hydrostratigraphic cross-section at the location of the former dry-cleaning facility.

Measurements and interpolation of groundwater head in the immediate area of the former dry-cleaning facility show two separate hydraulic gradients present at the site, one towards west and one towards south-east, see Figure 11. A groundwater divide is hypothesized to be located at the location of the former building, its precise placement unknown and deemed movable with variations in the system (WSP, 2023b).

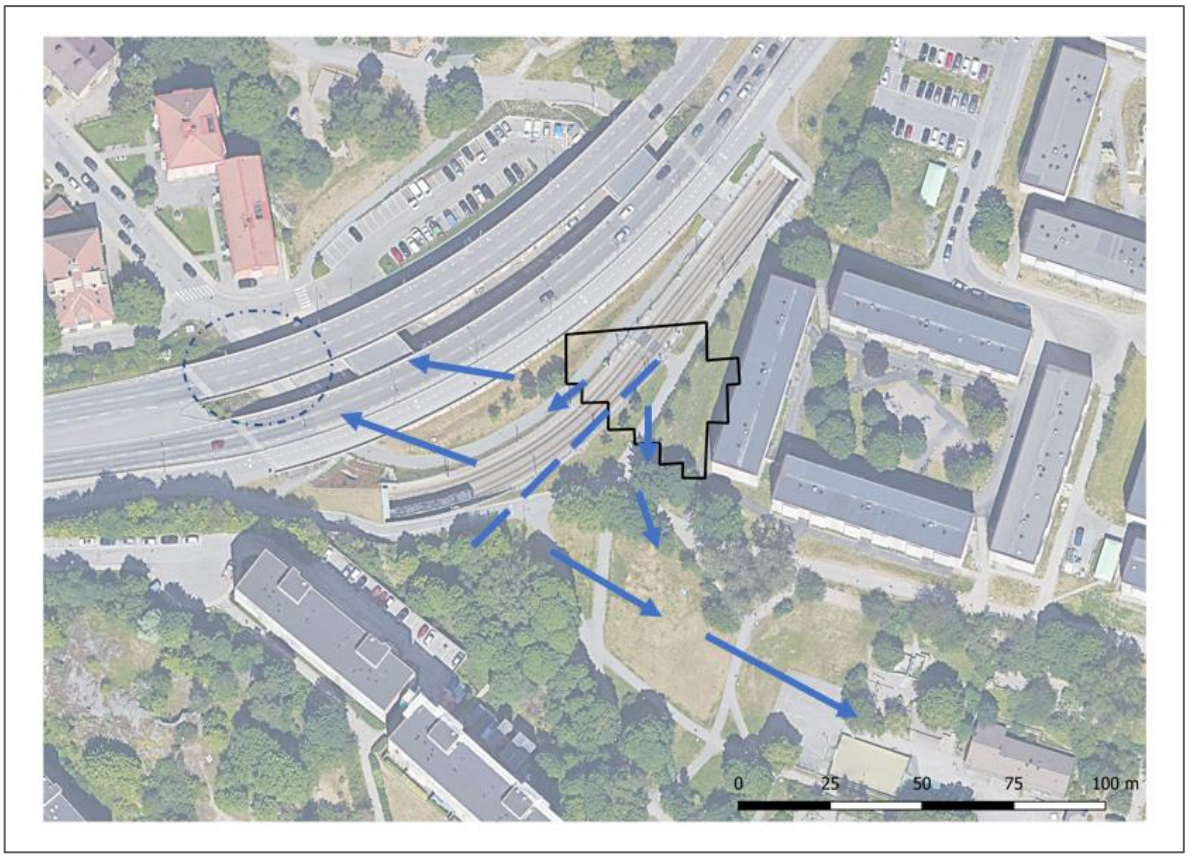

Figure 11. Groundwater flow (blue arrows) and the approximate placement of the groundwater divide (dashed blue line) in relation to the former building of the dry-cleaning facility (in black).

3.3.1 Hydraulic properties of soil materials

Limited data exist on the hydraulic properties of the geologic material at the investigated site. The filling material, that constitutes the upper unconfined aquifer, contains a variety of different geologic and anthropogenic materials, with large spatial variations (heterogeneities). The filling material is described as containing sand and gravel, and occasionally clay (WSP, 2023b). Probing performed adjacent to the former dry-cleaning facility found boulders across the filling material (WSP, 2023a). The permeability of the filling material is estimated to be moderate. Due to the uncertainties the filling material is modelled as isotropic.

The top of the clay layer is composed of drier clay which gradually becomes looser (WSP, 2023a). Probing show that thin layers of silt have been found in the clay at some sites. The distinction between the clay and the sand layer is not very clear at certain locations. The clay is deemed to behave as a confining layer, with significantly lower hydraulic conductivity than the adjacent layers. The layers of clay and sand are conceptualized as anisotropic, meaning that the hydraulic conductivity is the same in the (horizontal) x- and y-direction, however the hydraulic conductivity is assumed to be three times lower in the vertical direction, giving an anisotropy ratio of 1:3. This is due to the depositional characteristics of the material.

The sand layer is found to have an increasing grain size, from fine sand below the clay to coarse sand close to the bedrock (WSP, 2023b). Estimations of the hydraulic conductivity of the sand that constitutes the confined aquifer are presented by WSP (2019b) based on three slug tests performed at a site located west of the former dry-

cleaning facility. The results give an estimated hydraulic conductivity between $1.04 * 10^{-5}$and $3.46 * 10^{-4}$ m/s indicating moderate permeability, and sand, possibly silty sand (Freeze & Cherry, 1979), which coincides with the description of the material from performed probing in the area surrounding the former dry-cleaning facility. An anisotropy ratio of 1:3 is assumed (i.e., the same as for clay). As the tests are performed at a separate location, they cannot be seen as representative of the area of interest for modelling. While this gives an indication of the hydraulic properties of the sand, calibration of the parameter is needed.

The effective porosity of the soil materials and the bedrock are estimated based on ranges of values presented by Woessner & Poeter (2020) and Hölting & Coldewey (2019). The estimated hydrogeologic properties of the soil materials that constitute the hydrogeologic units are presented in Table 1.

Table 1. Estimated hydraulic conductivity and effective porosity of the soil materials.

Material	K_x=K_y (m/s)	K_z (m/s)	Effective porosity (-)
Filling material	1.0E-05	1.0E-5	0.10
Clay	1.0E-09	3.3E-10	0.03
Sand	1.8E-04	6.1E-05	0.25

The esker is described as containing coarse glaciofluvial sediments with a high hydraulic conductivity (Eriksson, 2009). The aquifer is at least 20 m deep and is according to the SGU (n.d.-a) composed of gravel, thereby a hydraulic conductivity of $5*10^{-3}$ m/s is estimated for the material.

3.3.2 Evaluation of hydraulic conductivity of the bedrock

The hydraulic conductivity of the bedrock decreases with depth, thereby the hydraulic conductivity of the rock has been evaluated for seven different layers. The hydraulic properties of the rock have been estimated based on an analysis of data from the open well archive by the Geological Survey of Sweden (SGU, 2022).

Data for wells within an 3,8 km radius from the site of the former dry cleaner were selected. Data points without any coordinates, water quantity, or pipe length have been excluded from the data set. Data points with a total depth below 20 meters have also excluded. For data points with a water quantity of 0, the water quantity was set to 5. The data set contained many duplicate values. Duplicates of data points with respect to water quantity, total depth and depth of the borehole were identified and deleted. The hydraulic conductivity, K (m/s) of the crystalline rock was calculated for 612 wells according to equation (8) by Ryd (2017) as recommended by the SGU (2019a),

$$K = \frac{0.076 * Q^{1.026}}{L} \tag{8}$$

where Q is the well capacity (m^3/d) and L is the length of borehole that is drilled in rock (m).

The frequency of different depths (L) of the data set was investigated. Based on the distribution of the depth of the data points, the data is separated into three populations: 100 m, 170 m, and 250 m. The hydraulic conductivity of the bedrock is assumed to be log-normally distributed, and log-normal distributions are fitted for each interval. The

effective hydraulic conductivity in large scale, K_{3D} was thereafter derived for each intervals using equation (9) by Gustafson (2009),

$$K_{3D} = K_g * e^{\sigma_{lnK}{}^2/6} \tag{9}$$

where K_g is the geometric mean of the fitted lognormal-distribution and σ_{lnK} is the log-standard deviation of the fitted distribution. The hydraulic conductivity of the bedrock is assumed to decrease with depth according to equation (10) from Naturvårdsverket (1997),

$$K = C * d^L = 6{,}0 * 10^{-4} * d^{-2} \tag{10}$$

where C is a constant representing the trend of the shallow rock, L is a constant describing the trend for the decrease by depth, and d is the vertical depth (m). The constants C and L have been determined through fitting of summarized transmissivity in a developed experimental model that follows equation (10) against values of K_{3D} for the three depth ranges. This provides a representative depiction of the decreasing of the hydraulic conductivity within the studied area.

The bedrock is modelled as isotropic. The bedrock contains several weak zones which have increased hydraulic properties, K_{zone}. The cells within the weak zones were determined to be modelled as having a conductivity 7 times larger than adjacent cells in that layer. The evaluated rock layers and their hydraulic properties are presented in Table 2. Detailed calculations are presented in Appendix C.

A graph was thereafter fitted through the values of K_{3D} plotted against depth, representing the variations of the hydraulic conductivity with depth

Table 2. Evaluated hydraulic conductivity and estimated effective porosity of the rock and weak zones of each layer, with depth from rock surface, and thickness of each rock layer presented.

Material	Layer	Thickness (m)	K_x=K_y= K_z (m/s)	K_{zone} (m/s)	Effective porosity (-)
Superficial rock	Rock 1	10	1.9E-07	1.3E-06	0.05
	Rock 2	10	1.1E-07	7.7E-07	
	Rock 3	20	4.2E-07	2.9E-06	
Deep rock	Rock 4	30	1.2E-07	8.4E-07	
	Rock 5	40	5.7E-08	4.0E-07	
Very deep rock	Rock 6	60	2.5E-08	1.8E-07	
	Rock 7	60	1.2E-08	8.4E-08	

3.3.3 Installations and rock tunnels

The area contains a large variety of underground installations, such as drinking water pipes, stormwater pipes, sewers, telephone lines and gas pipes. The flow patterns of the unconnected hydrogeological unit of the filling material are thought to be highly affected by these underground installations in the area (WSP, 2023b).

The area also contains two tunnels drilled into the bedrock: a sewage tunnel and a stormwater tunnel. The two tunnels are located west of the former dry-cleaning facility, on the other side of the dual carriageway, stretching around 500 m north-east parallel

to each other. The sewage tunnel is reportedly 2200-2400 mm wide and located at +3.5 to +5.7 (RH2000) (WSP, 2023b). The stormwater tunnel is located at +3.9 m (RH2000). It is probable that the sewage tunnel was constructed in 1969, however the stormwater tunnel is believed to be older (WSP, 2023b). As no information of the volume of groundwater that drains into the two tunnels exist, the drain leakance, a coefficient that describes the head loss between the drain element and the surrounding groundwater system, needs to be estimated during model calibration. The head loss is caused by "converging flow patterns near the drain, the presence of foreign material around the drain, channel bed materials, the drain wall, and the degree to which the drainpipe openings may be blocked by chemical precipitates, plant roots, etc" (Waterloo Hydrogeologic, 2022).

3.3.4 Hydrology and groundwater recharge

Figure 12 presents the drainage basins of the investigated area. According to data from the SMHI (2016a) a main drainage divide stretches along the elevated bedrock area north of the dry-cleaner. The northern basin drains into the bay located west of the investigated area, while the southern basin drains into the southern bay.

The small lake is located approximately 1 km northwest of the former dry-cleaner. The lake is shallow and muddy, with an average depth of 2 m (Svensson, 2017). The lake is connected to the nearby eastern bay and is located at sea level according to data from SMHI (2020).

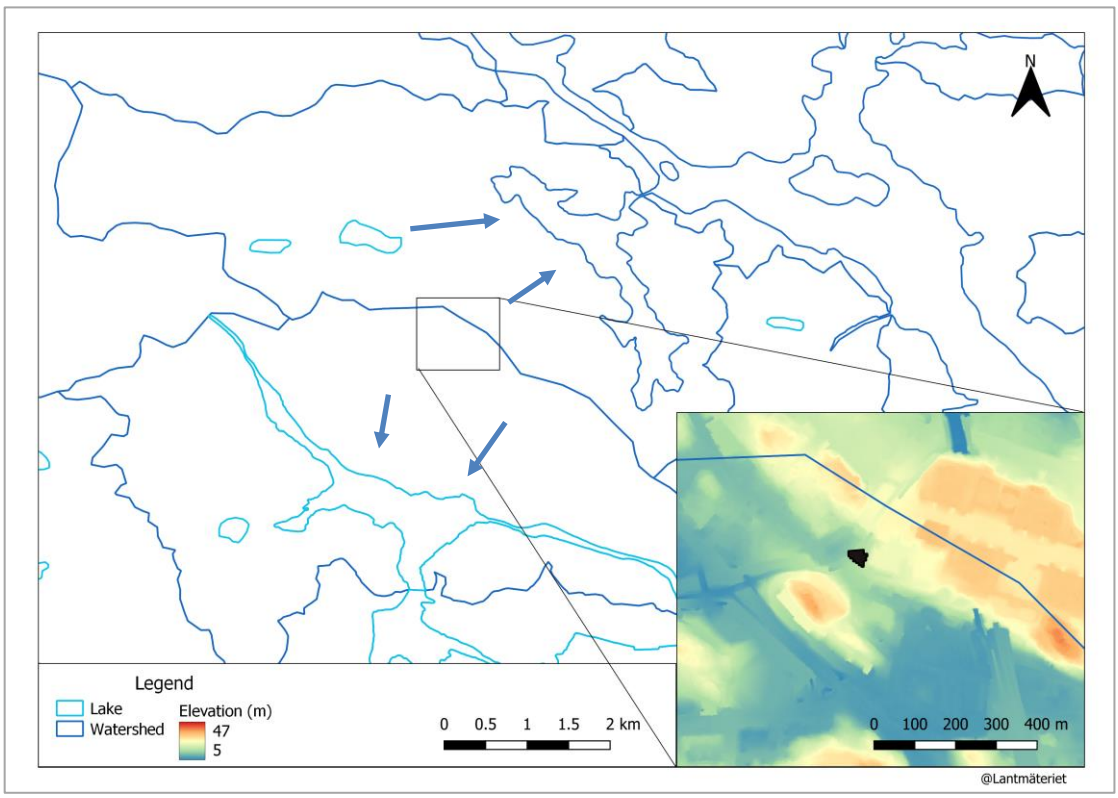

Figure 12. Map of nearby surface waters and watersheds, with the topography of the immediate area of the former dry-cleaning facility. Blue arrows indicate the flow of the surface water within the drainage basin. Map created using data from SMHI (2016a; 2016b) and Lantmäteriet.

The upper unconfined aquifer is recharged primarily through precipitation. Calculations of the water balance have been performed to estimate the recharge of the aquifer. The calculations are based on open data of the sum of precipitation for 24h from the Swedish Metrological Institute (SMHI, n.d.-a) and mean air temperature for 24h (SMHI, n.d.-b) the years 1961-2020 for the weather station *Observatoriekullen* in Stockholm. The sum of precipitation and mean of air temperature was calculated for each year. The mean precipitation and temperature per year over the time periods 1961-1990 and 1991-2020 was thereafter calculated. Using the calculated mean precipitation and mean temperature of the time periods, the evapotranspiration, ET (mm), was calculated using Turcs formula presented in equation (11),

$$ET = \frac{P}{\sqrt{0.9+\left[\frac{P}{L}\right]^2}} \tag{11}$$

where P is yearly average precipitation (mm) and L is calculated through the formula L=300 + 25 T + 0,05 T^3 (mm), where T is the mean air temperature (°C). The type and degree of vegetation has a large impact on ET rates (Eveborn et al., 2017). ET is generally found to be lower in urban areas compared to non-urban areas (Mazrooei et al., 2021), and thereby a reduction of 20% was applied to the ET in order to better represent conditions in an urban area.

The increase in temperature and change in precipitation due to climate change needs to be considered in the calculations. The corrected precipitation, P_k was calculated for each year between 1961-2050 based on data of precipitation (mean deviation) per year for the RCP 8.5 climate scenario (SMHI, n.d.-c) and a reference normal of Pk set to the mean of the time period 1961-1990. Similarly, the temperature was calculated for each year based on data of the mean deviation of the temperature for each year based on RCP 8.5 climate scenario (SMHI, n.d.-d) and a reference normal of the temperature set according to the mean temperature of the time period 1991-1990. The increase of precipitation and temperature between the mean of each time period was thereafter calculated. This increase was thereafter applied to the historical data in order to get an estimation of the precipitation and temperature for the future case of the period 2021-2050.

Next, in order to perform calculations of the water balance for all three time periods, a factor F is derived in order to describe the increase in precipitation and in calculated ET between the time periods. Finally, using calculated values for the time period 1961-1990 (P_k=539 mm and ET=294 mm) as the starting point, the water balance was performed for the three time periods using the relationship (12),

$$Q = P_k * \mathrm{F}_P - ET * F_{ET} \tag{12}$$

where Q is the recharge (mm/year), P_k is the corrected precipitation (mm/year), ET is evapotranspiration (mm/year), and F the factors of increase between the time periods. Table 3 presents the calculated water balance for the three different time periods based on data from SMHI. Complete calculations are presented in Appendix D.

The derived estimation of a recharge of 235 mm per year is in the same range as other estimations for the location. Sanner & Grahn (1995) calculated the effective precipitation to 150-300 mm at the location of the studied area (Eveborn et al., 2017). Rodhe et al. (2006) calculated the groundwater recharge of the location to 225-200 mm/year for coarse soil (sand and gravel).

Table 3. Calculated water balance.

	1961-1990	1991-2020	2021-2050	Unit
Pk	539	546	561	mm/year
ET	294	310	326	mm/year
Q	245	237	**235**	mm/year

3.3.5 Contamination of soil and groundwater

Primarily the compounds PCE and TCE and further degradation products have been detected at the site. There is information of an annual use of 20-40 tons of TCE during the 1940s according to the documentation of the Swedish Environmental Protection Agency's methodology for contaminated areas (MIFO) (WSP, 2019a). PCE was likely handled and used in the later years of the dry-cleaning business. The handling of chemicals is known to have taken place in the north-western corner of the building, where the process of dry-cleaning was performed.

Results from previously performed investigations at the site are presented by WSP (2018, 2019a, 2021). Investigations have continued since 2021, with investigations being performed and evaluated gradually. Initially sampling was performed through screening (soil gas and tree cores), before more invasive investigations, such as Membrane Interface Probing (MIP) and sampling of soil and groundwater was performed (WSP, 2023a). The investigations are under evaluation (WSP 2023b), with the risk assessment of the site to be completed during 2023.

The findings regarding the source zone and the contamination of groundwater are briefly presented here. Figure 13 shows an interpolation of PCE-levels in groundwater based on performed MIP. Visualization of TCE levels can be found in Appendix E. The source area of PCE and TCE is located in the northwestern corner of the former building, where high concentrations are found in both soil and groundwater. The highest concentrations of PCE in soil are found in the deeper clay, close to the sand layer, at between 2800 – 3100 mg/kg TS. Very high concentrations of PCE, TCE and further degradation products are found in the groundwater below the clay in the source area, with the highest found concentration of PCE at 2 000 000 µg/l and TCE at 2 600 000 µg/l. Due to the results, it is considered probable that PCE exist in free phase in the source area.

The former dry cleaner is as previously discussed located at a groundwater divide, and results from groundwater sampling indicate two contaminant plumes in the lower aquifer, one directed southwest towards the dual freeway, and one towards southeast. The highest concentrations in groundwater are found in the lower aquifer (sand) directly below the clay. The southwestern plume contains high concentrations of TCE and the degradation product DCE. The southeastern plume contains significantly lower concentrations than the southwestern.

Recent sampling of leaching groundwater from the inside of the sewage tunnel show presence of chlorinated ethenes at significant concentrations. The investigations and sampling from inside the two tunnels have been performed at the same time as this thesis has been under development. Sampling of groundwater in rock has also been performed, indicating limited spreading.

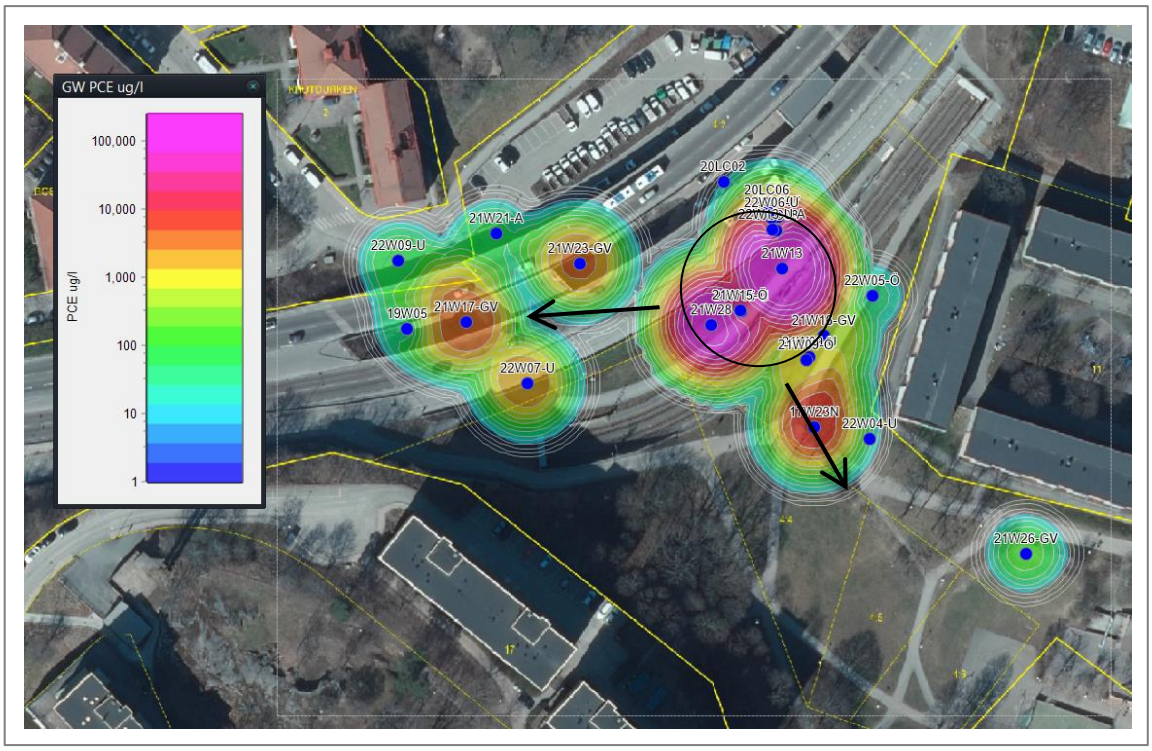

Figure 13. Interpolated PCE levels in groundwater (µg/l). The source area is marked with a circle. The spreading of PCE with the groundwater in two contaminant plumes are indicated with arrows.

4 Development of the numerical model

This section details the development of a numerical flow model. A steady-state numerical model was chosen to be developed to represent the long-term state of the hydrogeologic system. The numerical flow model was developed based on the CSM.

Initially, the model structure was defined, after which the model was discretized. Boundary conditions and material properties were then assigned to the discretized model. Post-processing tools (MODPATH and ZONEBUDGET) were coupled to the model. Thereafter the model was calibrated according to data from available groundwater wells. A sensitivity analysis was then performed on the calibrated model. Finally, the area of influence of the tunnels was derived.

4.1 Software

The three-dimensional hydrogeological groundwater flow (GWF) model was developed in Visual MODFLOW Flex (VMF), version 6.1, which is one of the most used graphical user interfaces (GUI) of MODFLOW. MODFLOW is an open-source groundwater flow model that is developed by the US Geological Survey (Harbaugh, 2005). The MODFLOW-NWT flow engine has been used for flow modelling, as it is developed to prevent problems regarding dry cells for unconfined aquifers (Niswonger et al., 2011). In addition, the post-processing tools ZONEBUDGET (Harbaugh, 1990) and MODPATH (Pollock, 2017) have been used; ZONEBUDGET to investigate the inflow into the tunnels and MODPATH for application of particle tracking in order to investigate flow paths and travel times of the groundwater.

4.2 Model structure

The model boundary was chosen to cover the whole confined aquifer and to accommodate as many topographic boundaries as possible. The final model area covered 4,87 km^2. The coordinate reference system SWEREF 99 TM was used for all input data. The model consists of 11 input grids, forming the layers of the model. The input grids were created in the software Surfer. The top layer of the model is a topographical layer based on data ordered from the Swedish Land Survey authority (Terrain model, 1+). Layer two, the layer of the top of the clay layer, is created from the topographical layer based on the assumption of the layer of filling material to be 2.5 m thick.

A rock surface was initially created using the topography layer and data of soil depth from a file originally retrieved from SGU. Based on a number of points with measurements of the rock elevation in the adjacent area of the former dry-cleaner, a surface was interpolated. This interpolated surface has thereafter been joined with the rock surface from the soil depth in order to create a more accurate rock surface layer (layer 4). Sharp edges of the rock layer, and the edges between the joined surfaces, were smoothed out in Surfer. Layer 3, representing the boundary between the clay and sand, was defined after discretization of the model (detailed in Section 3.3.3). The clay compromised 30% and the sand 70% of the vertical distance between layer 2 and 4. The seven rock surfaces have been created from the rock surface according to the evaluation of the hydraulic conductivity, detailed in Section 3.2.2.

4.3 Model discretization

The model was discretized using an irregularly spaced structured FD grid. The FD method was chosen as this traditionally is the most commonly applied method, and less computationally demanding than the FEM. An initial grid with 40x40m cells was created, and thereafter refined a number of times giving the central area of interest in the model cells with an area of 5x5 m. Care was taken in order for the size difference between adjacent cell not to be too large. The model grid is presented in Figure 14, and is composed of 179 rows and 195 columns, giving a total of 34 905 cells. The model was discretized vertically with each layer one cell thick, giving the model 10 layers.

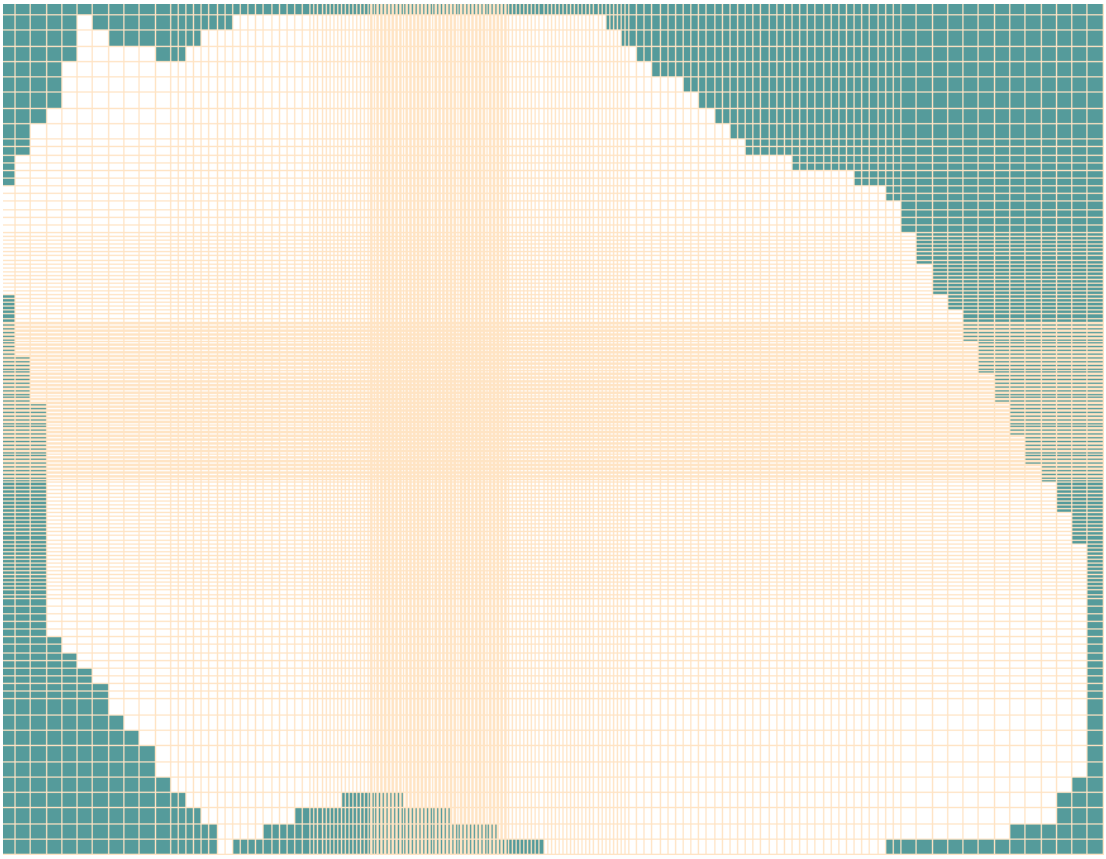

Figure 14. The FD grid used for discretizing of the model. Teal denotes inactive cells.

4.4 Property assignment

The discretized model was divided into a number of property zones, i.e., zones with certain hydrogeological properties. The property zones of the top three layers have been created based on the soil map by SGU (n.d.-a). Polygons of different soil types were digitized in GIS according to the soil type map. The edge of the clay layer was corrected slightly according to other data in the area surrounding the former dry-cleaning facility, as the SGU soil map is found to deviate from measurements of the soil layering at the location of the former dry-cleaning facility (as discussed in Section 3.1). The property zones of layer 1 are shown in Figure 15. Each layer of the rock constitutes a property zone. Weak zones are represented as polylines, forming separate property zones in each layer of the model A cross-section showing the property zones of the model can be

found in Appendix F. The property zones were thereafter assigned hydraulic properties according to the defined material properties according to the CSM (see Section 3.2.1).

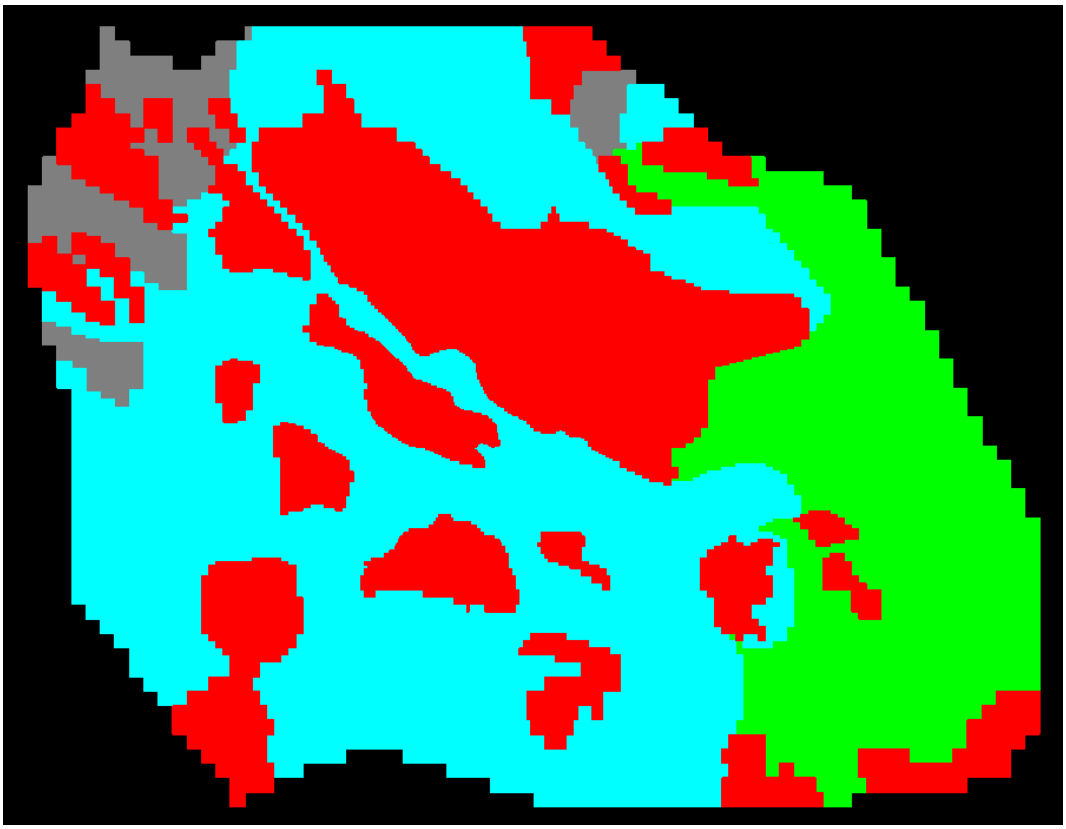

Figure 15. The created property zones of model layer 1; Turquoise – filling material, red – bedrock, green – glacial sand, dark grey – clay.

4.5 Boundary conditions

The boundary conditions of the model domain are presented in Figure 16. The lake and esker constitute physical boundary conditions, as they are permanent hydrogeologic and geologic features. They are in the model each represented as constant head boundaries. The constant head boundary serves as an infinite source of water in the model (Waterloo Hydrogeologic, 2022). The constant head of the lake is set to +1.6 m. A zone west of the lake constitutes a hydraulic hydrogeological boundary, where a constant head was set to 2 m below the surface elevation. No data of the level of the groundwater table of the esker at the edge of the model area has been attained, and an estimation is therefore used. The head of the esker is estimated to +3 m along the boundary of the model area.

For simulating recharge of the upper unconfined aquifer, the boundary condition type Recharge in VMF (specified flow) was applied to the top layer over the whole model area. The rock tunnels have been modelled as drain elements using polylines. The sewage tunnel set at +4.6 m and the stormwater tunnel at +5 m (RH2000). The water that discharges to the drain is removed from the model, thus simulating the drainage of water into the tunnels as the water pressure on the outside of the tunnels is higher than the inside. For modelling of drainage elements in VMF, a value of the drain leakance (m^2/day) is needed. An initial value of LCOND (leakance per unit length of the drain in each grid cell (m/day)) was assigned to the cells, from which the leakance per cell

(m^2/day) is calculated by VMF. For simplicity, the leakance is assumed to be the same for both tunnels. In addition, a drain has been applied over the whole model area, simulating drainage in an urban setting (such as through installations and basements). The drain was set at 1.5 m below the topographic surface, with the leakance (per unit length) set to 0.1 m/day. The initial heads of the model are set to ground elevation.

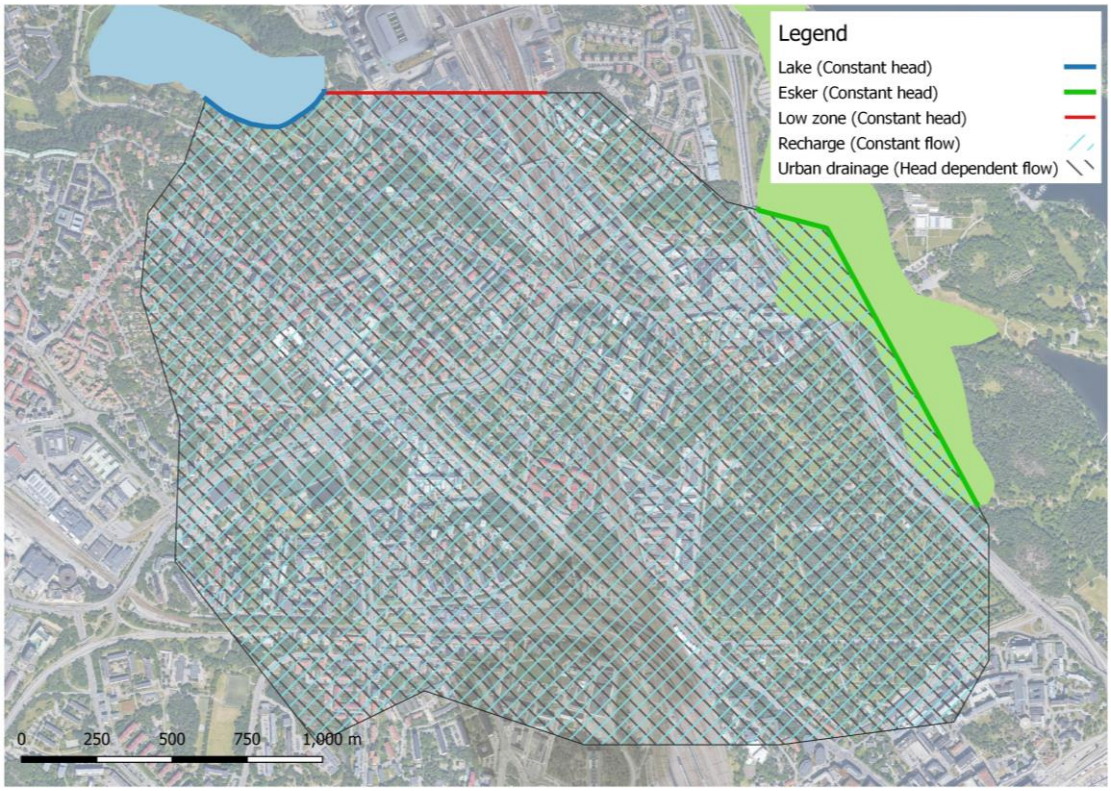

Figure 16. Boundary conditions applied to the model area. The drain elements that represent the two rock tunnels are not included in the figure.

4.6 Particle tracking

Particle tracking is used to visualize the movement of groundwater through the developed model with the generation of flow paths. The particles, that can be thought to represent a discrete volume of water, move along a flow path according to the average linear velocity, v_L (equation 7) (Anderson et al., 2015). Thereby particle tracking can also be though to represent advective transport of a solute (such as a contaminant). Dispersion, sorption, and chemical reactions are thereby not included in the simulation, meaning that the simulated contaminant is assumed to be non-reactive. The travel time of the particles along the flow path is calculated, which gives an estimation of the time of the groundwater or contaminant in the flow system.

The purpose of the particle tracking is to give an estimation of the average travel time of the groundwater and advective transport of dissolved particles of chlorinated ethenes, from the location of the former dry-cleaning facility. The starting point of the particles were defined in the sand layer in the immediate area of the former building of the dry-cleaning facility in WMF, according to the approximate placement of the source plume, located at the centre of the sand layer. Forward tracking was applied. In order for calculation of groundwater velocity, particle tracking requires input of values of

effective porosity into the model (presented in Section 3.2.1), applied through the creation of separate property zones in VMF.

ZONEBUDGET is run with the model to investigate the inflow of groundwater into the two tunnels. Two separate ZONEBUDGET zones are created, one zone for the sewage tunnel and one for the stormwater tunnel.

4.7 Model calibration

Data of 23 observation wells located in the confined sand aquifer were used in the calibration of the model, see Figure 17. An analysis of the number of observations and the distribution of heads for each well was performed. The mean of the observations of the heads in a well was defined as the calibration target in VMF. Detailed data of the well observations can be found in Appendix G. Manual calibration, meaning trial and error, was performed. Calibration statistics provided in VMF were used as tools for calibration.

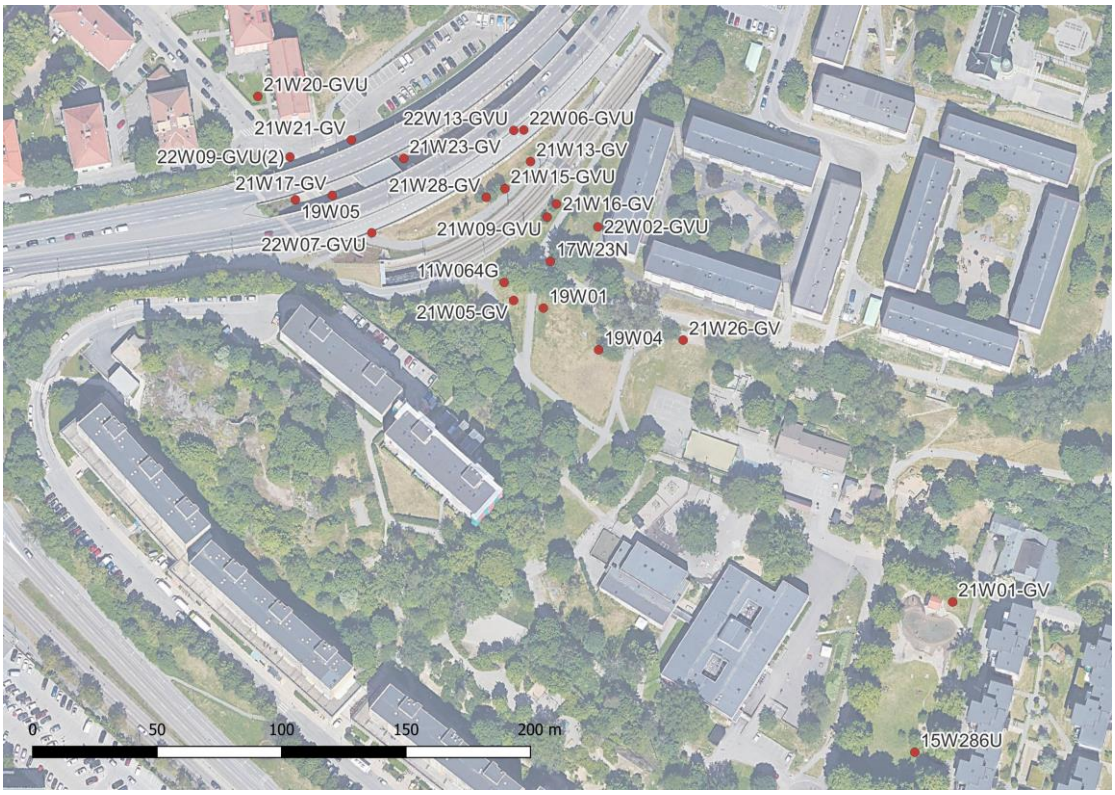

Figure 17. Observation wells used in calibration of the numerical model.

4.8 Sensitivity analysis

The sensitivity analysis was performed on the calibrated model. The sensitivity analysis aims to evaluate the model response to variations in input parameters and boundary conditions. The calibration performance of the model is evaluated using the maximum residual and Mean Average Error (MAE), see Section 2.3.3. The design of the sensitivity analysis was largely based on insight from the performed model calibration. Beyond the hydraulic conductivity of the model layers, three additional parameters were investigated: the recharge rate, the factor of increase of the hydraulic conductivity of weak zones compared to the surrounding bedrock (Kzone/K), and the leakance (LCOND) of the drain elements that represent the tunnels in the model.

The parameters have been individually varied within a reasonable range, which is dependent on each parameter. The recharge rate was varied between 150 and 320 mm, in line with the reported effective precipitation in the area by Sanner & Grahn (1995). The leakance (LCOND) was varied between 0.01 and 10, a determined reasonable interval, based experience from the process of calibration. Regarding the hydraulic conductivity of the weak zones, the K_{zone}/K was varied from 1 (meaning no weak zones in the model) to a value of 14.

In order to facilitate comparison of the sensitivity regarding hydraulic conductivity of the geologic material of the model, the hydraulic conductivity of the layers filling material, clay, sand, and bedrock (including weak zones) was increased and decreased with a factor. The hydraulic conductivity of the layer of filling material, clay and sand were varied within the reasonable interval for each geologic material according to values supplied by Hölting & Coldewey (2019) and Carlsson & Gustafson (1991). The hydraulic conductivity of the layers of bedrock was varied in an interval determined based on experience from the process of calibration.

The sensitivity of the four parameters have been evaluated regarding their effect on the flow of groundwater into the sewage and stormwater tunnel using ZONEBUDGET, and the computed average travel time of particles placed in the sand layer below the former dry-cleaning facility using MODPATH, thus giving an estimation of the advective transport of a dissolved ethene contaminant.

4.9 Area of influence

The impact of the two rock tunnels on the local groundwater levels can be illustrated through calculation of the area of influence ("influensområde" in Swedish), which is defined by SGU (2019b) as the zone in which the groundwater level is affected by groundwater withdrawal. Commonly, the area of influence is defined in regard to a specified limit, referred to as "påverkansområde" in Swedish by SGU (2019b). The area of influence of the tunnels is here defined as the area of the cone of depression in which the water-level decline is greater than 0.1 m in soil and 0.3 m in bedrock. This definition is based on similar calculations performed in a relating project (Svensson & Lissel, 2017). In this project, the groundwater withdrawal is in the form of the drainage into the sewage and stormwater tunnels. The drawdown of the tunnels is evaluated for the sand aquifer and for the bedrock (layer 6, located 20 to 40 m below ground level).

5 Results

This chapter presents the calibrated numerical model, the results of the conducted sensitivity analysis, and the findings from the investigations regarding the influence of the modelled rock tunnels on the hydrogeological system.

5.1 The calibrated model

Figure 18 presents a scatterplot of the calculated hydraulic heads versus observed heads of the calibrated model. The final calibrated parameter values of the model are presented in Appendix H.

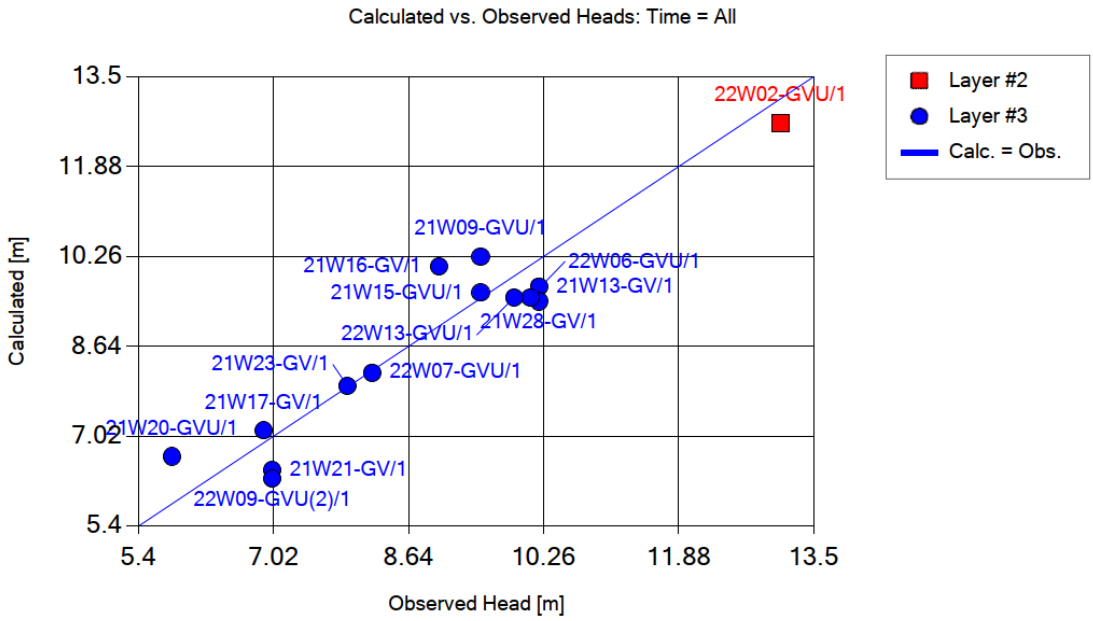

Figure 18. Calculated hydraulic heads versus observed hydraulic heads.

The model had problems in accurately reproducing the groundwater heads southeast of the former dry-cleaning facility. Due to this, the model was calibrated according to the 14 observation wells that are located along the south-western gradient, as shown in Figure 19.

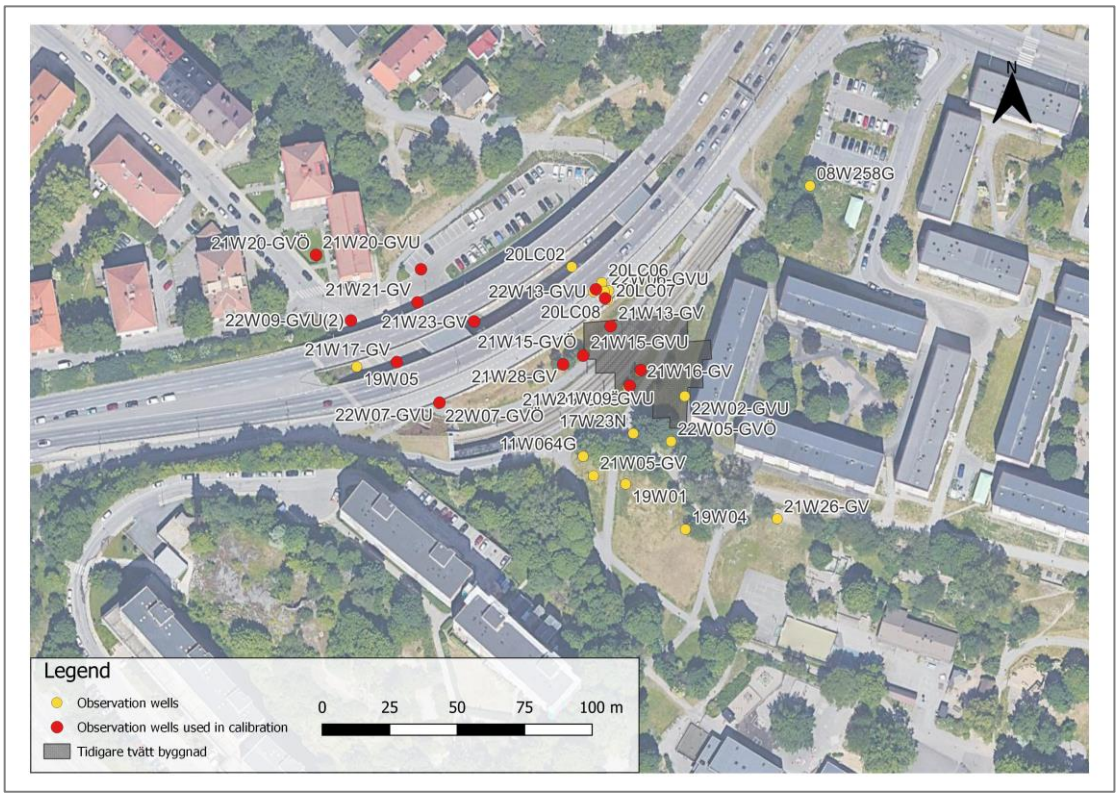

Figure 19. Map with the 14 observation wells used for calibration of the model marked in red.

5.2 Investigations regarding the impact of the tunnels

The area of influence of the drainage of groundwater through the two rock tunnels in the sand aquifer and in the bedrock are presented in Figure 20. The area of influence of the rock tunnels in the sand aquifer is calculated to be around 100 000 m^2. The area of influence in the rock (20-40 m below ground level) is calculated to around 60 000 m^2.

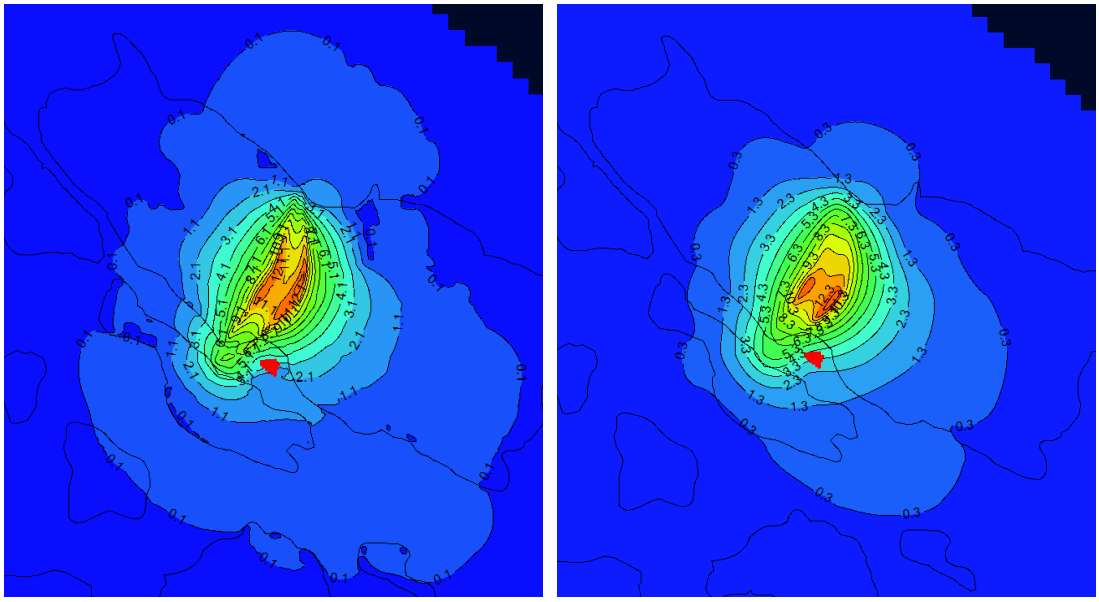

Figure 20. The drawdown of the rock tunnels in (a) the sand aquifer and (b) the bedrock (20-40 m below the surface). The building of the former dry-cleaning facility is marked in red. The outer line corresponds to the area of influence of the tunnels in the layer of (a) sand and (b) bedrock layer.

The figures below present the flow paths of seven particles assigned to the location of the former building of the dry cleaner in two scenarios; Figure 21 depicting the scenario with the rock tunnels included in the model and Figure 22 depicting the scenario without the rock tunnels included in the model.

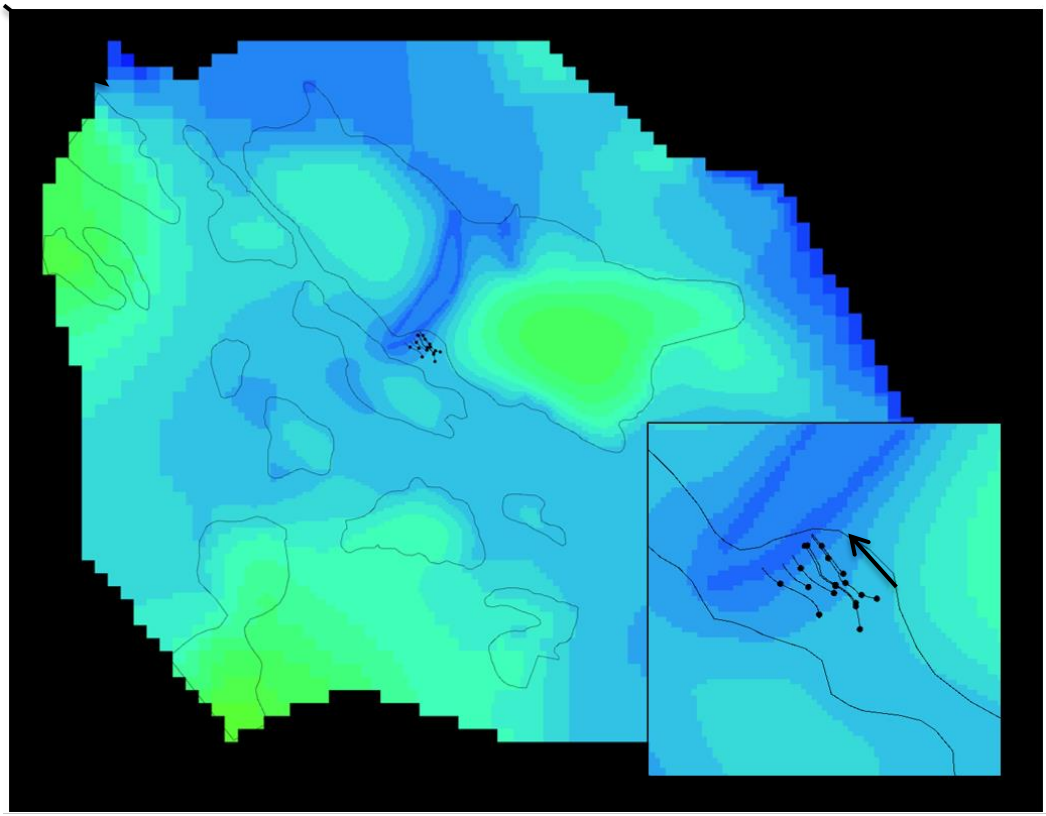

Figure 21. Particle flow paths with the rock tunnels included in the model. The arrow indicates the flow direction.

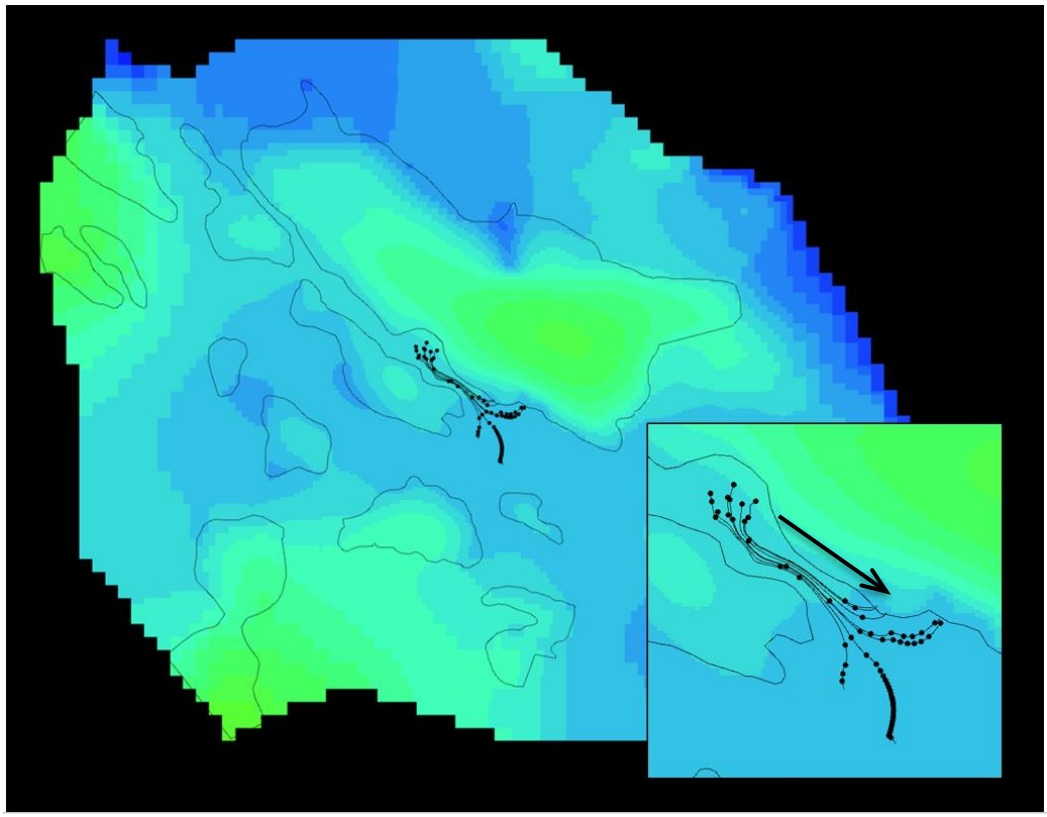

Figure 22. Particle flow paths without the rock tunnels included in the model. The arrow indicates the flow direction.

5.3 Results of the sensitivity analysis

The subsequent sections present how variations in the recharge rate, ratio of Kzone/K, leakance parameter of modelled rock tunnels, and the hydraulic conductivity of model layers impact the calibration of the model (maximum residual head and mean absolute error, MAE), the inflow to the two tunnels and the computed particle travel times.

5.3.1 Degree of calibration

Figure 23 illustrates the changes in the maximum head residuals and the mean absolute error (MAE), in response to variations in the recharge rate of the model. Decreasing the recharge rate produces a slight rise in the MAE, whereas a corresponding increase appears to have no discernible impact. Concerning the maximum residual, it increases with an increase in the recharge rate, and decrease with a decrease of the recharge rate.

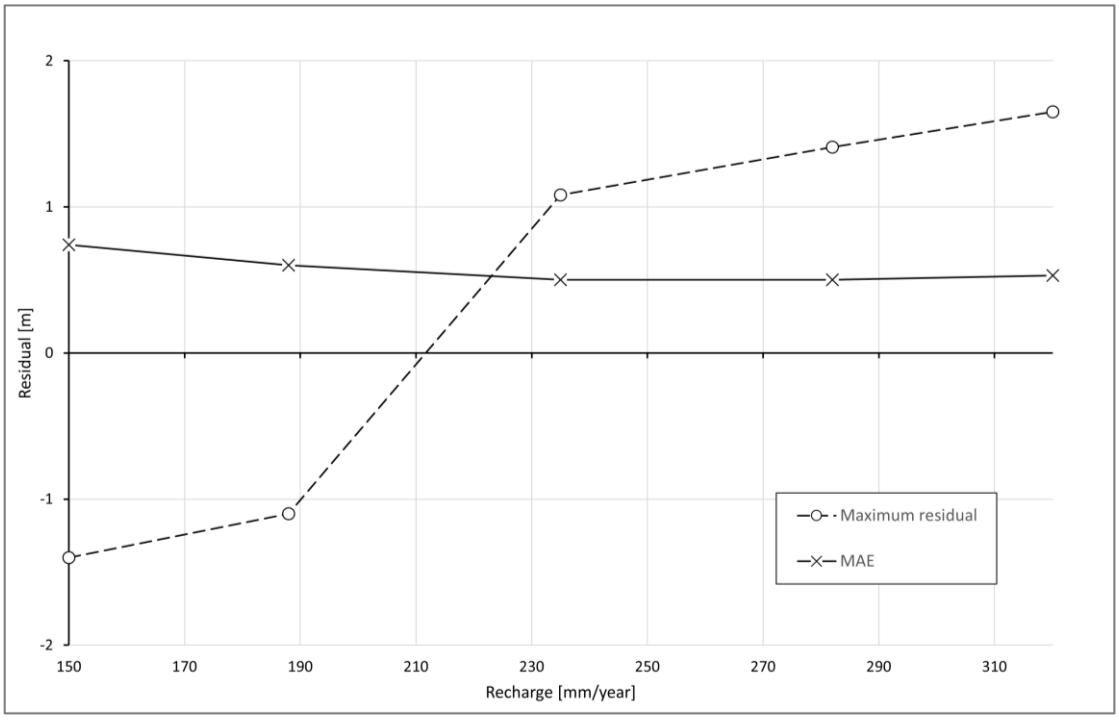

Figure 23. The change in maximum hydraulic head residual and the mean absolute error (MAE) in response to variations of the recharge rate of the model.

Figure 24 illustrates the changes in the maximum head residuals and the mean absolute error (MAE), in response to variations in the leakance (LCOND) of the drain elements that represent the rock tunnels in the model. The maximum residual and the MAE decrease similarly with an increase of the leakance from 0.01 to 0.1 m/day, with the MAE thereafter stabilize at value of approximately 0.5 m. The maximum residual however shows slightly more variations.

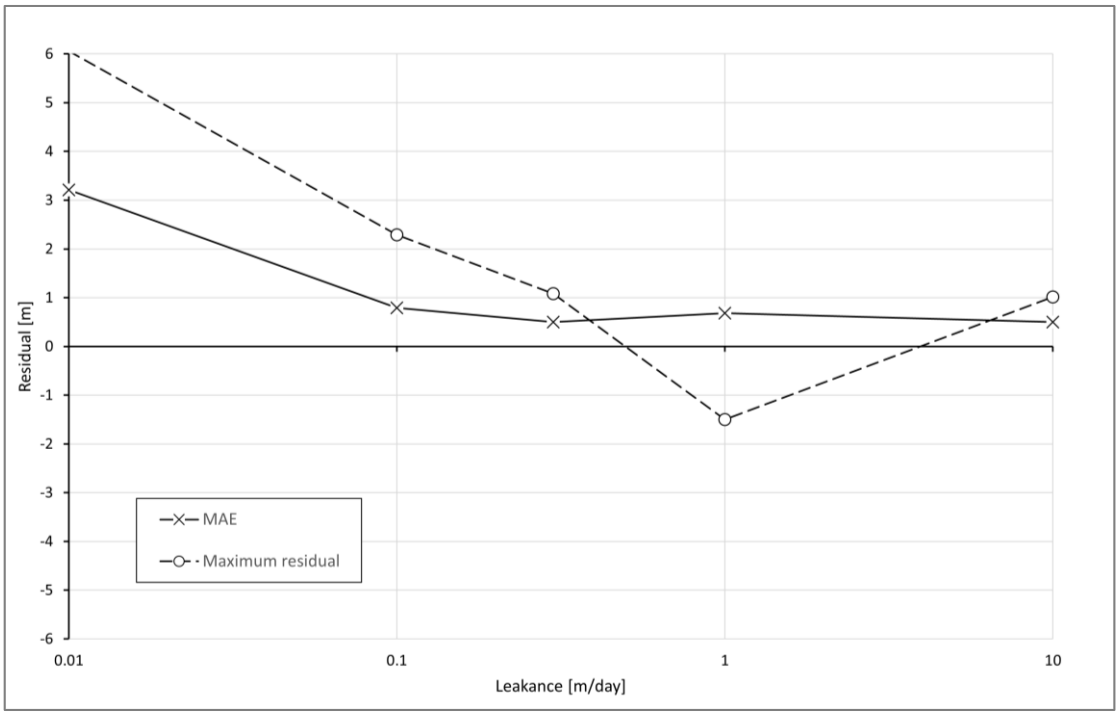

Figure 24. The change of the maximum hydraulic head residual and mean absolute error (MAE) in response to variations of the leakance of the two tunnels.

Figure 25 illustrates the changes in the maximum head residuals and the mean absolute error (MAE) in response to variations of the ratio of Kzone/K, representing the hydraulic conductivity of the weak zones compared to the surrounding bedrock. Miniscule change is seen regarding the MAE, however the maximum residual switches from a value around 1 to -1 at a Kzone/K above 10.5.

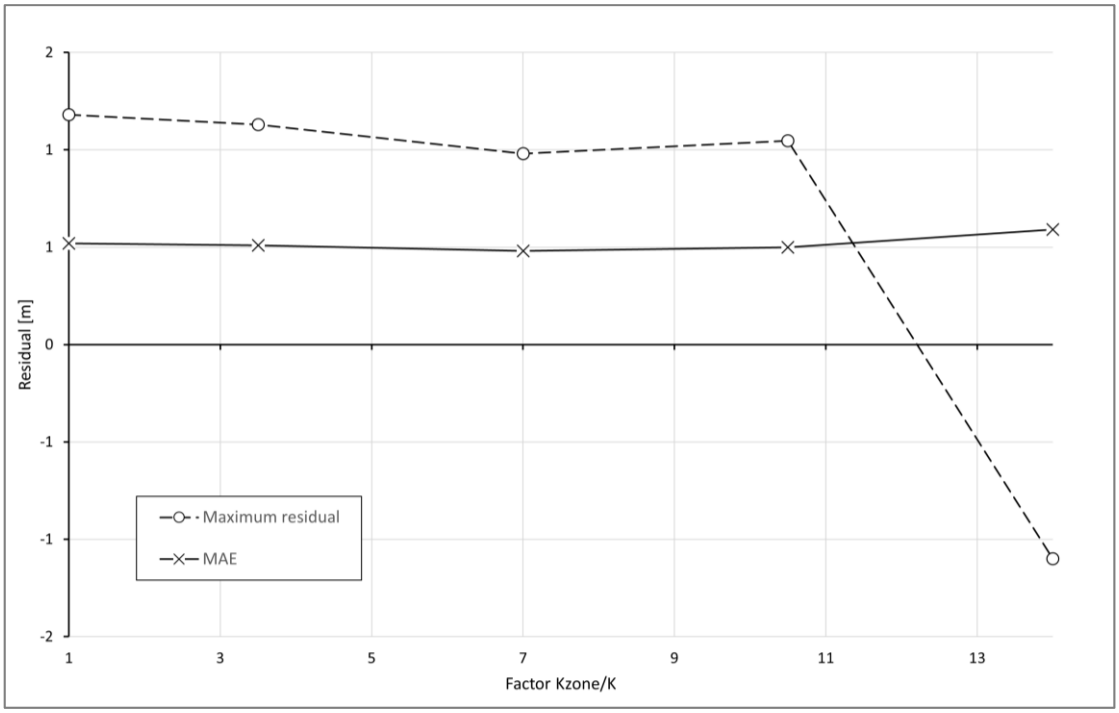

Figure 25. The change in maximum hydraulic head residual and mean absolute error (MAE) in response to variations in the ratio of K_{zone}/K, representing the hydraulic conductivity of the weak zones compared to the surrounding bedrock.

Figure 26 shows the changes in the maximum head residual and the mean absolute error (MAE), in response to variations in the hydraulic conductivity of the filling material, clay, sand and bedrock. Varying the hydraulic conductivity of the filling material and clay produces miniscule change in the maximum head residual and MAE. However, the maximum residual (and the MAE to a lower degree) is sensitive to changes in the hydraulic conductivity of the sand and bedrock.

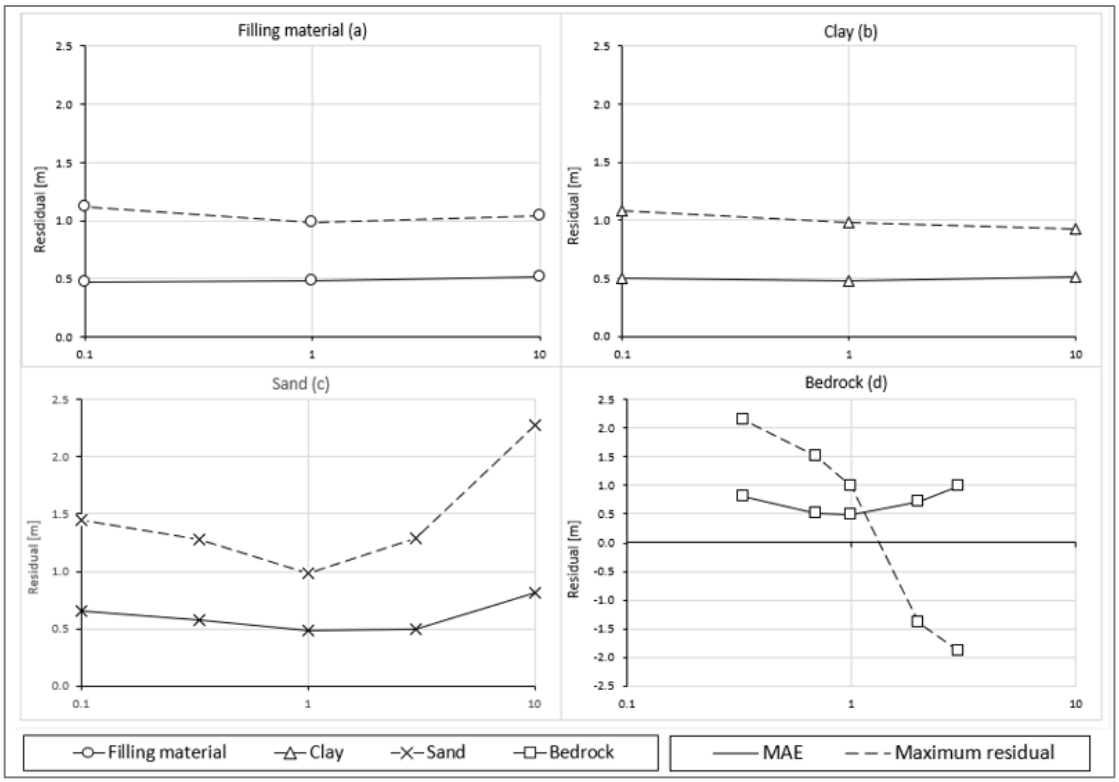

Figure 26. The change in maximum head residual and mean average error (MAE) in response to variations of the hydraulic conductivity of the filling material, clay, sand, and bedrock. Notice the negative y-axis of (d).

5.3.2 Inflow to tunnels

Figure 27 presents the change in the flow rate into the two tunnels with variations of the recharge rate. As can be seen in the figure, the inflow into the tunnel varies significantly between the two tunnels, with the inflow of the sewage tunnel at 38 m^3/day and the inflow to the stormwater tunnel at 16 m^3/day (at the calibrated recharge of 235 mm). The inflow is shown to increase relative linearly with the recharge rate for both of the tunnels. The effect is similar for both tunnels, a decrease of the recharge rate to 150 mm/year produces a decrease of 19% in the inflow to the sewage tunnel and a decrease of 23% in the inflow to the stormwater tunnel.

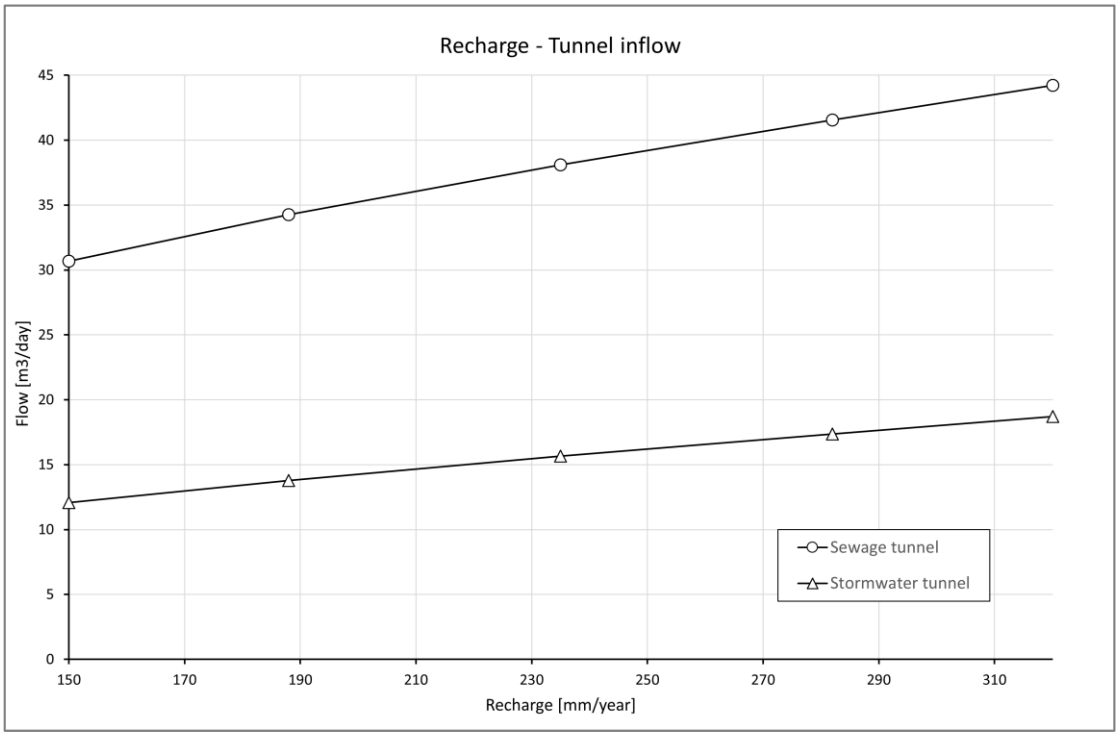

Figure 27. The change in inflow of the sewage and stormwater tunnel in response to variations of the recharge rate.

Figure 28 presents the change in the flow rate into the two tunnels with variations of the leakance (LCOND) of the drainage elements that are used to model the rock tunnels. The rate of inflow is shown to rapidly increase as the leakance is raised from 0.01 m/day, eventually reaching a stabilization point at a leakance of 1 m/day. This corresponds to a flow rate of approximately 40 m^3/day in the sewage tunnel and 16 m^3/day in the stormwater tunnel.

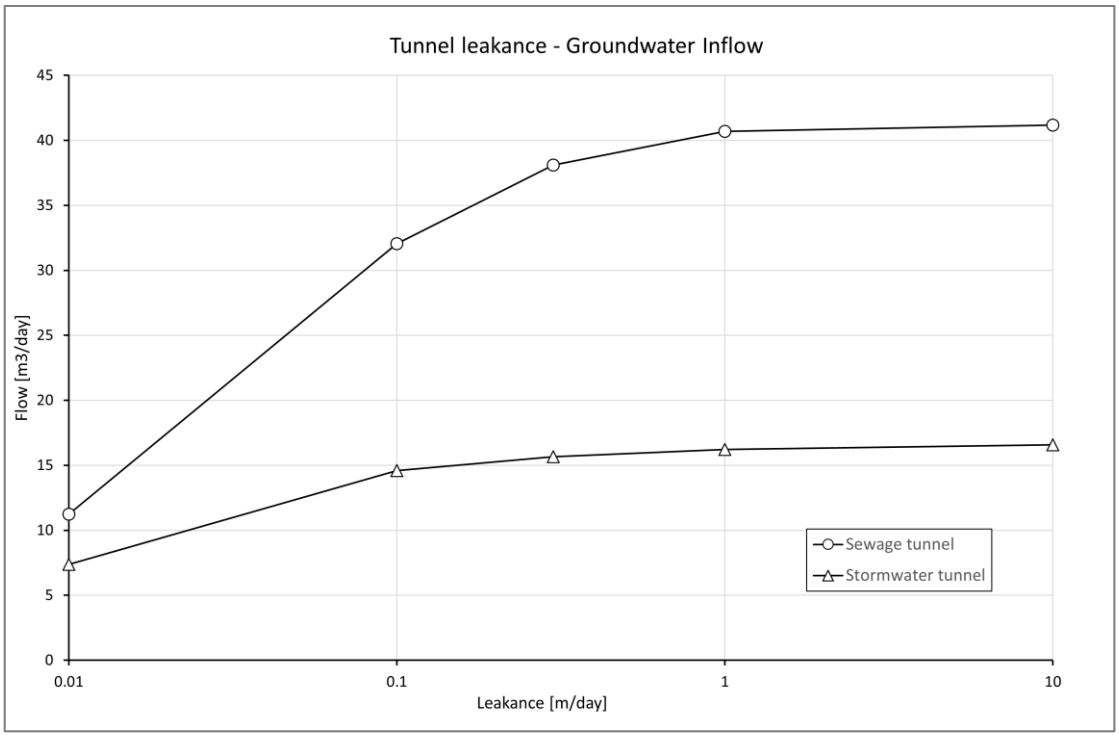

Figure 28. The change in flow rate of the sewage and stormwater tunnel in response to variations in the leakance of the tunnels.

Figure 29 presents the sensitivity of the inflow to the tunnels to changes to the ratio of K_{zone}/K, representing the hydraulic conductivity of the weak zones compared to the surrounding bedrock. The inflow is shown to decrease significantly at an increase of the K_{zone}/K from 10.5 to 14, with a 90% reduction of the inflow to the sewage tunnel and a 55% reduction of the inflow to the stormwater tunnel.

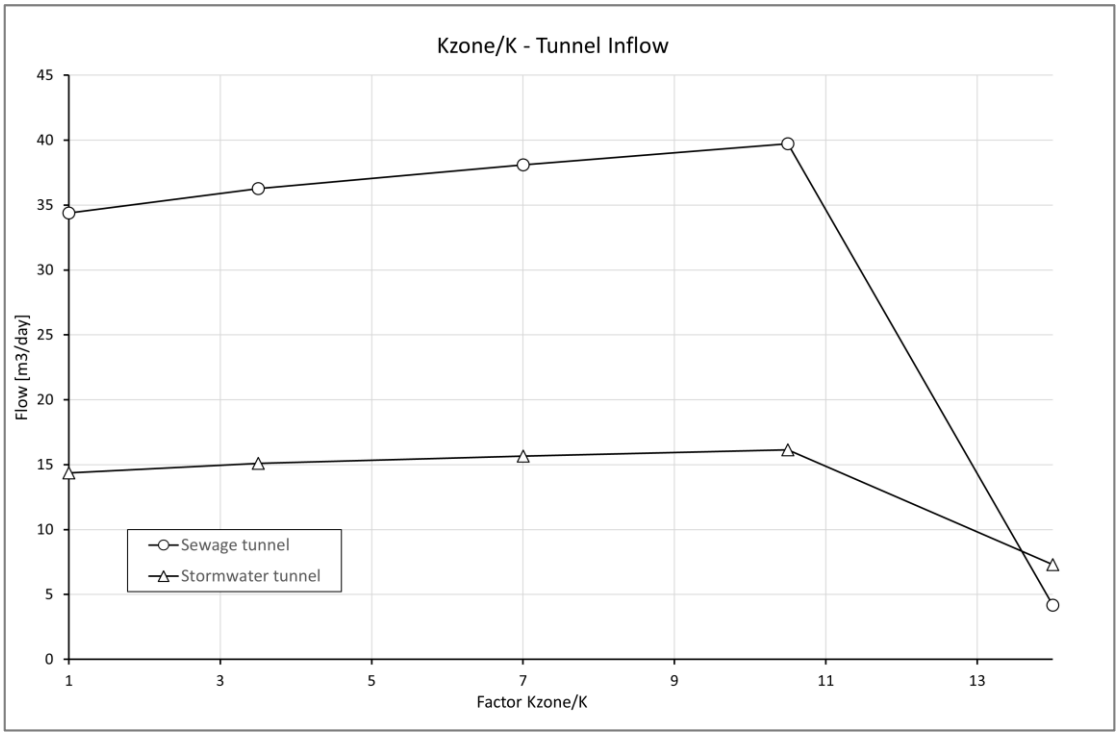

Figure 29. The change in flow rate of the sewage and stormwater tunnel in response to variations of the ratio of K_{zone}/K, representing the hydraulic conductivity of the weak zones compared to the surrounding bedrock.

Figure 30 presents the change in the flow rate into the two tunnels with variations of the hydraulic conductivity of the filling material, clay, sand, and bedrock. Changes in the hydraulic conductivity of the filling material and clay had a minimal impact on the flow of the tunnels.

However, the flow rate of the sewage tunnel showed a comparable responsiveness to changes in both the hydraulic conductivity of the sand layer and the bedrock. For both the sand and rock, increasing the hydraulic conductivity by a factor of three results in a flow rate at approximately 50 m^3/day. The flow rate of the stormwater tunnel displays a lower degree of sensitivity to variations of the hydraulic conductivity compared to the sewage tunnel. When considering the hydraulic conductivity of the sand, a decrease has no effect on the flow rate.

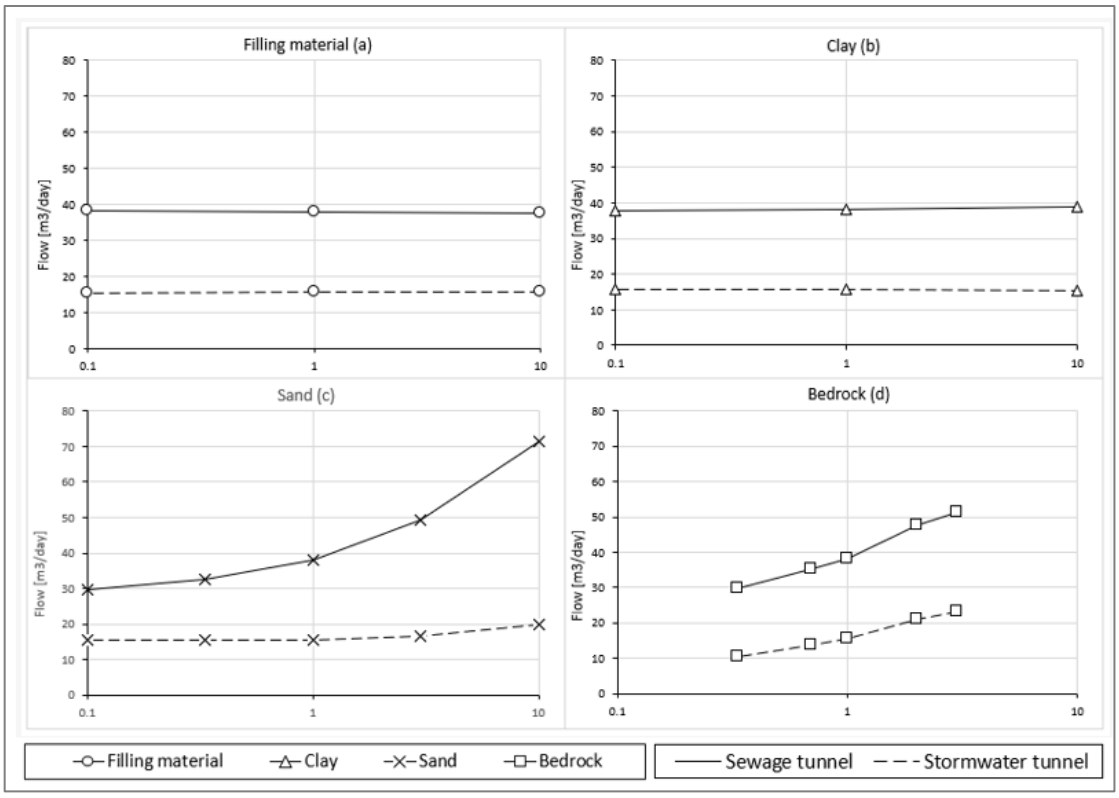

Figure 30. The flow rate of the sewage and stormwater tunnel in response to variations of the hydraulic conductivity of the filling material, clay, sand, and bedrock.

5.3.3 Particle travel time

Figure 31 presents the change in the particle travel time with variations of the recharge rate. The particle travel time is found to decreases with an increase in recharge rate. Reducing the recharge rate to 150 mm/year results in an 29% increase of the travel time, while a similar increase in recharge (85 mm) leads to an 12% decrease.

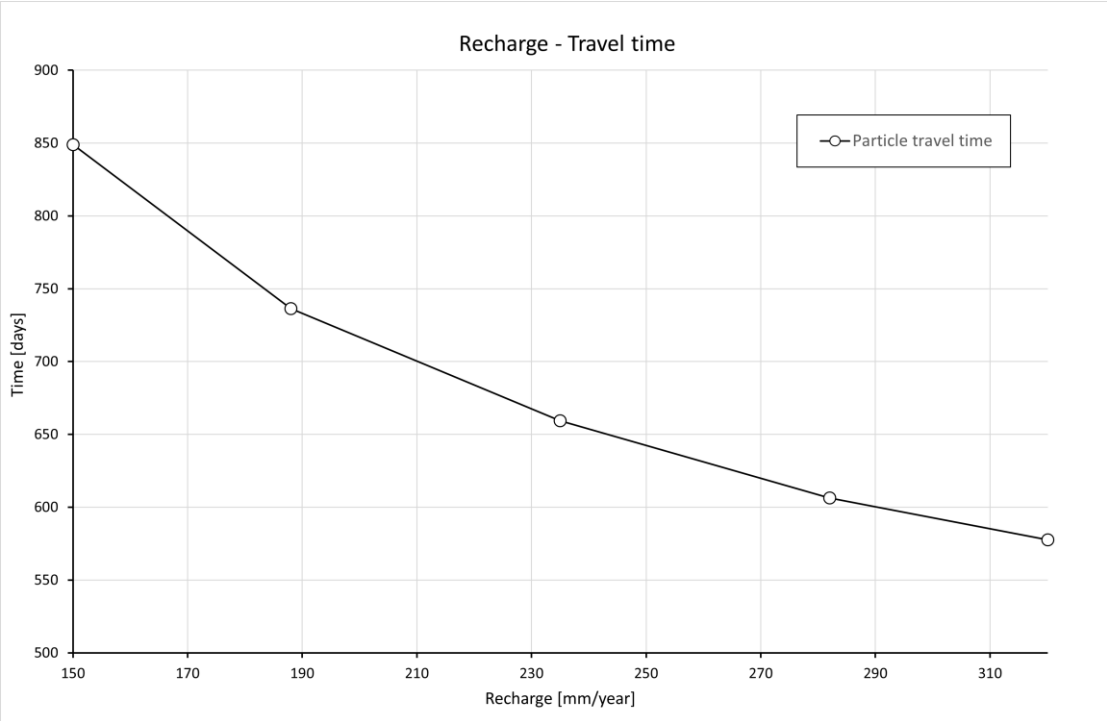

Figure 31. The change in computed particle travel time in response to variations of the recharge rate.

Figure 32 presents the sensitivity of the inflow to the tunnels to changes to the parameter of leakance (LCOND) of the drainage elements that are used to model the rock tunnels. The results show that the travel time is sensitive to variations in the leakance, especially of a lowering of the leakance. A leakance around 0.01 m/day producing a travel time of 4 663 days.

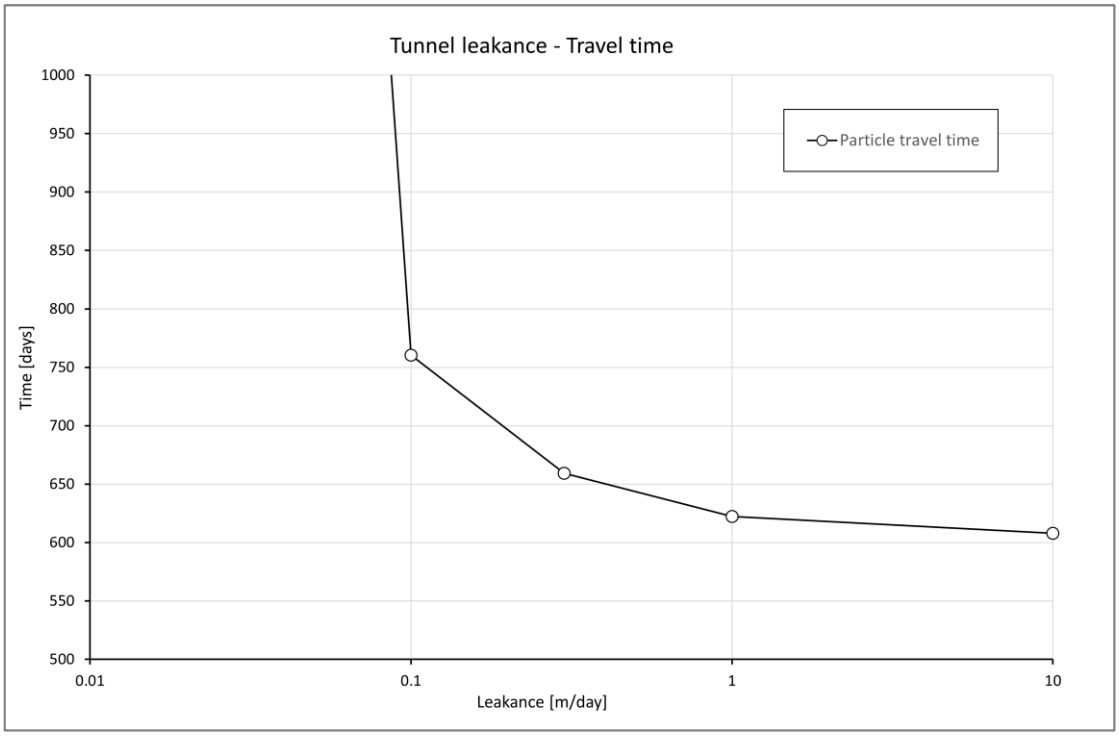

Figure 32. The change in computed particle travel time in response to variations of the leakance of the two tunnels.

Figure 33 presents the change in the particle travel time by changes to the ratio of K_{zone}/K, representing the hydraulic conductivity of the weak zones compared to the surrounding bedrock. As can be seen in the figure, an increase in the ratio of K_{zone}/K produces a slight increase of the travel time, while a decrease leads to a similar reduction of the travel time.

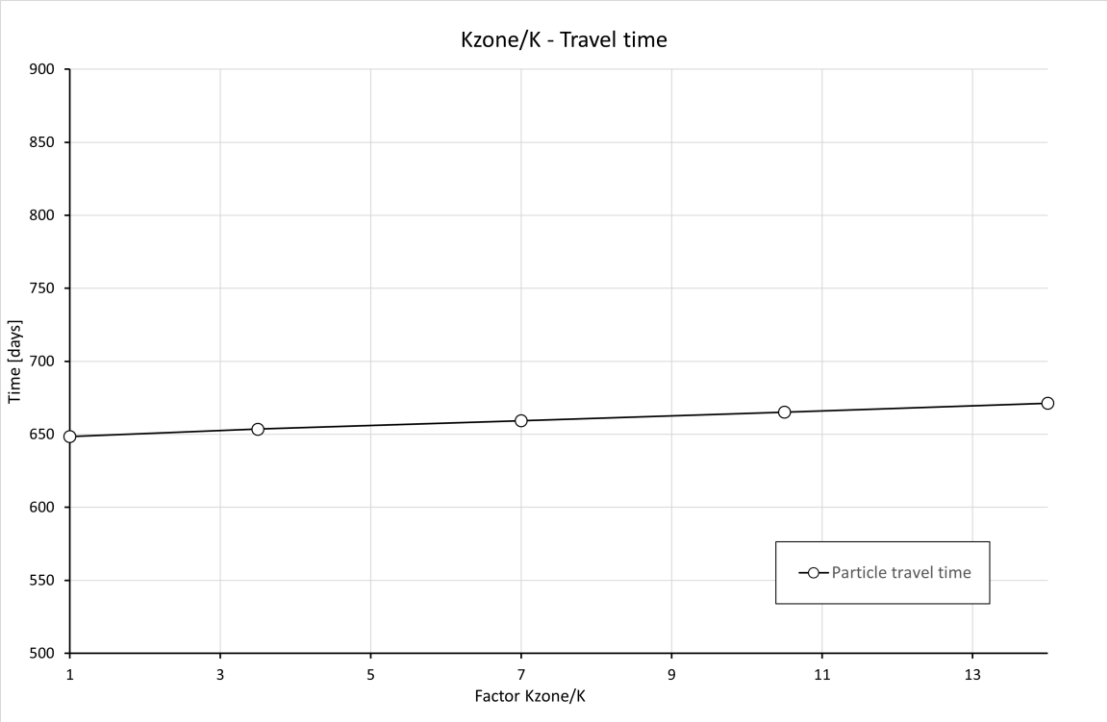

Figure 33. The change in particle travel time by variations of the ratio of K_{zone}/K, representing the hydraulic conductivity of the weak zones compared to the surrounding bedrock.

Figure 34 presents the change in the computed travel time due to variations in the hydraulic conductivity of filling material, clay, sand, and bedrock. Variations of the hydraulic conductivity of the filling material gave no response, while a slight response can be noted for the clay. The travel time showed great sensitive to variations of the hydraulic conductivity of the sand layer, with a decrease by a factor of ten producing a travel time of 2 424 days and an increase by a factor of ten producing a travel time of 294 days (see Figure 34c). The model also showed sensitivity to increasing of the hydraulic conductivity of the bedrock, resulting in a notably reduced travel time.

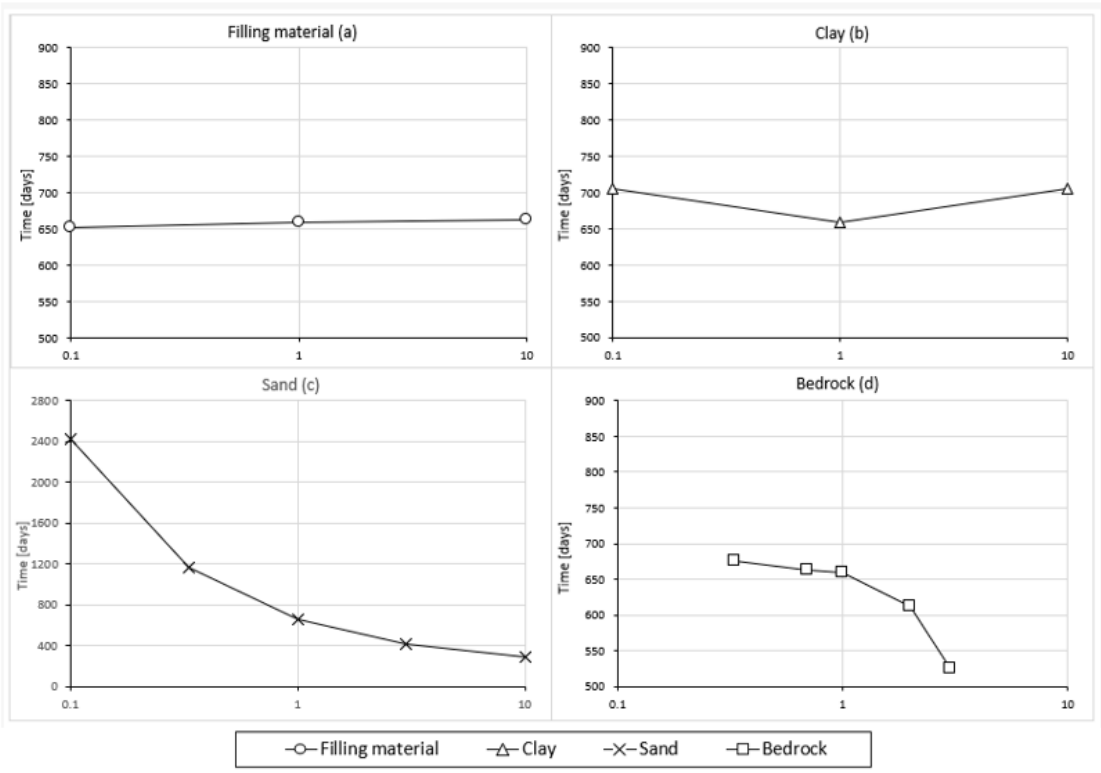

Figure 34. The change in computed travel time in response to variations of a factor describing the change in hydraulic conductivity of the filling material, clay, sand, and bedrock. Notice the difference in the scale of the y-axis of (c).

5.3.4 Evaluation of the sensitivity analysis

Table 4 presents a summary of the performed sensitivity analysis regarding the deemed effect of each parameter on the model calibration, inflow to tunnels and particle travel time.

Table 4. Categorization of the evaluated parameters (and intervals) in the sensitivity analysis according to their impact on the degree of calibration of the model, groundwater inflow to tunnels and calculated particle travel time. K denotes hydraulic conductivity.

	Impact	
	Significant	Insignificant
Calibration performance	LCOND < 0.1 m/day Kzone > 10.5 K_{sand} K_{rock}	Recharge LCOND > 0.1 m/day Kzone/K < 10.5 K_{sand} (1–3) $K_{filling}$ K_{clay}
Groundwater inflow to tunnels	Recharge LCOND (0.1- 1 m/day) Kzone/K > 10.5 K_{sand} K_{rock}	Kzone/K < 10.5 $K_{filling}$ K_{clay}
Travel time	Recharge LCOND (0.1- 1 m/day) K_{sand} K_{rock}	Kzone/K $K_{filling}$ K_{clay}

6 Discussion

This chapter discusses the results obtained in Chapter 5. The discussion is structured into four segments: the tunnels, uncertainties in the conceptual site model, discussion of the performed sensitivity analysis and finally an evaluation of the used method.

6.1 Hydrogeology of the site

The initial model produced little variation in groundwater head, and calibration of the model was needed. In the process of calibration, the area south-east of the dry-cleaning facility was assigned a slightly higher hydraulic conductivity, which together with the calibration of the leakance of the tunnel produced a more accurate variation in hydraulic heads. The drainage elements that represent the tunnels were found to be crucial in the calibration of the model, with extremely low values of leakance having a substantial effect on the calibration of the model compared to the scenario of no tunnels.

Two distinct groups of wells with similar behaviour were identified during calibration, wells west of the dry-cleaner and wells south-east of the dry-cleaner, as shown in figure 19. The model was found difficult to calibrate against both groups. This divide between the group of observation wells corresponds to the likely placement of the groundwater divide, further indicating two separate systems at the site. Calibration of the model was directed at accurately predicting the western hydraulic gradient. This produced an overprediction of the hydraulic heads south-east of the dry-cleaner.

Variations in the recharge rate were tested, however the calculated value of 235 mm was found to fit the model well. The parameter of recharge is further discussed in Section 6.3.1. The leakance of the rock tunnels was estimated purely based on calibration. The hydraulic conductivity of the third layer (sand) was generally decreased and a number of separate property zones were created, which represent the variations (heterogeneities) of the hydraulic conductivity of the layer. The hydraulic conductivity of three most superficial layers of bedrock was decreased.

The derived area of influence in the sand aquifer and rock (Figure 20), show the significant reduction in groundwater head produced by the tunnels in the adjacent area. The investigated scenarios using particle tracking (Figure 21 and 22) illustrates the impact of the tunnels on the flow patterns of the area. Without the rock tunnels included in the calibrated model, the groundwater flow, and subsequently modelled advective flow of contaminant particles from the dry cleaner, is directed towards east, instead of south-west. The rock tunnels have a clear impact on the groundwater flow patterns at the site.

6.2 Uncertainties in the CSM

The developed model has large uncertainties in the geological representation. The geology of the investigated area is complex, with large variations in the bedrock surface and geological layers. This includes the bedrock depression south-east of the former dry cleaner, for which the used data is known to be insufficient.

The used representation of the rock surface was created based on data of soil depth from SGU, which is known to be general and unspecific, thus containing large uncertainties. Measurements of the elevation of the rock surface are limited to the adjacent area surrounding the source zone, and interpolation of the measurements was found to be challenging. Additional measurements of the rock surface elevation could improve the representation of the rock surface in the model.

In addition, many of the observation wells that served as the basis of the calibration of the model only had a few observations, giving rise to uncertainties in the calibration of the model. Observation wells were limited to the immediate area surrounding the former dry-cleaning facility.

The difficulties in calibration of the model to observation wells located both west and south-east of the former dry-cleaning facility (discussed in Section 6.1) give rise to questions regarding the performance of the model and the accuracy of the conceptual model. From the process of calibration and the sensitivity analysis it is evident that the groundwater heads west and south-east of the dry cleaner do not behave in a similar manner, and that they likely belong to two separate systems. This fault in the model performance can likely be traced to the conceptual model. The conceptual model does not separate the areas located east and west of the groundwater divide; the same parameters are largely used across the whole model area. To improve the conceptual model (and subsequently the numerical model), the areas might have to be looked upon as separate units.

In addition, the site is located in a highly urban area with a wide range of possible parameters impacting the hydrogeological systems at the site, many of which are likely unknown. As for the south-eastern system, an underground railway tunnel is located nearby, stretching through the elevated rock area, with the opening of the tunnel located further to the east of the site of the dry-cleaning facility. The possible influence this tunnel and other known or unknown subsurface infrastructure might have on the systems present at the site are not detailed, largely due to time restraints and difficulties in obtaining information.

6.3 The sensitivity of model parameters

The following sections discusses the sensitivity of the model parameters of recharge, leakance of the tunnels and the hydraulic conductivity of the geologic material.

6.3.1 Recharge

The recharge rate is generally subject to calibration in numerical models. According to the calculations of water balance the groundwater recharge is estimated to 235 mm. In these calculations the effective precipitation is assumed to be equal to the groundwater recharge, which as is discussed in Section 2.2.3 can be considered a valid assumption in Nordic conditions (Barthel et al., 2021). However, surface covering will have an influence on the degree of recharge, with a greater portion of precipitation contributing to surface runoff within urban regions. How much the surface covering impacts the recharge rate at the site is unknown. Additional contribution to recharge from ground installations is a further factor with great uncertainties. However, the calculated recharge rate of 235 mm was found to fit the model well.

The effect of the recharge rate on the MAE of the model was minimal, although slight at a lowering of the recharge rate to 150 mm, see Figure 23. The maximum head residual showed a clearer sensitivity to the recharge rate, increasing with an increase in the recharge and vice versa. However, the recharge rate has a clear impact on the inflow of the tunnels and the travel time of the groundwater.

This result indicates that the recharge is an important parameter in the model, as when looking at the MAE a small uncertainty in the calibration of the model contribute to a large uncertainty in the computed inflow of the tunnels and particle travel time. Reducing the uncertainties of such parameter, referred to as Sensitivity Type 4 by

ASTM (2016), would thereby contribute to the reduction of the model uncertainties regarding prediction.

6.3.2 Tunnel leakance

The tunnel leakance is a lumped coefficient, difficult to estimate based on measured data (Waterloo hydrogeologic, 2022). Thus, calibration is necessary to estimate, or at least adjust the parameter in the model. Below a leakance of 0.1 m/day, the leakance has a large effect on the maximum residual head and MAE otherwise little variations is seen in the degree of calibration of the model, see Figure 24. Values of the leakance below 0.1 m/day produces a low degree of calibration and extreme values of tunnel inflow and computed travel time. However, a value above 0.1 m/day corresponds to a calibrated model although relatively large variations in the computed travel time, and inflow of the sewage tunnel still can be seen. Increasing the leakance further produce little variations in both calibration and the model output. This indicates that there is an interval between a leakance of approximately 0.1 to 1 m/day in which the model is sensitive to variations. Thus, the leakance of the drain elements is a parameter to investigate further in order to limit uncertainties of the model.

6.3.3 Hydraulic conductivity

Material parameters form important input parameters of the numerical model. As has been partly discussed in the conceptual model (Section 3.2.1) little data of material properties exist; therefore, calibration of the model has been used to estimate the hydraulic properties. However, different values of hydraulic conductivity of the material of the model can produce similar output, meaning that there is no single true solution. The hydraulic conductivity of the filling material and clay was found to have little impact on the model calibration as well as model outputs. They can therefore be categorized as parameters of Sensitivity Type 1 and are not considered important in reducing uncertainties of the model, see Section 2.3.3.

The model was however found to be sensitive to changes in the hydraulic conductivity of the sand and bedrock. The MAE of the sand showed little variations at an increase of three times the calibrated value, however a further increase produced a significantly higher MAE. A slight sensitivity to a decrease of the value was seen. The maximum hydraulic head increased significantly at an increase of the hydraulic conductivity of a factor of 3. Regarding the output of the model, variations of the parameter showed a clear impact on the particle travel time, especially a decrease of the parameter value, which produced extreme values. The inflow to the tunnels (primarily the sewage tunnel) showed sensitive to an increase of the hydraulic conductivity.

The importance of the parameter of hydraulic conductivity of the sand regarding the minimization of uncertainties is not as straight forward as previous parameters. The parameter is deemed to show a Type 4 sensitivity only between a value around 1-3 times the calibrated hydraulic conductivity. Outside of this interval, the parameter cannot be categorized as a Sensitivity Type 4. Therefore, the impact of variations in the value are only of interest of a limited range.

There are almost certainly heterogeneities in the hydraulic conductivity of the sand layer, which gives rise to uncertainties in the parameter values as well as the model structure of the sand layer. The created property zones of the model during the process of calibration show the impact of heterogeneities on the model. The performance of hydrogeological investigations, such as slug tests would give more detailed information of the hydraulic properties of the sand layer. It is however unknown whether these

investigations would result in a substantial enhancement of the numerical model. In addition, more detailed data would increase the complexity of the model.

Regarding the hydraulic conductivity of the bedrock, the MAE and the maximum head residual showed equally sensitive to both an increase and decrease of the value. The parameter was shown to have an equal distinct impact on the inflow to both the sewage and stormwater tunnel. The particle travel time was found to vary little with a decrease of the hydraulic conductivity of the bedrock, however sensitive to an increase of the value. These results suggest the hydraulic conductivity of the bedrock is not a prioritized parameter to minimize uncertainties of the model.

Variations in the factor of Kzone/K produce a limited impact on calibration performance of the model, unless increased above a value of 10.5, see Figure 25. Similarly, variations in the factor are found to have a limited impact on the inflow to the tunnels unless modelled with a hydraulic conductivity 10.5 times higher than the surrounding bedrock or more. In addition, the hydraulic conductivity of the weak zones shows little impact on the particle travel time. Thus, the parameter is not considered as important to investigate further to limit uncertainties of the model.

6.4 Evaluation of method

Hydrogeological flow modelling serves as an excellent way to visualize, increase the understanding and to explore a hydrogeologic system and the governing conditions. In this project, the developed model has been focused on investigating the impact of the nearby rock tunnels on the hydrogeological system. This use could be expanded for further investigations of hydraulic conditions at the site. The developed model could also serve as the basis of the development of a transport model of the spreading of contaminants at the site.

The process of developing of a three-dimensional numerical groundwater flow model is resource demanding task, requiring time and knowledge. The model was developed with a certain simplicity in mind, and could as always, be further improved and developed into a more complex model.

7 Conclusion

According to the developed model, the tunnels play an integral role in shaping the flow patterns of the nearby area, impacting the groundwater flow from the location of the former dry-cleaning facility. The model suggests that the tunnels, primarily the sewage tunnel, acts as a contaminant pathway of chlorinated solvents originating from the source area at the former dry-cleaning facility.

The groundwater levels south-east of the former dry-cleaning facility are found to be governed by unknown hydraulic conditions, which were not identified and included in the conceptual model.

The performed sensitivity analysis indicates that the most important parameters to investigate further in order to limit uncertainties of the model prediction of inflow to the tunnels and the particle travel time, are the boundary conditions of recharge and leakance of the drainage elements that are used to model the tunnels. In addition, the hydraulic property of the sand is a parameter that for which further investigations should be considered.

8 References

Anderson, M. P., Woessner, W. W., & Hunt, R. J. (2015). Applied Groundwater Modeling - Simulation of Flow and Advective Transport (2nd ed.) Elsevier.

Andréasson, P.-G. (Ed.). (2015). *Geobiosfären* (2nd ed.) (The Geobiosphere. In Swedish). Studentlitteratur.

ASTM. (2016). *Standard Guide for Conducting a Sensitivity Analysis for a Groundwater Flow Model Application* (ASTM D5611-94 (2016)). https://compass.astm.org/document/?contentCode=ASTM%7CD5611-94R16%7Cen-US.

Barthel, R., Stangefelt, M., Giese, M., Nygren, M., Seftigen, K., & Chen, D. (2021). Current understanding of groundwater recharge and groundwater drought in Sweden compared to countries with similar geology and climate. *Geografiska Annaler, Series A: Physical Geography*, 103(4), 323–345. https://doi.org/10.1080/04353676.2021.1969130

Burri, N. M., Weatherl, R., Moeck, C., & Schirmer, M. (2019). A review of threats to groundwater quality in the anthropocene. *Science of the Total Environment*, 684, 136–154. https://doi.org/10.1016/j.scitotenv.2019.05.236

Carlsson, L. & Gustafson G. (1991). Provpumpning som geohydrologisk undersökningsmetodik: reviderad utgåva av R41:1984 (In Swedish). R66:1991. Retrieved through Gothenburg University, https://gupea.ub.gu.se/handle/2077/47991

Chen, D., Zhang, P., Seftigen, K., Ou, T., Giese, M., & Barthel, R. (2021). Hydroclimate changes over Sweden in the twentieth and twenty-first centuries: a millennium perspective. *Geografiska Annaler, Series A: Physical Geography*, 103(2), 103–131. https://doi.org/10.1080/04353676.2020.1841410lee

Cwiertny, D. M. & Scherer, M. M. (2010). Chlorinated Solvent Chemistry: Structures, Nomenclature and Properties. In H. Stroo & C. Ward (Eds.), *In Situ Remediation of Chlorinated Solvent Plumes*. SERDP/ESTCP Environmental Remediation Technology. Springer, New York, NY. https://doi.org/10.1007/978-1-4419-1401-9_2

Damgaard, I., Bjerg, P. L., Bælum, J., Scheutz, C., Hunkeler, D., Jacobsen, C. S., Tuxen, N., & Broholm, M. M. (2013). Identification of chlorinated solvents degradation zones in clay till by high resolution chemical, microbial and compound specific isotope analysis. *Journal of Contaminant Hydrology*, 146, 37–50. https://doi.org/10.1016/j.jconhyd.2012.11.010

Dennedy-Frank, P. J. (2019). Including the subsurface in ecosystem services. *Nature Sustainability*, *2*(6), 443–444. https://doi.org/10.1038/s41893-019-0312-4

Enemark, T., Peeters, L. J. M., Mallants, D., & Batelaan, O. (2019). Hydrogeological conceptual model building and testing: A review. *Journal of Hydrology*, 569, 310–329. https://doi.org/10.1016/j.jhydrol.2018.12.007

Eriksson, A. (2009a). *Grundvattenmagasinet Stockholmsåsen – Solna* (Groundwater reservoir Stockholmsåsen – Solna. In Swedish). Sveriges geologiska undersökning K 154. https://resource.sgu.se/dokument/publikation/k/k154karta/k154-karta.pdf

Eveborn, D., Vikberg, E., Thunholm, B., & Hjerne och Mattias Gustafsson, C.-E. (2017). *Grundvattenbildning och grundvattentillgång i Sverige* (Groundwater recharge in Sweden. In Swedish). Geological Survey of Sweden. https://resource.sgu.se/dokument/publikation/rr/rr201709rapport/RR1709.pdf

Fetter, C. W. (1993). *Contaminant Hydrogeology*. Macmillan Publishing Company.

Fitts, C. R. (2012). *Groundwater Science* (2nd ed.) Academic Press. https://doi.org/10.1016/C2009-0-62950-0

Freeze, R. A., & Cherry, J. A. (1979). *Groundwater*. Provided by the Groundwater project, https://gw-project.org/books/groundwater/

Geological Survey of Sweden [SGU]. (2019a). *Beräkningsexempel hydraulisk konduktivitet* (Example of calculations of hydraulic conductivity. In Swedish). https://www.sgu.se/anvandarstod-for-geologiska-fragor/bedomning-av-influensomrade-avseende-grundvatten/utgangslage-och-utredningsstrategi/berakningsexempel-hydraulisk-konduktivitet/

Geological Survey of Sweden. (2019b). *Bedömning för influensområde avseeende grundvatten* (Assessment of the area of influence. In Swedish). https://www.sgu.se/anvandarstod-for-geologiska-fragor/bedomning-av-influensomrade-avseende-grundvatten/

Geological Survey of Sweden. (2022). *Wells, open data* {Data set}. Retrieved Mars 20, 2023, from https://resource.sgu.se/oppnadata/grundvatten/brunnar/v1/lan/01?format=csv

Geological Survey of Sweden. (n.d.-a). Jordarter 1:25 000–1:100 000 (Soil types) {Data set}. https://resource.sgu.se/service/wms/130/jordarter-25-100-tusen

Geological Survey of Sweden. (n.d.-b). Berggrund 1:50 000 – 1:250 000 {Data set}. https://resource.sgu.se/service/wms/130/berggrund-50-250-tusen

Geological Survey of Sweden. (n.d.-c). *Map viewer: groundwater reservoirs*. Retrieved April 21, 2023, from https://www.sgu.se/en/products/maps/map-viewer/

Gogu, C. R., Gaitanaru, D., Boukhemacha, M. A., Serpescu, I., Litescu, L., Zaharia, V., Moldovan, A., & Mihailovici, M. J. (2017). Urban hydrogeology studies in Bucharest City, Romania. *Procedia Engineering*, 209, 135–142. https://doi.org/10.1016/j.proeng.2017.11.139

Gustafson, G. (2009). Hydrogeologi för bergbyggare (Hydrogeology for Rock Engineers. In Swedish). Forskningsrådet Formas.

Harbaugh, A.W. (2005). *MODFLOW-2005, the U.S. Geological Survey modular ground-water model – the Ground-Water Flow Process* (U.S. Geological Survey Techniques and Methods 6-A16). U.S. Geological survey. https://doi.org/10.3133/tm6A16

Harbaugh, A.W., (1990). *A computer program for calculating subregional water budgets using results from the U.S. Geological Survey modular three-dimensional ground-water flow model* (U.S. Geological Survey Open-File Report 90-392). U.S. Geological Survey. https://doi.org/10.3133/ofr90392

Hölting, B., & Coldewey, W. G. (2019). *Hydrogeology*. Springer. https://doi.org/https://doi.org/10.1007/978-3-662-56375-5

Howard, K. W. F. (2015). Sustainable cities and the groundwater governance challenge. *Environmental Earth Sciences*, 73(6), 2543–2554. https://doi.org/10.1007/s12665-014-3370-y

International Agency for Research on Cancer. (2008). *IARC Monographs on the Evaluation of Carcinogenic Risks to Humans, vol 97: 1,3-Butadiene, ethylene oxide and vinyl halides (vinyl fluoride, vinyl chloride and vinyl bromide)*. International Agency for Research on Cancer. https://publications.iarc.fr/115

International Agency for Research on Cancer. (2014). *IARC Monographs on the evaluation of carcinogenic risks to humans, vol 106: Trichloroethylene, tetrachloroethylene, and some other chlorinated agents*. International Agency for Research on Cancer. https://publications.iarc.fr/130

Kresic, N., & Mikszewski, A. (2012). Hydrogeological Conceptual Site Models: Data Analysis and Visualization. CRC Press. https://doi.org/https://doi.org/10.1201/b12151

Lantmäteriet. (n.d.-a). *RH2000*. https://www.lantmateriet.se/en/geodata/gps-geodesi-och-swepos/reference-systems/height-systems/swedish-height-systems/RH-2000/

Lantmäteriet. (n.d.-b). *SWEREF99, projections*. https://www.lantmateriet.se/en/geodata/gps-geodesi-och-swepos/reference-systems/two-dimensional-systems/SWEREF-99-projektioner/

Lapworth, D. J., Boving, T. B., Kreamer, D. K., Kebede, S., & Smedley, P. L. (2022). Groundwater quality: Global threats, opportunities and realising the potential of groundwater. In *Science of the Total Environment* (Vol. 811). Elsevier B.V. https://doi.org/10.1016/j.scitotenv.2021.152471

Leeson, A., Stroo, H. F., & Ward, C. H. (Eds.). (2013). Bioaugmentation for Groundwater Remediation. Springer. https://doi.org/10.1007/978-1-4614-4115-1

Mazrooei, A., Reitz, M., Wang, D., & Sankarasubramanian, A. (2021). Urbanization impacts on evapotranspiration across various spatio-temporal scales. *Earth's Future*, 9 (8). https://doi.org/10.1029/2021EF002045

Middlemis, H., Merrick, N., Rozlapa, K., & Ross J. (2001). *Groundwater Flow Modelling Guideline.* Murray-Darling Basin Commission. South Perth, Australia.

Naturvårdsverket. (1997). Grundvattenströmning i kristallint berg (Groundwater flow in crystalline rock. In Swedish). Rapport 4818. Naturvårdsverket, Stockholm.

Niswonger, R.G., Panday, S., & Ibaraki, M. (2011). *MODFLOW-NWT, A Newton formulation for MODFLOW-2005* (U.S. Geological Survey Techniques and Methods 6–A37, 44 p.). U.S. Geological Survey. https://pubs.usgs.gov/tm/tm6a37/

Pankow, J. F., & Cherry, J. A. (1996). *DENSE CHLORINATED SOLVENTS and other DNAPLs in Groundwater: History, Behavior, and Remediation*. Waterloo Press. Provided by the Groundwater project, https://gw-project.org/books/dense-chlorinated-solvents-and-other-dnapls-in-groundwater/

Persson, L. (1998). Engineering geology of Stockholm, Sweden. *Bulletin of Engineering Geology and the Environment*, 57, 79–90.

Pollock, D.W. (2017). *MODPATH v7.2.01: A particle-tracking model for MODFLOW.* U.S. Geological Survey Software Release, 15 December 2017. http://dx.doi.org/10.5066/F70P0X5X.

Puigserver, D., Herrero, J., Nogueras, X., Cortés, A., Parker, B. L., Playà, E., & Carmona, J. M. (2022). Biotic and abiotic reductive dechlorination of chloroethenes in aquitards. *Science of The Total Environment*, *816*, 151532. https://doi.org/10.1016/j.scitotenv.2021.151532

Rapantova, N., Tylcer, J., & Vojtek, D. (2017). Numerical modelling as a tool for optimisation of ground water exploitation in urban and industrial areas. *Procedia Engineering*, 209, 92–99. https://doi.org/10.1016/j.proeng.2017.11.134

Rodhe, A., Lindström, G., Rosberg, J., & Pers, C. (2006). *Grundvattenbildning I svenska typjordar – översiktlig beräkning med en vattenbalansmodell* (In Swedish). Uppsala University, Department of Earth Sciences, Hydrology.

Ryd, E. (2017). *Relationship between capacity during drilling and transmissivity in crystalline and sedimentary rock.* {Master thesis, Uppsala University}. SGU. http://www.w-program.nu/filer/exjobb/Ellinor_Ryd.pdf

Sanner, H. & Grahn, G. (1995). *Effektiv nederbörd i Sverige – beräknad med HBV-modellen* (Effective precipitation in Sweden- calculated using the HBV-model. In Swedish). Swedish Meterological and Hydrological Institute.

Schirmer, M., Leschik, S., & Musolff, A. (2013). Current research in urban hydrogeology - A review. *Advances in Water Resources*, 51, 280–291. https://doi.org/10.1016/j.advwatres.2012.06.015

Schöpfel, J. (2010). *Towards a Prague Definition of Grey Literature*. https://archivesic.ccsd.cnrs.fr/sic_00581570

Statistics Sweden (2015). Hårdgjord mark (tätorter med mer än 30 000 invånare) per tätort. År 2010 – 2015 {Data set}. Retrieved Mars 20, 2023 from https://www.statistikdatabasen.scb.se/pxweb/sv/ssd/START__MI__MI0805__MI0805A/GYHgMarkTo37/

Stephens, D. B., Hsu, K. C., Prieksat, M. A., Ankeny, M. D., Blandford, N., Roth, T. L., Kelsey, J. A., & Whitworth, J. R. (1998). A comparison of estimated and calculated effective porosity. *Hydrogeology Journal*, *6*(1), 156–165. https://doi.org/10.1007/s100400050141

Sun, Y., Lu, X., Petersen, J. N., & Buscheck, T. A. (2004). An Analytical Solution of Tetrachloroethylene Transport and Biodegradation. In *Transport in Porous Media* (Vol. 55).

Svensson, H. (2017). *PM hydrogeologi*: *Miljöprövning för tunnelbana till Arenastaden* (Memo of environmental assessment of subway line to Arenastaden. In Swedish). Stockholms läns landsting, förvaltning för utbyggd tunnelbana. FUT 2016-0025

Svensson, H. & Lissel, P. (2017). Bilaga C6 Hydrogeologiska beräkningar, PM Hydrogeologi: Miljöprövning för tunnelbana till Arenastaden (Appendix C6 hydrogeological calculations, memo of environmental assessment of subway line to Arenastaden. In Swedish). Stockholms läns landsting, förvaltning för utbyggd tunnelbana.

Swedish Meteorological and Hydrological Institute. (2020). Vattenytor 2016 {Data set}. Retrieved April 15, 2023, from https://www.smhi.se/data/utforskaren-oppna-data/vattenytor-svar2016

Swedish Meterological and Hydrological Institute. (n.d.-a). Precipitation, sum of 24 hours: Stockholm- Observatoriekullen {Data set}. Retrieved Mars 24, 2023, from https://www.smhi.se/data/meteorologi/ladda-ner-meteorologiska-observationer/#param=precipitation24HourSum,stations=core,stationid=98210

Swedish Meterological and Hydrological Institute. (2016a). Delavrinningsområden, SVAR. {Data set}. Retrieved from https://www.smhi.se/data/hydrologi/sjoar-och-vattendrag/ladda-ner-data-fran-svenskt-vattenarkiv-1.20127

Swedish Meterological and Hydrological Institute. (2016b). Vattenytor, SVAR. {Data set}. Retrieved from https://www.smhi.se/data/hydrologi/sjoar-och-vattendrag/ladda-ner-data-fran-svenskt-vattenarkiv-1.20127

Swedish Meterological and Hydrological Institute. (n.d.-b). Air temperature, mean of 24 hours: Stockholm- Observatoriekullen {Data set}. Retrieved Mars 24, 2023, from https://www.smhi.se/data/meteorologi/ladda-ner-meteorologiska-observationer/#param=airtemperatureMean24h,stations=core,stationid=98210

Swedish Meterological and Hydrological Institute. (n.d.-c). In-depth climate scenario service: Stockholm County {Data set}. Retrieved Mars 24, 2023, from https://www.smhi.se/klimat/framtidens-klimat/fordjupade-klimatscenarier/met/stockholms_lan/medelnederbord/rcp45/2071-2100/year/anom

Swedish Meterological and Hydrological Institute. (n.d.-d). In-depth climate scenario service: Stockholm County {Data set}. Retrieved Mars 24, 2023, from https://www.smhi.se/klimat/framtidens-klimat/fordjupade-klimatscenarier/met/stockholms_lan/medeltemperatur/rcp45/2071-2100/year/anom

Takeuchi, M., Kawabe, Y., Watanabe, E., Oiwa, T., Takahashi, M., Nanba, K., Kamagata, Y., Hanada, S., Ohko, Y., & Komai, T. (2011). Comparative study of microbial dechlorination of chlorinated ethenes in an aquifer and a clayey aquitard. *Journal of Contaminant Hydrology*, 124(1–4), 14–24. https://doi.org/10.1016/j.jconhyd.2011.01.003

Tobiszewski, M., & Namieśnik, J. (2012). Abiotic degradation of chlorinated ethanes and ethenes in water. *Environmental Science and Pollution Research*, *19*(6), 1994–2006. https://doi.org/10.1007/s11356-012-0764-9

Waterloo Hydrogeologic. (2022). *User's manual: Visual MODFLOW Flex 8.0 Integrated Conceptual & Numerical Groundwater Modeling Software*. https://www.waterloohydrogeologic.com/wp-content/uploads/2021/01/VMODFlex_UsersManual.pdf

Woessner, W. W., & Poeter, E. P. (2020). *Hydrogeologic properties of earth materials and principles of groundwater flow.* The Groundwater Project, Guelph, Ontario, Canada.

WSP. (2018). *Översiktlig miljöteknsisk undersökning, Stockholms län* (Environmental investigation, Stockholm County. In Swedish). Project nr. 10251928, 577-7306-2017, Kemtvättar i Stockholms län. WSP Environmental Sverige.

WSP (2019a). *Förstudie* (Prestudy of the former dry cleaner. In Swedish). Project nr. *10284481*. WSP Environmental Sverige.

WSP. (2019b). *Hydrogeologisk utredning Kv Motorn.* (Hydrogeological investigation of housing block Motorn. In Swedish). WSP Environmental Sverige.

WSP. (2021). *Resultatrapport: Provtagningsrapport utförda undersökningar 2020-2021, certifierad provtagning* (Results of sampling performed 2020- 2021. In Swedish). Project nr. *10307352. WSP Environmental* Sverige.

WSP. (2023a). *Resultatrapport: provtagningsrapport utförda undersökningar 2020-2022, certifierad provtagning,* (Results of performed sampling during 2020-2022. In Swedish). [Draft report 2021-12-15]. Project nr. 10307352. WSP Environmental Sverige.

WSP. (2023b). *Sammanställning av föroreningssituation: Utvärdering av utförda undersökningar.* (Compilation of the information regarding the contamination at the former dry-cleaner: evaluation of performed investigations. In Swedish) [Draft report 2023-04-28]. Project nr. 10307352. WSP Environmental Sverige.

Appendices

A. The glaciofluvial esker

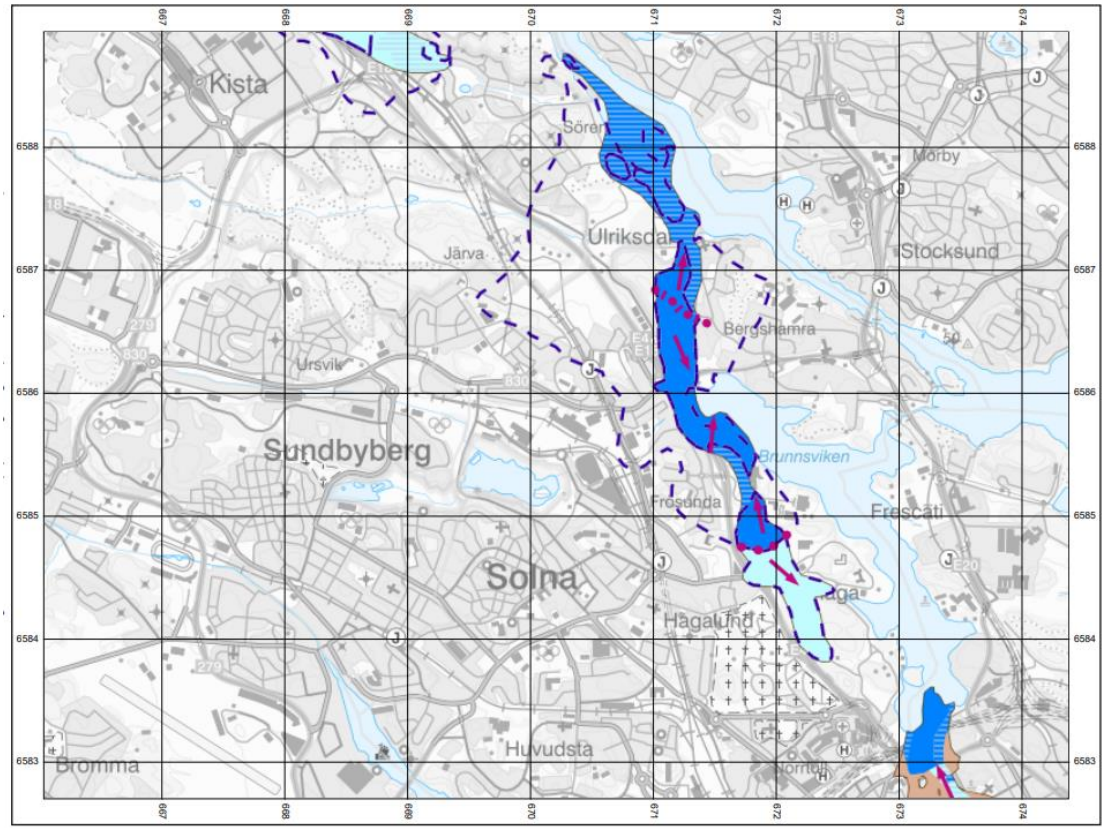

Figure A1. Map over the reservoir of the glaciofluvial esker from the SGU (n.d.-c) map viewer. Scale 1:50 000. The dark blue area indicates the delineation of the northern reservoir and the turquoise the southern reservoir. The purple arrows indicate the estimated direction of the groundwater flow in quaternary deposits and the purple dots represent groundwater divides. The dark blue dotted line represents the boundary of catchment area.

B. Groundwater flow direction

Figure B1. The estimated flow direction of the confined aquifer based on previous hydrogeological investigations performed in the area.

C. Calculations of the hydraulic conductivity of the bedrock

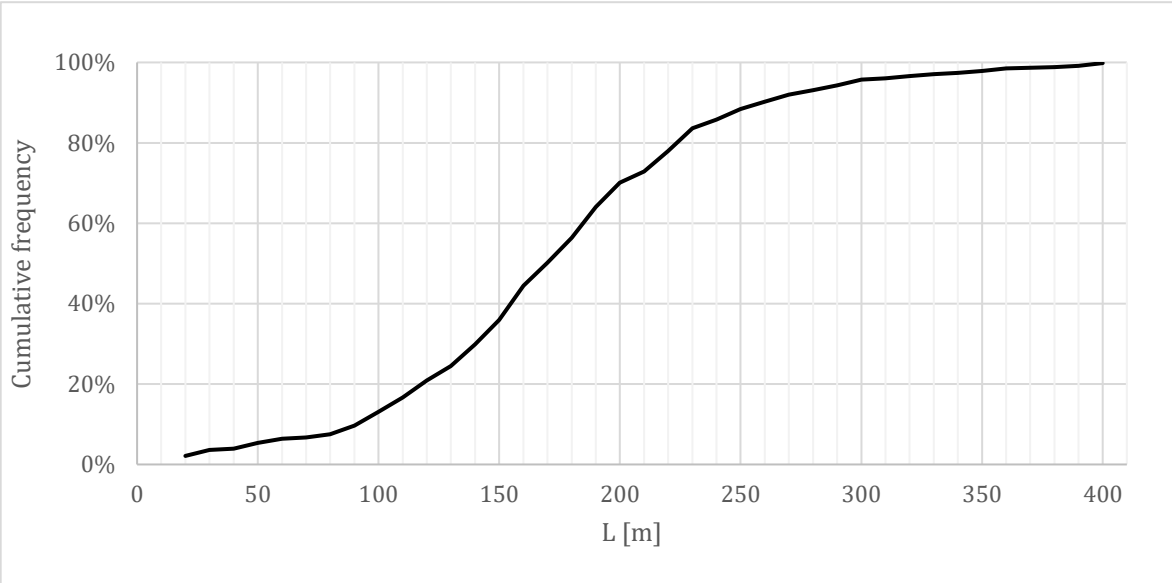

Figure C1. Cumulative frequency of the length of boreholes used for evaluation of the hydraulic properties of the bedrock.

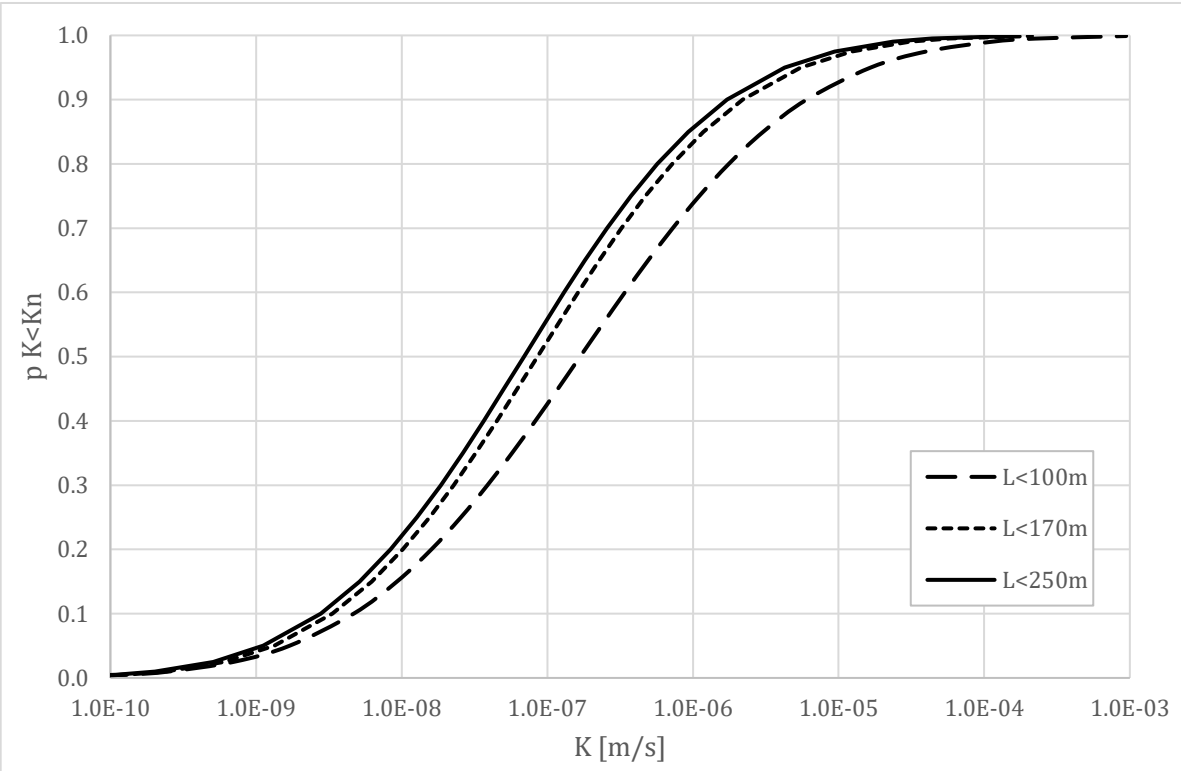

Figure C2. The fitted curves of the three populations of data.

D. Calculations of water balance

Table D1. Calculated mean temperature and precipitation based on historical observations, and the calculated evapotranspiration using Turc's formula and a reduction of 20%.

Time period	Precipitation (mm/year)	Temperature (°C)	ET (mm/year)
Mean 1961-1990	539	6.7	294
Mean 1991-2020	546	7.9	310

Table D2. Calculated increase in precipitation and temperature between the time periods based on data from SMHI:s climate model.

Time period	Increase in precipitation (%)	Increase in temperature (°C)
1961-1990	-0.1%	-0.2
1990-2020	2.6%	0.9
2021-2050	4.6%	2.1

Table D3. Calculated mean precipitation and mean temperature of the future scenario of 2021-2050 based on increase of precipitation and the temperature between the time periods 1990-2020 and 2021-2050 calculated from the SMHI climate model (Table D2) and the calculated values in Table D1. ET is calculated based on these values using Turc's formula and a reduction of 20%.

Time period	Precipitation (mm/year)	Temperature (°C)	ET (mm/year)
2021-2050	558	9.1	326

Table D4. Factor of increase derived from the data in Table D1, D2 and D3 between the time periods 1961-1990 and 1991-2020, and between 1991-2020 and 2021-2050.

	1961-1990	1991-2020	2021-2050
F_P	1	1.014	1.026
F_{ET}	1	1.053	1.054

Figure D1. Comparison of calculated and observed precipitation.

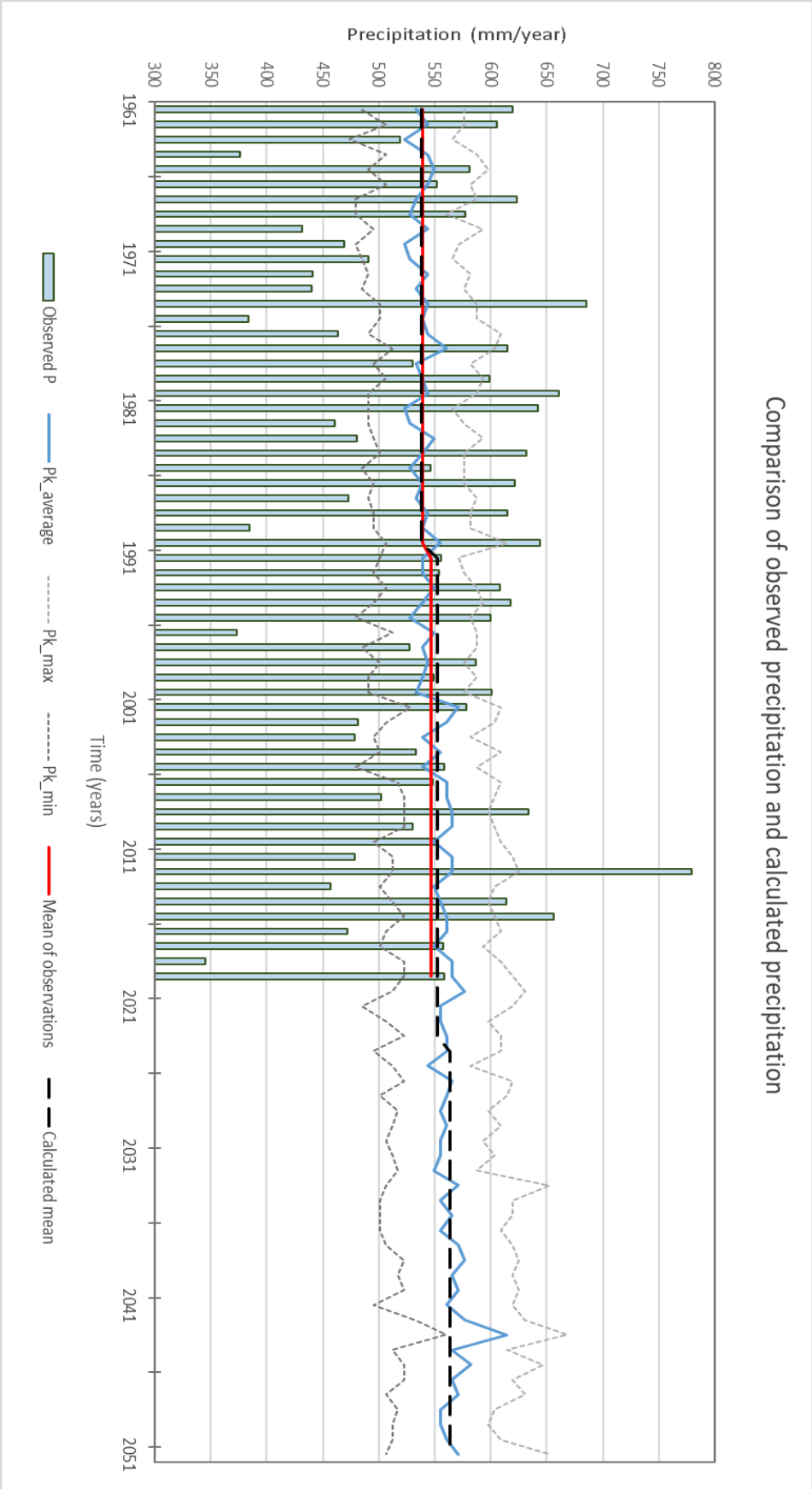

E. TCE levels in groundwater

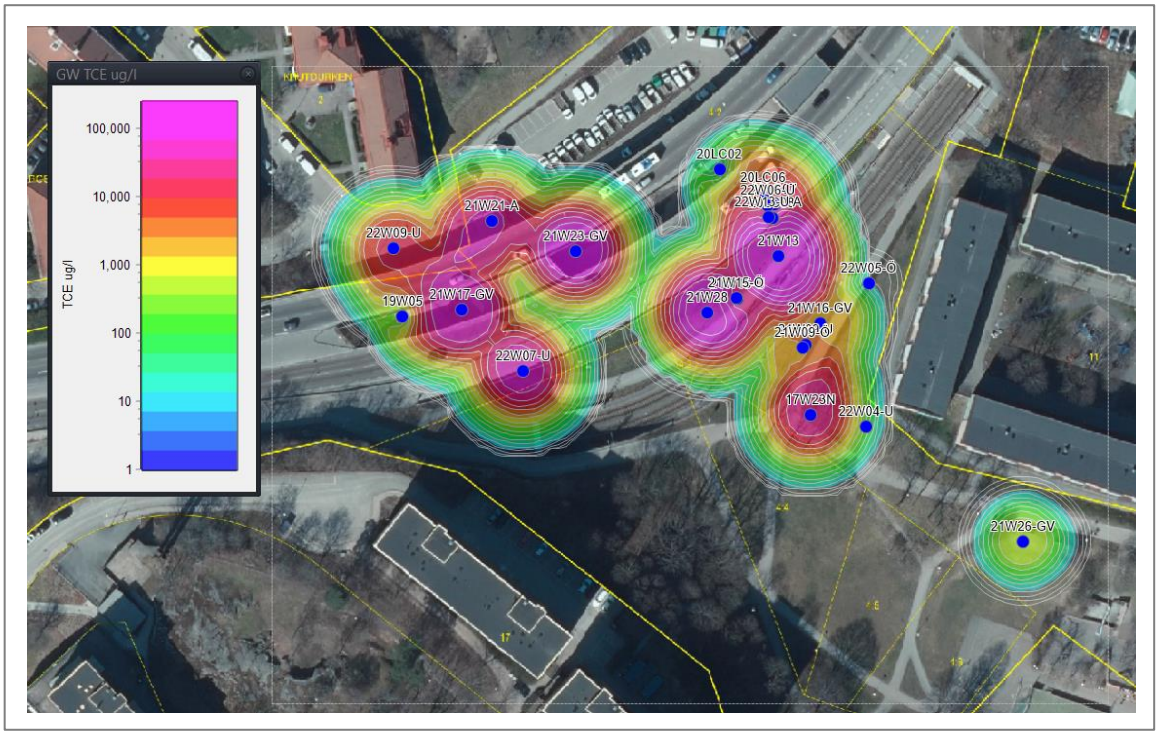

Figure E1. TCE levels in groundwater (µg/l).

F. Property zones

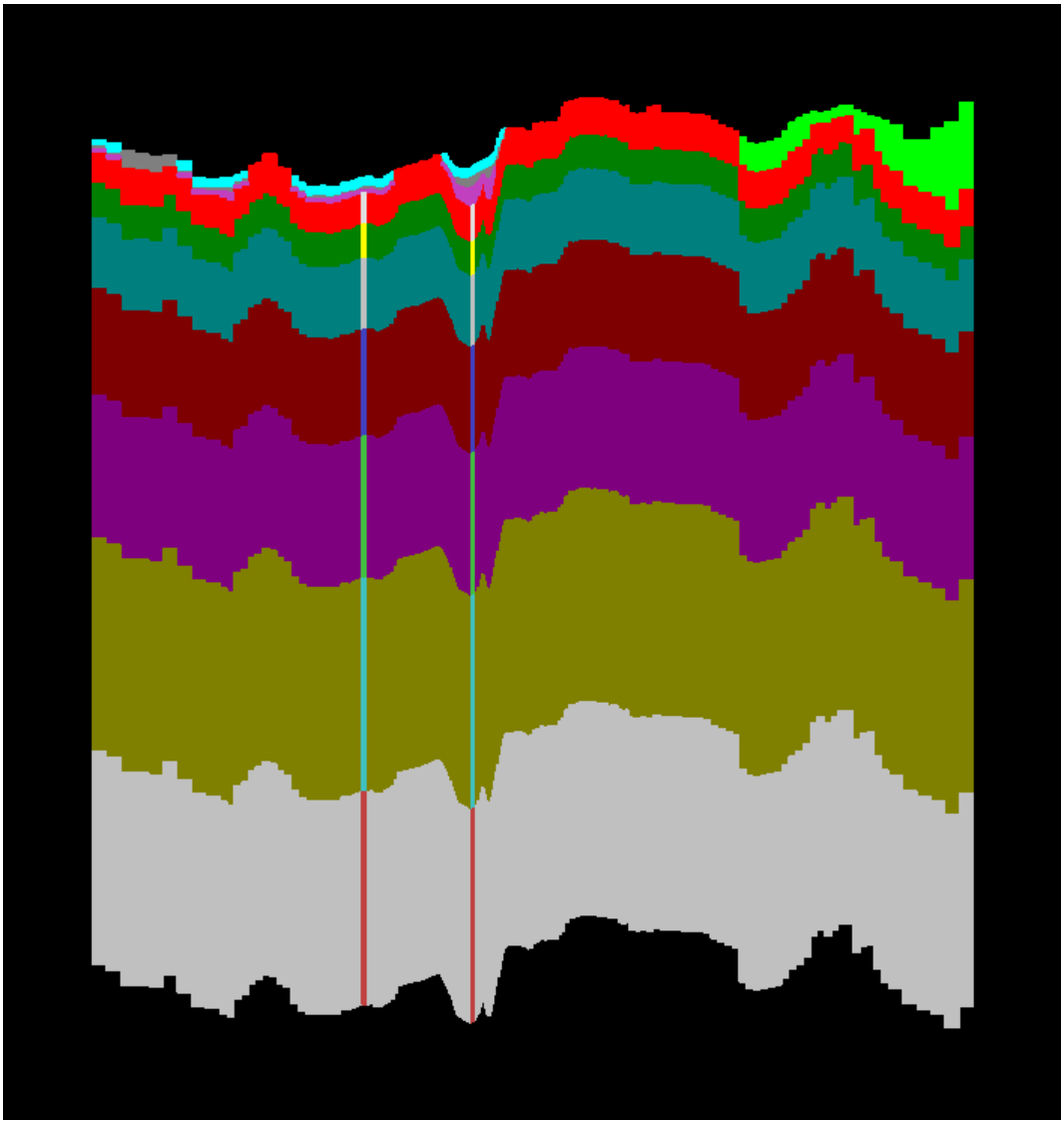

Figure F1. The property zones of the developed model, row 80.

G. Groundwater observation wells

Table G1. Data of groundwater observations used for calibration of the model. Logger z is calculated as the well bottom elevation plus the filter height. Coordinates in SWEREF99TM. Elevation in RH2000.

Well ID	X	Y	Elevation (Z)	Well bottom elevation	Filter height (m)	Logger z elevation	Assigned layer	Observed head (m)				Nr. of observations
								Min	Average	Median	Max	
11W064G	670796.4648	6584184.094	15.0	2.8	1	3.8	3	5.8	6.6	6.5	8.4	95
15W286U	670961.4394	6583995.536	8.7	-0.1	1	0.9	3	5.1	6.2	6.1	7.4	58
17W23N	670815.0337	6584192.577	16.0	-2.2	1	-1.2	3	7.5	7.8	7.7	8.2	9
19W01	670812.2314	6584173.811	15.0	1.5	1	2.5	3	7.0	7.9	7.8	9.2	8
19W04	670834.3851	6584157.046	15.1	2.3	1	3.3	3	7.2	8.3	8.3	9.2	8
19W05	670712.5784	6584217.299	12.7	-2.6	1	-1.6	3	5.3	6.2	6.2	7.9	9
21W01-GV	670976.64	6584055.833	9.4	-3.1	1	-2.1	3	6.9	7.3	7.1	8.1	6
21W05-GV	670800.287	6584176.891	14.8	2.5	2	4.5	3	7.9	8.4	8.3	9.3	4
21W09-GVU	670813.733	6584210.302	15.7	4.6	1	5.6	3	8.9	9.5	9.1	11.7	6
21W13-GV	670807.0586	6584232.608	15.2	5.3	2	7.3	3	9.7	10.2	10.0	11.1	6
21W15-GVU	670796.8073	6584221.738	14.5	3.7	2	5.7	3	9.1	9.5	9.4	10.0	6
21W16-GV	670817.4699	6584215.578	15.7	3.6	1	4.6	3	8.5	9.0	8.8	10.0	6
21W17-GV	670727.4266	6584219.058	12.7	3.8	2	5.8	3	6.3	6.9	6.7	8.2	6
21W20-GVU	670697.5001	6584258.78	12.8	1.7	2	3.7	3	5.2	5.8	5.4	7.0	4
21W21-GV	670735.1029	6584241.282	12.4	3.5	2	5.5	3	6.5	7.0	6.8	7.9	6
21W23-GV	670756.171	6584233.855	12.0	4.5	2	6.5	3	7.7	7.9	7.9	8.2	4
21W26-GV	670868.3836	6584160.967	18.3	0.1	2	2.1	3	6.9	8.7	7.7	11.0	5
21W28-GV	670789.2451	6584218.293	14.2	5.2	2	7.2	2	9.5	10.2	9.7	12.2	6
22W02-GVU	670834.1173	6584206.384	18.8	10.8	2	7.7	3	-	13.1	-	-	2
22W06-GVU	670804.3352	6584245.301	13.0	5.7	2	7.7	3	10.0	10.1	10.1	10.2	3
22W07-GVU	670743.2673	6584204.023	13.1	5.1	1	7.1	3	7.4	8.2	7.5	9.6	3
22W09-GVU(2)	670710.404	6584234.464	12.7	4.7	2	6.7	3	6.5	7.0	6.7	7.9	3
22W13-GVU	670800.3394	6584245.121	13.0	6.5	2	8.5	3	9.7	9.9	9.8	10.2	3

H. Calibrated model parameter values

Table H1. Initial and calibrated hydraulic conductivity of the model layers. K_{xy} denotes horizontal hydraulic conductivity, while K_z denotes vertical hydraulic conductivity.

		Hydraulic conductivity (m/s)				
		Initial value		Final calibrated value		
Layer	Material	K_{xy}	K_z	K_{xy}	K_z	K_{zone}
1	Filling material	1.0E-05	-	1.0E-05	-	-
2	Clay	1.0E-09	3.3E-10	1.0E-09	3.3E-10	-
3	Sand	1.8E-04	6.1E-05	1.0E-05	3.3E-06	-
4	Rock 1	1.2E-07	-	9.0E-07	-	6.3E-06
5	Rock 2	1.2E-07	-	3.0E-07	-	2.1E-06
6	Rock 3	8.5E-07	-	2.0E-07	-	1.4E-06
7	Rock 4	2.0E-08	-	1.2E-07	-	8.4E-07
8	Rock 5	5.7E-08	-	5.7E-08	-	4.0E-07
9	Rock 6	2.4E-08	-	2.5E-08	-	1.8E-07
10	Rock 7	1.2E-08	-	1.2E-08	-	8.4E-08

Table H2. Calibrated parameter values.

Parameter	Calibrated value
Recharge	235 mm
LCOND	0.3 m/day

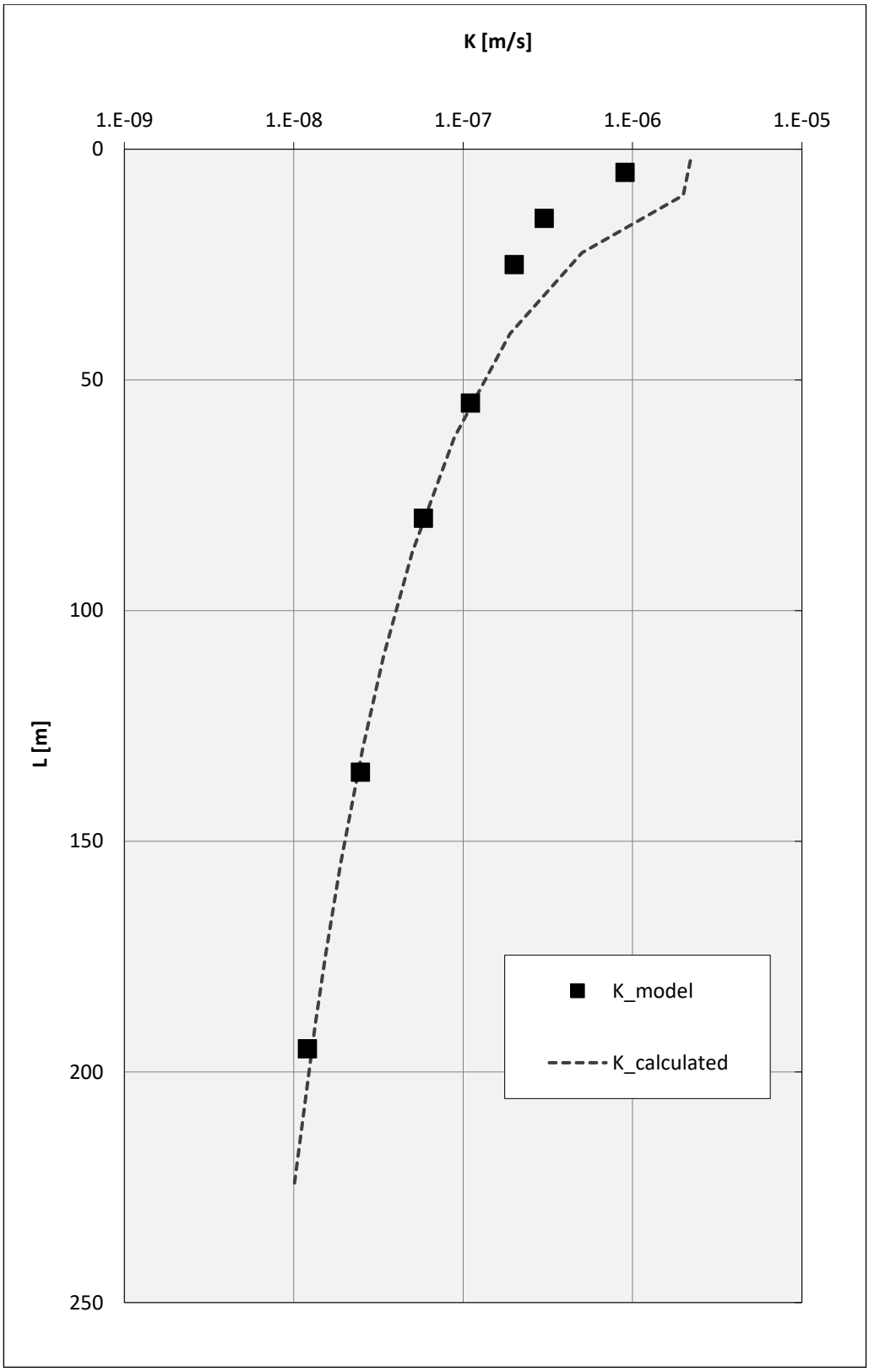

Figure H1. Comparison of the hydraulic conductivity of the bedrock of the calibrated model (K_{model}) and the calculated hydraulic conductivity ($K_{calculated}$). For details on the derivation of the calculated hydraulic conductivity of the bedrock, see Section 3.2.2.

DEPARTMENT OF ARCHITECTURE AND CIVIL ENGINEERING
CHALMERS UNIVERSITY OF TECHNOLOGY
Gothenburg, Sweden 2023
www.chalmers.se

CHALMERS
UNIVERSITY OF TECHNOLOGY